12-2011

Adaptive Intensity Modulated Radiation Therapy Planning Optimization with Changing Tumor Geometry and Biology Enforcing Both Cumulative and Fraction Size Dose Constraints

Behlul Saka
University of Arkansas, Fayetteville

ADAPTIVE INTENSITY MODULATED RADIATION THERAPY PLANNING OPTIMIZATION WITH CHANGING TUMOR GEOMETRY AND BIOLOGY ENFORCING BOTH CUMULATIVE AND FRACTION SIZE DOSE CONSTRAINTS

ADAPTIVE INTENSITY MODULATED RADIATION THERAPY PLANNING OPTIMIZATION WITH CHANGING TUMOR GEOMETRY AND BIOLOGY ENFORCING BOTH CUMULATIVE AND FRACTION SIZE DOSE CONSTRAINTS

A dissertation submitted in partial fulfillment
of the requirements for the degree of
Doctor of Philosophy in Industrial Engineering

By

Behlul Saka
Sabanci University
Bachelor of Science in Manufacturing Systems Engineering, 2005
University of Arkansas
Master of Science in Industrial Engineering, 2007

December 2011
University of Arkansas

ABSTRACT

Intensity Modulated Radiation Therapy (IMRT) is a modern technique of delivering radiation treatments to cancer patients. In IMRT technology, intensities must be chosen for the many small unit grids into which the beams are divided to produce a desired distribution of dose at points throughout the body with the goal of maximizing dose delivered to the tumor while sparing healthy tissues from excessive radiation and keeping dose homogeneous across the tumor. Although IMRT plans are optimized as a single overall treatment plan, they are delivered over 30-50 treatment sessions (fractions) and both cumulative and per-fraction dose constraints apply.

The extended time period of treatment allows for periodic re-imaging of the changing tumor geometry and for adapting the treatment plan accordingly. This research presents promising iterative optimization approaches that re-optimize and update the treatment plans periodically by incorporating the latest tumor geometry information. Two realistic lung cases simulating practice, based on anonymized archive datasets, are used to test the effectiveness of the proposed adaptive planning approaches. The computed optimal plans both satisfy cumulative and per-session dose constraints while improving the objective (average tumor dose) as compared to non-adaptive treatment.

In addition to tracking tumor geometrical changes through the treatment, recent advances in imaging technology also provide more insight on tumor biology which has been traditionally disregarded in planning. The current practice of delivering homogeneous physical dose distributions across the tumor can be improved by nonhomogeneous distributions guided by the biological responses of the tumor points. This research is one of the first efforts in developing

radiation therapy planning optimization methods with tumor biology information while maintaining both cumulative and per-fraction dose constraints. The proposed biological optimization models generate treatment plans reacting to the tumor biology prior to the treatment as well as the changing tumor biology throughout the treatment. The optimization models are tested on a simulated head and neck test case. Results show computed biologically optimized plans improve on tumor control obtained by traditional plans ignoring biology, and also with adaptive over non-adaptive methods.

This dissertation is approved for recommendation to the Graduate Council

Dissertation Director:

DR. RONALD L. RARDIN

Dissertation Committee:

MARK P. LANGER (M.D.)

DR. HEATHER L. NACHTMANN

DR. SARAH E. ROOT

DISSERTATION DUPLICATION RELEASE

I hereby authorize the University of Arkansas Libraries to duplicate this dissertation when needed for research and/or scholarship.

Agreed _____

Behlul Saka

Refused _____

Behlul Saka

ACKNOWLEDGEMENTS

First and foremost, I would like to acknowledge my Ph.D. advisor, Professor Ronald Rardin, for being a great professor, teacher, colleague, and friend to me from the beginning of my Ph.D. journey until now. I would like to thank him for listening to me patiently at our discussions, giving guidance to me during the most challenging times in my dissertation research and sharing the best moments of my achievements both inside and outside the department. Secondly, I am very thankful to Mark Langer (M.D.) for his patience towards me in understanding the basic concepts of radiation therapy and his role in motivating me to work on medical decision problems and even to start a related career. Without our continuous collaboration for the past three years, this research would not be possible to happen. I also thank Professor Heather Nachtmann and Professor Sarah Root for their valuable time and serving in my committee.

Special thanks go out to the faculty members of the Industrial Engineering Department that I was fortunate to take courses from or work with on the research projects. I am also thankful to the very helpful staff at our department and my friends from graduate school.

I would like to take this opportunity to thank my relatives in Turkey and my wife's relatives in U.S.A. for their belief in me during my Ph.D. studies. Especially, I want to thank my three brothers, Talha, Bilal, and Abdullah, for always thinking highly of me and considering me as an inspiration in their lives. Although he is not with us now, my grandfather always deserves the most special thanks due to his support through my education life prior to coming U.S.A. I also want to thank my sweet grandmother for just being herself.

Above all, my wife Clarissa and my daughter Mina here with me and my mother and father in Turkey deserves the most special thanks for their endless support and patience, baring with me during the most disappointing times in my research, and motivating me to finish this challenging task of my life. Without your help, I would not be able to achieve what I had done.

Lastly, I want to thank the National Science Foundation (NSF) for funding my research. This research is sponsored in part by NSF grant 0813896.

DEDICATION

This dissertation is dedicated to my mother, Ayse Saka, and my father, Ismail Saka.

TABLE OF CONTENTS

LIST OF FIGURES

LIST OF TABLES

1 Introduction

According to the American Cancer Society, "Cancer is the second most common cause of death in the US, exceeded only by heart disease, and cancer accounts for nearly 1 of every 4 deaths". In 2011, over 570,000 Americans are expected to die of cancer, more than 1,500 people a day, and the new cases that are expected to be diagnosed are about 1.6 million (Cancer Facts &Figures, 2011). Treatment methods to cure cancer include surgery, radiation therapy, chemotherapy, hormone therapy, biological therapy, and targeted therapy. Radiation therapy can be used alone or in combination with other treatment methods. Over half of all cancer patients receive radiation therapy at some point during their treatment (Bortfeld *et al.*, 2008).

1.1 IMRT Technology

Radiation therapy aims to destroy cancer cells or slow their rate of growth by using high energy rays without exposing the healthy tissues to excess dose. When applying radiation therapy to a patient, a device mounted on a gantry called a *linear accelerator* rotates around the patient and shoots radiation from different beam angles aiming at targets (Figure 1.1). Using different beam angles helps better sparing the healthy tissues since a particular surrounding healthy tissue will not be heavily exposed to radiation consistently.

Figure 1.1: Radiation Therapy Environment

Intensity Modulated Radiation Therapy (IMRT) is illustrated on a lung case *slice* in Figure 1.2. A slice is defined as an image of the particular cross section of the body and outlines the structures of interest. Each structure is discretized into a collection of three dimensional volume elements called *voxels* representing particular *points* in the structure. In IMRT, radiation is delivered through a set of virtual *beamlets* (e.g. 0.5 cm to 0.5 cm) rather than whole beam (e.g. 10 cm to 10 cm) by modulating the beams using a multi-leaf collimator (Figure 1.3) which allows for the radiation dose to conform more precisely to the three-dimensional shape of the tumor while more effectively sparing healthy tissues (Webb, 2003). A multi-leaf collimator has leaves on two sides of the beam which open/close in front of the beam in order to arrange a set of beamlets, called an *aperture*. Radiation dose can be defined as the measure of physical effect at each point of the body receiving radiation (ICRU 50, ICRU 62). Although the power of the beam is constant throughout the treatment, each beam angle can have a non-uniform beamlet intensity map in IMRT as shown in Figure 1.2 by blocking parts of the beam during its exposure. *Intensity* (or *fluence*) is the measure of radiation delivered from the beamlet.

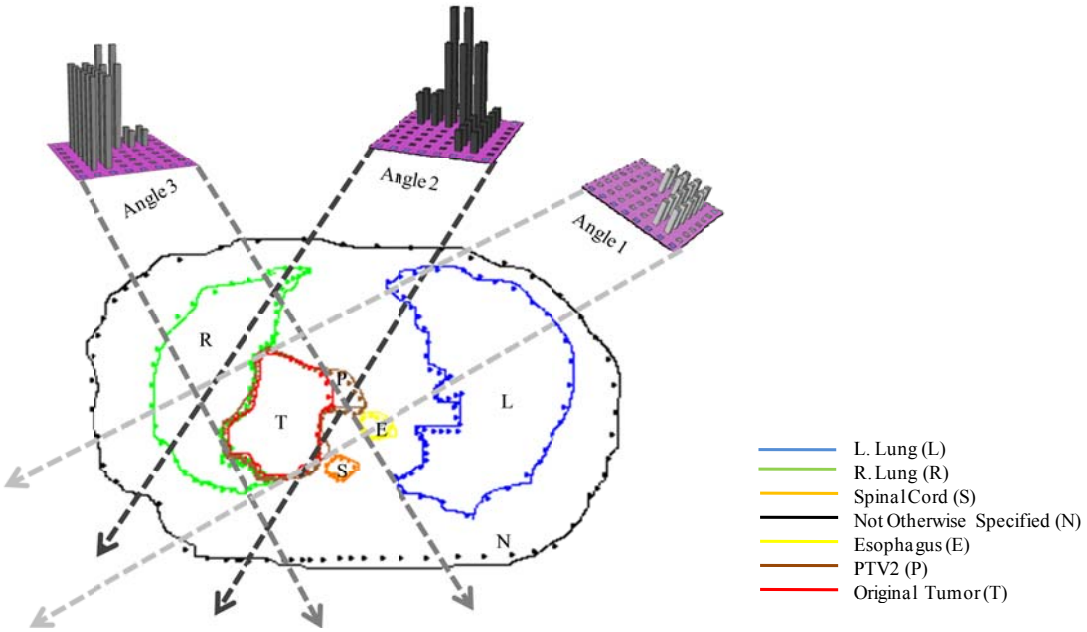

Figure 1.2: Intensity Modulated Radiation Therapy (IMRT)

Figure 1.3: Modulating a Beam by a Multi-leaf Collimator

1.2 IMRT Planning

Traditional IMRT planning optimization uses penalty based methods where the excess dose on healthy tissues and dose deficiency on targets are penalized in the objective function. By contrast, the approach taken in this research chooses intensity/fluence levels for the beamlets of selected beam angles which maximize the min/average tumor dose subject to explicitly enforced cumulative dose constraints across the entire treatment including tumor dose homogeneity

requirements, dose maxima on healthy tissues, dose-volume limits of protected fractions of healthy tissues (both a maximum limit and a lesser dose threshold that a certain percentage of the healthy tissue can receive), and the minimum dose limits on secondary targets.

Although IMRT is planned as a single overall treatment, it is delivered over several weeks in a series of *fractions* or treatment sessions. In order to have more effective and applicable treatment plans, both cumulative and per-fraction dose constraints need to be taken into consideration (Wu *et al.*, 2000; Blanco and Chao, 2002). Table 1.1 shows a prescription for one of the lung cases used in this research. The table presents both cumulative and per-fraction (fraction size) dose objectives/limits for targets and healthy tissues in the prescription. For healthy tissues subject to dose-volume constraints, a mean dose limit based on a predictive model discovered in Europe and confirmed in the US that reduces the combinatorial complexity of planning (Kwa *et al.*, 1998; Bradley *et al.*, 2007) is used. This predictive model using mean lung dose has been shown to be a good predictor for radiation pneumonitis (frequent complication with symptoms of cough, fever, and shortness of breath found typically within 6 months after the start of radiotherapy) based on analysis of multiple datasets from different institutions which underlines the use of mean dose limits in the prescriptions.

Table 1.1: Prescription for the Lung Case Illustrating Both Cumulative and Fraction Size Dose Objectives/Limits

Structure	Structure Description	Prescription	
		Cumulative Dose Objective/Limit (Gy)	Fraction Size Dose Limit (Gy)
Tumor	Primary Target	Maximize avg. dose	≥ 2
		$\frac{\text{min. dose}}{\text{max. dose}} \geq 0.95$	
PTV2	Secondary Target	$100\% \geq 50$	≥ 2
Right Lung	Healthy Tissue	Avg. dose ≤ 17	≤ 2.1
Left Lung	Healthy Tissue	Avg. dose ≤ 17	≤ 2.1
Heart	Healthy Tissue	Avg. dose ≤ 35	≤ 2.1
Esophagus	Healthy Tissue	Avg. dose ≤ 35	≤ 2.1
Not Otherwise Specified Tissue	Healthy Tissue	$100\% \leq 100$	≤ 2.1
Spinal Cord	Healthy Tissue	$100\% \leq 45$	≤ 2.1

Numerous methods have been proposed in the literature to generate radiation therapy plans. Of these methods, optimization models using mathematical programming formulations have been developed to determine the best beamlet intensities (Langer *et al.*, 1990; Langer *et al.*, 1991; Langer *et al.,* 2003; Lee *et al.*, 2003; Romeijn *et al.*, 2003; Romeijn *et al.*, 2006; Preciado-Walters *et al.*, 2004, Lee *et al.*, 2006; Tuncel, 2008) and the best aperture intensities (Romeijn *et al.*, 2005; Preciado-Walters *et al.*, 2006), along with non-linear gradient techniques (Cho et al., 1998; Hristov and Fallone, 1998; Spirou and Chui, 1998; Wu and Mohan, 2000). Other methods include randomized approaches, such as simulated annealing (Webb, 1991; Morril *et al.*, 1990;

Mageras and Mohan, 1993; Langer *et al.*, 1996) and genetic algorithms (Langer *et al.*, 1996; Ezzel, 1996; Wu *et al.*, 2000).

1.3 Objectives of the Research

All of these available methods used to generate radiation therapy plans optimize a single cumulative treatment plan and neglect changes in the tumor geometry over time. However, with the recent advances in imaging technology, the Image Guided Radiation Therapy (IGRT) allows acquiring images throughout the treatment that capture the changes in the tumor geometry. This motivates devising adaptive optimization methodologies that re-optimize the treatment plan in response to the changing tumor geometry while maintaining both cumulative and fraction size dose constraints.

In addition, the recent molecular and functional imaging technology can provide more insight on the tumor biology and help incorporating the biological information, which has traditionally been unknown, into the treatment planning. The ability to understand the tumor biology and quantify the biological information invites developing optimization methodologies that would adjust IMRT plans by incorporating tumor biology information in order to achieve more effective treatment plans.

This dissertation research develops optimization models to meet the demand for optimization methodologies exploiting tumor geometry and biology information over the course of the treatment. The objectives of this dissertation research are as follows.

- To deal with both cumulative and fractionation constraints in adaptive IMRT planning optimization
- To develop, implement, and test adaptive optimization methodologies that re-optimize the treatment plan in response to the changes in the tumor geometry while satisfying both cumulative and fractionation dose constraints to achieve the best IMRT design for the overall treatment and for each fraction
- To develop, implement, and test static and adaptive optimization models that include the initial and changing tumor biology information into the optimization which helps adjusting IMRT plans to the tumor sensitivity in order to yield more effective treatment plans

1.4 Research Tools

The optimization models and methodologies developed in this dissertation research are implemented in C++ programming language by using ILOG Concert Technology Library. The formulations are solved by using CPLEX 11.2 software. Since the cuts generated by CPLEX do not help the optimization process, that feature of CPLEX is turned off. The other CPLEX parameters are kept at their default values. All the computational experiments are performed on the Industrial Engineering Department's Windows Server 2003 R2 Datacenter x64 Edition having 128 GB RAM and 16 processors at 2.93 GHz. The best performance is achieved by allocating single processor.

1.5 Dissertation Organization

This dissertation is organized as follows. Chapter 2 derives mathematical programming and related methods that optimize treatment plans where both cumulative and fraction size dose limits on each tissue are satisfied. Chapter 3 describes the fractionation challenge that is magnified in adaptive IMRT planning. Chapter 4 addresses the solution approaches for the fractionation challenge in adaptive IMRT by developing an adaptive planning optimization methodology with changing tumor geometry and fraction size limits and presents the computational experiments showing the benefit of adaptation. Biologically guided IMRT optimization methodologies are presented in Chapter 5 as well as the results demonstrating the improvements in the treatment outcomes. Finally, conclusions, contributions and future research are given in Chapter 6.

2 Models for Optimization of Treatment Plans Satisfying Fraction Size Requirements

2.1 Description of the CERRLung Test Case

This section describes one of the lung test cases, referred as "CERRLung", which is used in the computational experiments presented in Chapter 2 and 4. Table 2.1 shows the volume (cm^3), number of sampling voxels used for the optimization, the size of each voxel (cm^3/voxel), and the influence matrix density for each structure in the lung test case. The influence matrix represents all the voxels as its rows and all selected beamlets as its columns and each element of the matrix (*dose coefficient*) defines dose per unit beamlet intensity. The influence matrix density (%) for a structure indicates the ratio of its non-zero dose coefficients to its all dose coefficients in the influence matrix. The influence matrix for this test case is generated using a sample case found on the CERR website ("CERR: A Computational Environment for Radiotherapy Research") established to allow collaborative computational experimentation in radiation therapy. The prescription for this test case is presented in Section 1.2.

Table 2.1: Description of the Lung Test Case

Structure	Structure Description	Volume (cm^3)	Number of Sampling Voxels Used for Optimization	cm^3/Voxel in Optimization	The Influence Matrix Density
Tumor	Primary Target	90.6	2,133	0.04	94%
PTV2	Secondary Target	256.0	1,519	0.17	93%
Right Lung	Healthy Tissue	1,893.2	2,805	0.67	76%
Left Lung	Healthy Tissue	1,689.3	2,476	0.68	35%
Heart	Healthy Tissue	599.4	876	0.68	44%
Esophagus	Healthy Tissue	42.3	233	0.18	66%
Not Otherwise Specified	Healthy Tissue	31,430.0	11,425	2.75	40%
Spinal Cord	Healthy Tissue	56.2	316	0.18	52%
Beam Angles: 0 40 80 120 160 200 240 280 320 (780 beamlets)					

2.2 Notation

Tissues are represented by a collection of points (voxels). Let T denote the set of tumor points, S denote the set of points in the secondary target and H_k denote the set of points in k^{th} healthy tissue for $k \in K \cup \overline{K}$. Here, K and $\overline{K}$ denote the set of indices for the healthy and dose-volume healthy tissues, respectively.

The set of beamlets used from preselected beam angles is denoted by J. Dose coefficients a_{ij} denote the dose received by tissue point i per unit intensity of beamlet j. The coefficients for all tissues form the influence matrix for the problem as defined above. The dose received from beamlet j at point i is $a_{ij}x_j$ where $x_j \geq 0$ is the continuous decision variable defined as the value of intensity assigned to beamlet j.

Let variables d_i denote the dose received at point i. This research makes the standard assumption that the dose can be expressed as a linear combination of the individual beamlet intensities. Thus, for every point i,

$$d_i = \sum_{j \in J} a_{ij} x_j \tag{2.1}$$

Let D_{min} be a variable denoting the minimum tumor dose and coefficient α be a homogeneity ratio limit with $0 \leq \alpha \leq 1$. The prescribed minimum dose for the secondary target is denoted as l_{sec}^{total} whereas the prescribed maximum dose for healthy tissues $k \in K$ is denoted as u_k^{total}. The parameter μ_k represents the mean dose limit for the kth dose-volume healthy tissue.

The fraction size limits are represented by the following parameters. Let l_{tumor}^{daily} denote the minimum dose that any point in the tumor must receive during the fraction and l_{sec}^{daily} denote the minimum dose any point in the secondary target must receive during the fraction. u_k^{daily} denotes the maximum dose that any point in healthy tissue $k \in K \cup \overline{K}$ can receive during the fraction.

2.3 Optimization against Cumulative Dose Limits Alone

2.3.1 The Linear Programming (LP) Model

The LP formulation shown below and presented in Saka *et al.* (6) in 2010 is used to optimize the treatment plan against the cumulative dose limits alone. It maximizes the average tumor dose received over the entire treatment (2.2) subject to several overall treatment constraints. Constraint set (2.3) ensures that the average dose received across all points in k^{th} dose-volume healthy tissue is limited by the corresponding mean limit. Constraint sets (2.4) and (2.5) for the overall treatment guarantees that the upper dose limit for healthy tissues and the lower dose limit for secondary target tissue are satisfied, respectively. Constraint set (2.6) is the dose consistency constraint assuring secondary target doses do not exceed the maximum tumor dose. Constraint (2.7) satisfies the tumor dose homogeneity by enforcing the ratio of the minimum and maximum tumor doses to be greater than or equal to homogeneity limit α.

$$\text{maximize} \quad \left(\sum_{i \in T} d_i\right) / |T| \tag{2.2}$$

$$\sum_{i \in H_k} d_i \le |H_k| \mu_k \qquad \forall k \in \overline{K} \tag{2.3}$$

$$d_i \le u_k^{total} \qquad \forall k \in K, \forall i \in H_k \tag{2.4}$$

$$d_i \ge l_{sec}^{total} \qquad \forall i \in S \tag{2.5}$$

$$d_i \leq \frac{D_{min}}{\alpha} \qquad \forall i \in S \tag{2.6}$$

$$D_{min} \leq d_i \leq \frac{D_{min}}{\alpha} \qquad \forall i \in T \tag{2.7}$$

2.3.2 Difficulties with Fractionating the Cumulative Plan

Traditionally, optimized treatment plans are delivered into 30-50 fractions for which fraction objectives apply (Wu et al., 2000; Blanco and Chao, 2002). The cumulative tolerances for normal tissues are valid only if delivered in doses per fraction no higher than about 2.1 Gy, and tumor eradication becomes uncertain when delivered dose per fraction falls below about 1.8 Gy (Stewart and Li, 2007). Successful treatment rests on delivering feasible fractions satisfying these stated fraction size dose objectives.

The optimized treatment plan cannot be divided into too many fractions since it is required to deliver the minimum fraction size dose to the primary and secondary target. This puts an upper bound on N denoted as $\overline{N}$. Here, N denotes the integer number of fractions the treatment plan will be given. $\overline{N}$ (not necessarily integer) is determined in the expression (2.8) as by taking the minimum of the number of fractions dividing the secondary target doses by the secondary target fraction size limit and the number of fractions dividing all the tumor doses by the tumor fraction size dose limit.

$$N \leq \overline{N} = min\left\{ \min_{i \in S}\left\{ \frac{d_i}{l_{sec}^{daily}} \right\}, \frac{D_{min}}{l_{tumor}^{daily}} \right\} \tag{2.8}$$

On the other hand, the treatment plan cannot be divided into too few fractions, because the healthy tissues cannot receive a dose more than their maximum fraction size limits during each fraction. This puts a lower bound on N denoted by $\underline{N}$ (not necessarily integer) determined in the expression (2.9) by taking the maximum of number of fractions dividing the maximum dose each healthy tissue receives by its fraction size dose limit.

$$N \geq \underline{N} = \max_{\substack{i \in H_k, \\ k \in K \cup \overline{K}}} \left\{ \frac{d_i}{u_k^{daily}} \right\} \tag{2.9}$$

When the treatment plan is optimized against the cumulative dose limits alone, the lower bound $\underline{N}$ may be greater than the upper bound $\overline{N}$; therefore, a feasible N to divide the treatment plan does not exist. This is demonstrated by the results given in Table 2.2. There, $\overline{N} = min\{50/2, 97.8/2\} = 25$ and $\underline{N} = 103.5/2.1 = 49.3$. The treatment plan can be divided at most in 25 fractions in order to satisfy the minimum fraction size limit (≥2 Gy) on the targets. On the other hand, it must be divided in at least $\lceil 49.3 \rceil = 50$ fractions in order not to violate the maximum fraction size limit (≤2.1 Gy) on the right lung. As a result, a feasible integer N that equally divides the cumulative treatment plan and satisfies both the minimum and maximum fraction size dose limits cannot be found.

Furthermore, when the cumulative doses are divided by the integer upper (N=25) or integer lower (N=50) bounds, the fraction size dose limits are significantly violated (4.14 Gy > 2.1 Gy for the right lung in integer upper bound division, 1.0 < 2.0 Gy for the secondary target PTV2 in integer lower bound division).

Table 2.2: Optimization against Cumulative Dose Limits Alone

Dose Statistics	Cum. Dose (Gy)	Fraction Size Dose Limit (Gy)	Feasible Integer Number of Fractions (N)	Fraction Size Dose (Gy) When $N = \lfloor \overline{N} \rfloor = 25$	Fraction Size Dose (Gy) When $N = \lceil \underline{N} \rceil = 50$
Min. Tumor	97.8	≥2	N≤48	3.91	**1.96**
Min. PTV2	50.0	≥2	**N≤25**	2.00	**1.00**
Max. Right Lung	103.5	≤2.1	**N≥50**	**4.14**	2.07

Notation: $\overline{N}$ (not necessarily integer) denotes the maximum number of fractions dividing all the targets' doses by their fraction size limit, and $\underline{N}$ (not necessarily integer) denotes the minimum number of fractions dividing all the healthy tissues' doses by their fraction size limit. PTV2 represents the secondary target.

2.4 Ratio Model: Optimization by Including Ratio Constraints and Rescaling

2.4.1 Ratio-Enforcing Constraints

In order to find a feasible N to divide the treatment plan, $\underline{N}$ needs to be at least less than or equal to $\overline{N}$. Thus:

$$\underline{N} = \max_{\substack{i \in H_k, \\ k \in K \cup \overline{K}}} \left\{ \frac{d_i}{u_k^{daily}} \right\} \leq \overline{N} = \min \left\{ \min_{i \in S} \left\{ \frac{d_i}{l_{sec}^{daily}} \right\}, \frac{D_{min}}{l_{tumor}^{daily}} \right\} \tag{2.10}$$

Let s_{min} be a variable that defines the minimum dose that the secondary target receives, so $s_{min} = \min_{i \in S} \{d_i\}$. Rewriting condition (2.10) by using this expression and then rearranging some terms gives the condition in (2.11) which states that the ratio of dose at any healthy tissue point to the dose at any primary or secondary tumor point cannot exceed the ratio of their respective fraction size limits.

$$\max_{i \in H_k} \{d_i\} \leq \min \left\{ s_{min} * \frac{u_k^{daily}}{l_{sec}^{daily}}, D_{min} * \frac{u_k^{daily}}{l_{tumor}^{daily}} \right\} \tag{2.11}$$

This condition is incorporated into the LP-formulation referenced in the previous section by adding ratio constraint sets (2.12) through (2.15) that ensure that the dose distribution healthy tissues receive are within a specified ratio of the dose distribution the targets receive. Constraint sets (2.12) and (2.13) capture the minimum secondary target and the tumor doses, respectively. Constraint sets (2.14) and (2.15) ensure that the maximum dose that each healthy tissue receives should be within a ratio of the minimum secondary target dose and the minimum tumor dose, respectively. The LP-formulation presented in Section 2.3.1 plus these ratio constraint sets constitute the *ratio model*.

$$d_i \geq s_{min} \qquad \forall i \in S \tag{2.12}$$

$$d_i \geq D_{min} \qquad \forall i \in T \tag{2.13}$$

$$d_i \leq \frac{u_k^{daily}}{l_{sec}^{daily}} * s_{min} \qquad \forall k \in K \cup \overline{K}, \forall i \in H_k \tag{2.14}$$

$$d_i \leq \frac{u_k^{daily}}{l_{tumor}^{daily}} * D_{min} \qquad \forall k \in K \cup \overline{K}, \forall i \in H_k \tag{2.15}$$

Table 2.3 shows the results from optimizing the treatment plan for the CERRLung test case by solving the ratio model. Based on the dose statistic, $\overline{N} = min\{72.4/2, 74.4/2\} = 36.2$ and $\underline{N} = 76/2.1 = 36.2$. However, there is still not an integer N between $\underline{N}$ and $\overline{N}$. In addition, when the cumulative doses are divided by the integer upper (N=36) or integer lower (N=37) bounds, the fraction size dose limits are still violated (2.11 Gy > 2.1 Gy for the right lung in integer upper bound division, 1.96 < 2.0 Gy for the secondary target PTV2 in integer lower bound division).

Table 2.3: Optimization including Ratio Constraints

Dose Statistics	Cum. Dose (Gy)	Fraction Size Dose Limit (Gy)	Feasible Integer Number of Fractions (N)	Fraction Size Dose (Gy) When $N = \lfloor \overline{N} \rfloor = 36$	Fraction Size Dose (Gy) When $N = \lceil \underline{N} \rceil = 37$
Min. Tumor	74.4	≥2	N≤37	2.07	2.01
Min. PTV2	72.4	≥2	**N≤36**	2.01	**1.96**
Max. Right Lung	76.0	≤2.1	**N≥37**	**2.11**	2.05

Notation: $\overline{N}$ (not necessarily integer) denotes the maximum number of fractions dividing all the targets' doses by their fraction size limit, and $\underline{N}$ (not necessarily integer) denotes the minimum number of fractions dividing all the healthy tissues' doses by their fraction size limit. PTV2 represents the secondary target.

2.4.2 Re-scaling to Achieve Feasibility

When N satisfying the integrality condition and $\lceil \underline{N} \rceil \le N \le \lfloor \overline{N} \rfloor$ cannot be found, the dose distribution can always be rescaled down on all plan intensities in order to get an N satisfying fraction size limits.

Proposition: It is always possible to find a rescaling factor r^* to achieve a feasible division of the treatment plans solving the ratio model.

Proof: Since $\overline{N}$ and $\underline{N}$ are within an integer bracket, it is always possible to find $0 < r^* \le 1$ that rescales $\underline{N}(1 - r^*)$ to $\lfloor \overline{N} \rfloor$ where $r^* = 1 - \lfloor \overline{N} \rfloor / \underline{N}$. Given $\overline{N} \ge \underline{N}$, rescaling $\overline{N}$ by r^* and rounding it down will give $\lfloor \overline{N} \rfloor$. Therefore, by rescaling doses down by $1 - \lfloor \overline{N} \rfloor / \underline{N}$, the treatment plan can always be divided into $\lfloor \overline{N} \rfloor$ feasible fractions. ■

Note that rescaling doses down may violate the minimum cumulative dose limit on the secondary target if $l_{sec}^{total} / l_{sec}^{daily}$ is fractional and the cumulative dose constraint on the secondary target (constraint set (2.5)) is active in the optimization implying $s_{min} = l_{sec}^{total}$. In order to avoid this violation, one can re-optimize the treatment plan by adding the fraction size dose (l_{sec}^{daily}) to the minimum cumulative dose limit on that tissue and then rescaling the dose distribution.

The effects of rescaling are demonstrated in Figure 2.1 by using the results in Table 2.3. Figure 2.1 shows the minimum doses the tumor and secondary target PTV2 receives and the maximum dose the right lung receives before and after rescaling. It also displays the bounds on the number of fractions to feasibly divide the corresponding doses. In this example, recall that $\overline{N} = \underline{N} = 36.2$, so the treatment plan cannot be divided more than 36 and less than 37 fractions. The rescaling factor is computed as r^*=0.005=1-(36/36.2). Rescaling the doses down by 0.5% allows treatment plan to be divided in 36 fractions.

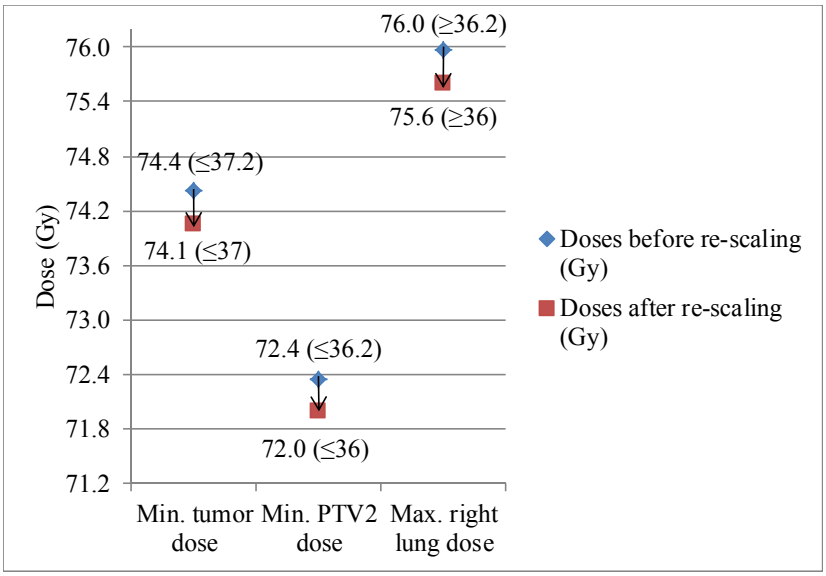

Figure 2.1: Rescaling Dose Distribution Received by Solving the Ratio Model (The bounds on the number of fractions into which the doses can be divided without violating fraction size requirement are given in the parenthesis. PTV2 represents the secondary target.)

2.5 Uniform Fractionation Model: Optimization Including Integer Fractionation Constraints

A single integer variable mixed-integer linear programming (MILP) model can be developed which generates higher quality treatment plans while explicitly satisfying the fraction size dose limits. The underlying concepts for this *uniform fractionation model* were first developed by Dink in 2005 and Dink *et al*. in 2011. The model maximizes the average tumor dose objective (2.2) subject to the overall treatment constraint sets (2.3) through (2.7) and the integer fractionation constraint sets (2.16) through (2.18) given below. Constraint sets (2.16) through (2.18) impose lower dose limits on the secondary target and tumor points, and the upper dose limits on all healthy tissue points for the N fractions in the plan. Here, N is an integer variable

and defined as the number of fractions in the plan. These integer fractionation constraints ensure that the plan can be delivered in N equal, feasible fractions.

$$d_i \geq l_{sec}^{daily} \times N \qquad \forall i \in S \tag{2.16}$$

$$d_i \geq l_{tumor}^{daily} \times N \qquad \forall i \in T \tag{2.17}$$

$$d_i \leq u_k^{daily} \times N \qquad \forall k \in K \cup \overline{K}, \forall i \in H_k \tag{2.18}$$

Figure 2.2 compares the average tumor doses obtained by solving the uniform fractionation model and the rescaled solution for the lung test case. The uniform fractionation model improves the average tumor dose of 75.9 Gy received from the rescaled solution to 76.2 Gy corresponding to a 0.3 Gy increase. These computational results illustrate the mathematical fact that the rescaled solution cannot be better than the optimal solution received from the uniform fractionation model, because the ratio solution is in the feasible space for the uniform fractionation model. In addition to offering the opportunity to produce better solutions, solving the uniform fractionation model will yield an optimal fractionation in every case if there is any.

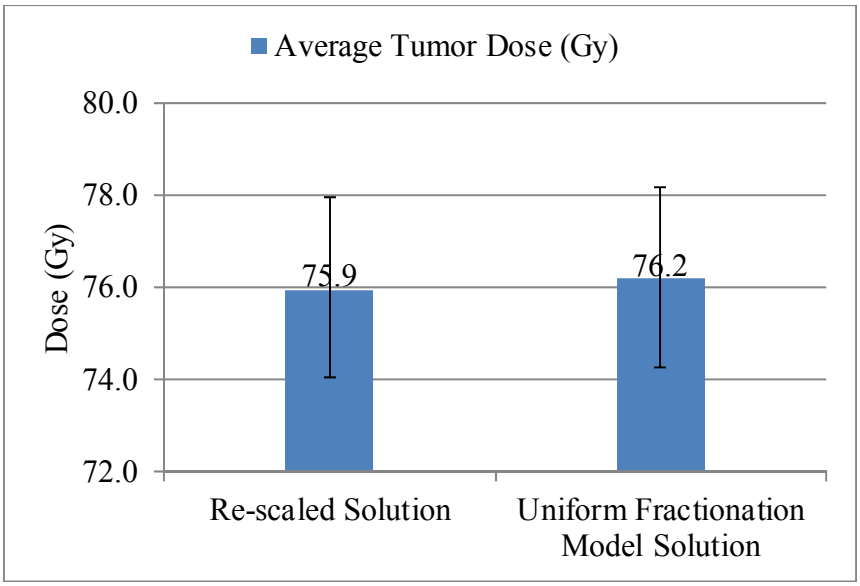

Figure 2.2: Rescaled Solution vs. Uniform Fractionation Model Solution (The minimum and maximum doses delivered to the tumor are shown with lower and upper bar on the columns, respectively.)

Although small in these results, the difference between the rescaled solution and the uniform fractionation model solution could worsen as the doses are rescaled down by a higher rescaling factor. Table 2.4 shows the highest possible values of $r = 1 - \lfloor \overline{N} \rfloor / \underline{N}$ for different values of $\lfloor \overline{N} \rfloor$. In this table, $\underline{N}$ is kept very close to $\lfloor \overline{N} \rfloor + 1$ in order to get an upper bound. As this table shows, the doses could be rescaled down significantly as the treatment plan is optimized on fewer fractions. For instance, for values of $\lfloor \overline{N} \rfloor <= 18$, the dose distribution could be rescaled down by more than 5% possibly causing the solution to perform significantly worse compared to the uniform fractionation model solution. As a result, solving the uniform fractionation model can be more beneficial when clinical conditions, such as using tighter cumulative dose limits on healthy

tissues or using higher fraction size limits, requires the treatment plan to be delivered in fewer fractions.

Table 2.4: Highest Possible Values of Re-scaling Factor (r) for Different $\lfloor \overline{N} \rfloor$

$\lfloor \overline{N} \rfloor$	$\underline{N}$	$r = 1 - \lfloor \overline{N} \rfloor / \underline{N}$
40	40.999	0.024
30	30.999	0.032
20	20.999	0.048
18	18.999	0.053
10	10.999	0.091
5	5.999	0.167
2	2.999	0.333

Notation: $\overline{N}$ (not necessarily integer) denotes the maximum number of fractions dividing all the targets' doses by their fraction size limit, and $\underline{N}$ (not necessarily integer) denotes the minimum number of fractions dividing all the healthy tissues' doses by their fraction size limit.

3 The Fractionation Challenge in Adaptive IMRT Planning

3.1 Background

Chapter 2 addressed the challenges that may arise in developing one cumulative plan (with secondary targets) and constraining or adjusting it to satisfy per fraction constraints. Still, the current standard practice of developing only one cumulative plan (without the secondary targets) at the onset of treatment often results in planned dose to primary target higher than that planned for any healthy tissue, and the minimum fraction dose for tumor slightly less than that of normal tissues. Then an integer number of equal fractions can easily be chosen to divide the overall treatment into feasible fractions and implicitly enforce per-fraction limits.

However, as the geometrical conditions change in adaptive planning, e.g. due to tumor shrinkage/growth (Kupelian *et al*., 2005; Siker *et al.*, 2006; Ramsey *et al.*, 2006; Underberg *et al.*, 2006; Bosmans *et al.*, 2006; Haasbek *et al.*, 2007) or inter-fractional motion (Yan and Lockman, 2001; Yan *et al.*, 2005), a normal tissue which would have satisfied its bound with slack in the initial plan is now pushed closer to its limit in the re-optimized plan. This creates a circumstance where the conditions for equal division of the adapted plan into fractions can no longer be satisfied easily.

This chapter demonstrates the problem of fractionating the adaptive plans by using another lung case simulating real practice. The optimization model is formulated as a linear programming formulation which is a mathematical representation of the prescription. The plan is first optimized over the entire set of cumulative constraints and delivered for the first sub-sequence of fractions (Epoch 1). Here, *epoch* defines a subsequence of fractions delivered as part of the

adaptive plan. After subtracting the delivered doses from the cumulative limits, the treatment plans are re-optimized partway through treatment in response to the changes in the tumor geometry. The challenge of fractionating the re-optimized plan is demonstrated by computational experiments performed with varying mean dose limit on both lungs and implicit minimum tumor fraction size dose limits.

3.2 Description of the Lung1 Test Case

This section describes the second lung test case treated here, referred as "Lung1", which is used in the computational experiments in Chapter 3 and 4. The points for optimization were distributed throughout the contours, determined randomly within each structure volume for computation efficiency rather than employing a uniform point set. They were more highly concentrated within the target and the critical structures of interest (Morrill *et al*., 1990; Niemierko and Goitein, 1990; Lu and Chin, 1993; Niemierko and Goitein, 1993; Acosta *et al*., 2009). Number of sample points used (the mean distance to the nearest neighbor point) is 683 (0.25 cm) for primary target PTV1, 95 (0.32 cm) for the esophagus, 400 (0.57 cm) for the heart, 500 (0.73 cm) on each of the lungs, 369 (0.21 cm) for spinal cord, and 2,580 (0.65 cm) for the Not Otherwise Specified tissue. The influence matrix of a_{ij} was calculated by using the standard radiation therapy software GRATIS (Sherouse Systems Inc.). For this test case, 9 co-planar beam angles are used, spaced at intervals of 40° within the range of 20°-340°.

Table 3.1 shows the prescription used in the computational experiments with the lung test case. The table presents both cumulative dose objectives and fraction size dose limits for the target and healthy tissues in the prescription. All of the points in each structure are subject to its

corresponding fraction size limit. Multiple values are shown for some structures varied in experiments to be reported below.

Table 3.1: Prescription for the Lung1 Test Case

Structure	Cumulative Dose Objective (Gy)	Fraction Size Dose Limit (Gy)
Primary Target (PTV1)	Maximize avg. dose	≥ 1.8, 1.9, 2.0
	$\frac{\text{min. tumor dose}}{\text{max. tumor dose}} \geq 0.95$	
Right Lung	Mean dose ≤ 20, 22, 25	≤ 2.1
Left Lung	Mean dose ≤ 20, 22, 25	≤ 2.1
Heart	Mean dose ≤ 35	≤ 2.1
Esophagus	Mean dose ≤ 35	≤ 2.1
Not Otherwise Specified Tissue	100% ≤ 100	≤ 2.1
Spinal Cord	100% ≤ 45	≤ 2.1

Note: PTV1 represents the planning target volume.

3.3 Adaptive Planning Optimization

The adaptive planning optimization approach taken in this study pursues the following steps. First, the LP-formulation presented in Section 2.3.1 is solved over all cumulative constraints. Then, an integer upper bound ($\overline{N}$) and an integer lower bound ($\underline{N}$) on the number of fractions (N) are computed. Upper limit $\overline{N}$ is calculated as the maximum number of fractions into which the tumor dose can be divided without violating fraction size requirement l_{tumor}^{daily}, i.e. $\lfloor D_{min} / l_{tumor}^{daily} \rfloor$. Similarly, lower limit $\underline{N}$ reflects the minimum number of fractions into which does for all healthy tissues k can be divided while enforcing fraction size maximum u_k^{daily}, i.e. $max\{d_i / u_k^{daily} : i \in H_k, k \in K \cup \overline{K}\}$. When there is a feasible outcome with $\overline{N} \geq \underline{N}$ the treatment

plan is divided into $\overline{N}$ fractions, and the first N_1 are delivered in Epoch 1 before the patient is re-imaged.

Following the first epoch, the PTV1 volume is updated based on the tumor shrinkage information extracted from simulated re-imaging. After revising the cumulative dose limits by subtracting the delivered doses, the treatment plan is re-optimized by solving the LP-formulation against the residual cumulative dose limits that maximizes the mean dose delivered to the residual tumor. Then, Epoch 2 fraction upper bound, $\overline{N_2} = \lfloor D_{min}^{remaining} / l_{tumor}^{daily} \rfloor$ fractions are delivered during the second epoch of the treatment where $D_{min}^{remaining}$ represents the minimum tumor dose achieved in the re-optimized plan.

3.4 Results

3.4.1 Computational Experiments – Overall Plan and Epoch 1

To illustrate the fractionation problem in adaptive planning, complete plans without adaptation are first computed for a range of mean doses of the lungs and tumor fraction limits. Table 3.2 shows that the optimized plan in the beginning of the treatment can be divided into integer number of feasible fractions (N) when ≥1.8 Gy tumor fraction size requirement applies. In this case, an integer N can be found within the range between lower and upper bound on N ($31 \leq N \leq 32$ for mean dose limit 20 Gy, $34 \leq N \leq 35$ for 22 Gy, $39 \leq N \leq 40$ for 25 Gy). For varying mean dose limits of 20 Gy, 22 Gy and 25 Gy on lungs, the treatment plan is divided into 32, 35, and 40 fractions, respectively, in which all the tumor points receive fraction size doses ≥1.8 Gy and all healthy tissue points receive fraction size doses ≤2.1 Gy.

Table 3.2: Optimal Non-Adaptive Plan Results over the Entire Range of Cumulative Constraints

Mean dose limit on both lungs (Gy)	Optimal Plan Results (All the cumulative dose requirements in Table 3.1 are satisfied.)							Upper and lower bound on integer number of fractions (N)			
									Tumor fx size limit		
									≥2.0	≥1.9	≥1.8
	Min. Tumor (Gy)	Max. Right Lung (Gy)	Max. Left Lung (Gy)	Max. Heart (Gy)	Max. Esoph. (Gy)	Max. N.O.S. (Gy)	Max. Cord (Gy)	$\underline{N}$	$\overline{N}$	$\overline{N}$	$\overline{N}$
≤20	58.8	60.9	43.2	55.8	45.6	64.8	45.0	31	29	30	**32**
≤22	64.4	67.2	46.9	61.3	49.4	71.4	45.0	34	32	33	**35**
≤25	72.8	76.4	52.4	70.4	55.2	80.8	45.0	39	36	38	**40**

Notation: $\underline{N}$ is the integer lower bound on N dividing all the healthy tissues' doses into fraction sizes of ≤2.1, $\overline{N}$ is the integer upper bound on N dividing all the target doses by the assumed tumor fraction limit. "N.O.S." is the abbreviation of "Not Otherwise Specified" tissue. Number of fractions to feasibly divide each plan is indicated in bold.

Following the adaptive planning approach of Section 3.3, the first 25 of those fractions are assumed to be delivered during the first epoch. Table 3.3 shows fraction size and the Epoch 1 cumulative dose statistics that result for the structures under interest. Note that all fraction limits are satisfied.

Table 3.3: Epoch 1 Optimal Plan Results

Mean dose limit on both lungs (Gy)	Epoch 1 (first 25 fractions) Optimal Plan Results (≥1.8 Gy tumor fraction size requirement applies.)								
	Min. Tumor (Gy)	Max. Tumor (Gy)	Avg. Tumor (Gy)	Max. Right Lung (Gy)	Max. Left Lung (Gy)	Max. Heart (Gy)	Max. Esoph. (Gy)	Max. N.O.S. (Gy)	Max. Cord (Gy)
≤20	45.8 [1.83]	48.3 [1.93]	47.1 [1.89]	47.6 [1.9]	33.7 [1.35]	43.6 [1.74]	35.6 [1.43]	50.5 [2.02]	35.2 [1.41]
≤22	46.0 [1.84]	48.4 [1.94]	47.3 [1.89]	47.9 [1.92]	33.6 [1.34]	43.7 [1.75]	35.2 [1.41]	50.9 [2.04]	32.1 [1.29]
≤25	45.4 [1.82]	47.8 [1.91]	46.7 [1.87]	47.8 [1.91]	32.8 [1.31]	44 [1.76]	34.5 [1.38]	50.5 [2.02]	28.1 [1.13]

Note: Fraction size doses are given in brackets below cumulative doses. "N.O.S." is the abbreviation of "Not Otherwise Specified" tissue.

3.4.2 Computational Experiments – Adaptation and Epoch 2

For the purpose of experimentation, the tumor shrinkage is simulated where the residual tumor corresponds to the 65% of the original tumor after fraction 25 (See Section 4.4.1 for details). After delivering 25 fractions in Epoch 1, the treatment plan is re-optimized based on the updated image against residual cumulative dose limits.

Table 3.4 shows the Epoch 2 dose statistics and fraction limits obtained from re-optimization. Only statistics related to Heart and Not Otherwise Specified tissues are shown here due to their

dominant role in determining the lower bound on the integer number of fractions that the re-optimized treatment plan can be delivered into (denoted N_2).

Table 3.4: Epoch 2 Optimal Plan Results

Mean dose limit on both lungs (Gy)	Epoch 2 Optimal Plan Results (In response to the tumor geometrical changes, the treatment plan is re-optimized against the residual cumulative dose limits.)					Upper and lower bound on the number of fractions in the re-optimized plan (N_2)			
							Tumor fx size limit		
							≥2.0	≥1.9	≥1.8
	Min. Tumor (Gy)	Max. Tumor (Gy)	Mean Tumor (Gy)	Max. Heart (Gy)	Max. Not Otherwise (Gy)	$\underline{N_2}$	$\overline{N_2}$	$\overline{N_2}$	$\overline{N_2}$
≤20	14.7	20.3	17.5	18.5	20.9	10	7	7	8
≤22	21.6	27.7	24.6	24.7	28.7	14	10	11	11
≤25	32.3	38.9	35.6	32.8	41.9	20	16	17	17

The cases show that the adapted plan in Epoch 2 using only cumulative constraints can only be divided into fractions satisfying tumor fraction size requirements at the price of violating the fraction size dose limits of some healthy tissue structures. Similarly, the adapted plan can be divided into fractions where all healthy tissue fraction size dose limits are satisfied without the tumor fraction size limit being satisfied. No number of fractions meets all requirements.

These violations are displayed in Figure 3.1(a-c) for different mean dose limits on each lung. For example, for mean dose limit 20 Gy, the adapted plan can be divided into 7 fractions satisfying ≥2 Gy tumor fraction size requirement while violating the ≤2.1 Gy requirement on Heart and Not Otherwise Specified tissue (2.64 Gy ≥ 2.1 Gy for Heart, 2.99 Gy ≥ 2.1 Gy for Not Otherwise Specified tissue). These plots illustrate that as the tumor fraction size requirement is relaxed from

≥2 Gy to ≥1.8 Gy, the ≤2.1 Gy requirement on Heart and Not Otherwise Specified tissues are less violated, but not fully satisfied.

Figure 3.1(a-c) also presents the number of fractions into which the adapted treatment plan can be divided in order to satisfy all the healthy tissue fraction size requirements. However, this causes tumor to be significantly underdosed (1.47 Gy minimum dose for mean dose limit 20 Gy, 1.54 Gy minimum dose for 22 Gy, and 1.62 Gy minimum dose for 25 Gy).

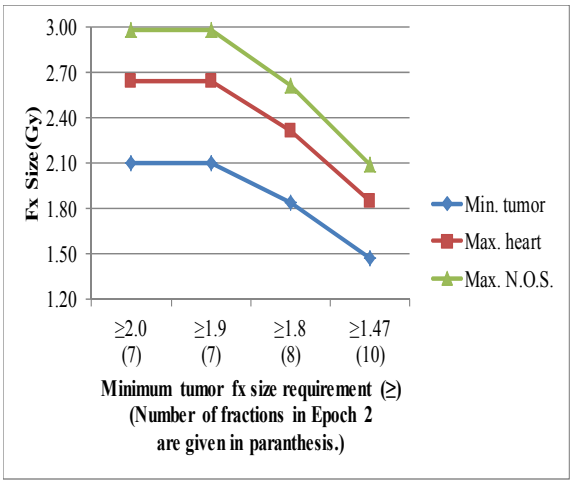

(a)

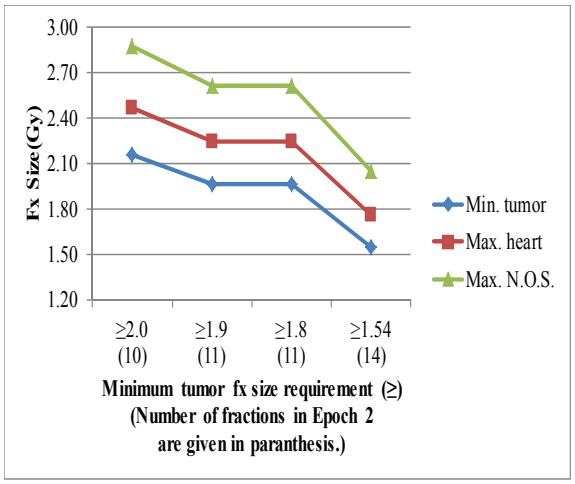

(b)

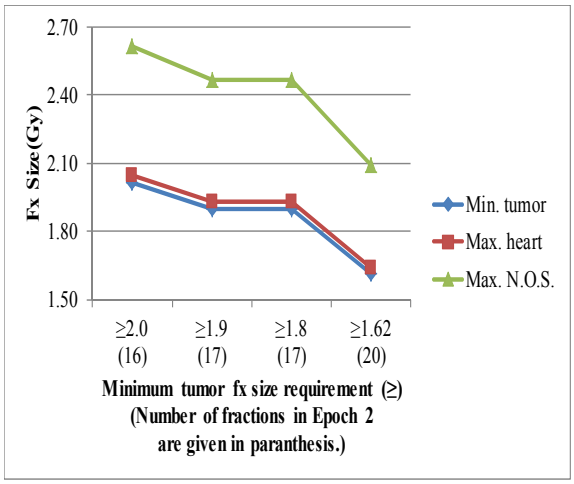

(c)

Figure 3.1: Sensitivity of Healthy Tissue and Target Fraction Size (fx) Doses in Epoch 2 (a) For Mean Dose Limit on Both Lungs 20 Gy (b) For Mean Dose Limit on Both Lungs 22 Gy (c) For Mean Dose Limit on Both Lungs 25 Gy ("NOS" is the abbreviation of "Not Otherwise Specified" tissue.)

3.4.3 Computational Experiments – Potential Gains with Adaptation

Although the above treatment plans generated by adaptation are not feasible due to the lack of fractionation in the second epoch, they are compared against plans generated by no adaptation in Table 3.2 to assess the gains that could be realized from adaptive planning. Figure 3.2 summarizes the mean tumor doses delivered to the tumor by no adaptation (Table 3.2) versus two-epoch adaptation (Epoch 1 in Table 3.3 and Epoch 2 in Table 3.4) for varying mean dose limits on the lungs. Here, ≥1.8 Gy tumor fraction size requirement is enforced in delivering Epoch 1. Adapting the treatment plan boosts the mean tumor dose from 60.3 Gy to 64.7 Gy for mean dose limit 20 Gy, from 66.2 Gy to 71.9 Gy for 22 Gy, and from 74.6 Gy to 82.2 Gy for 25 Gy. These improvements correspond to a 7% to 10% gain in the doses delivered to the tumor.

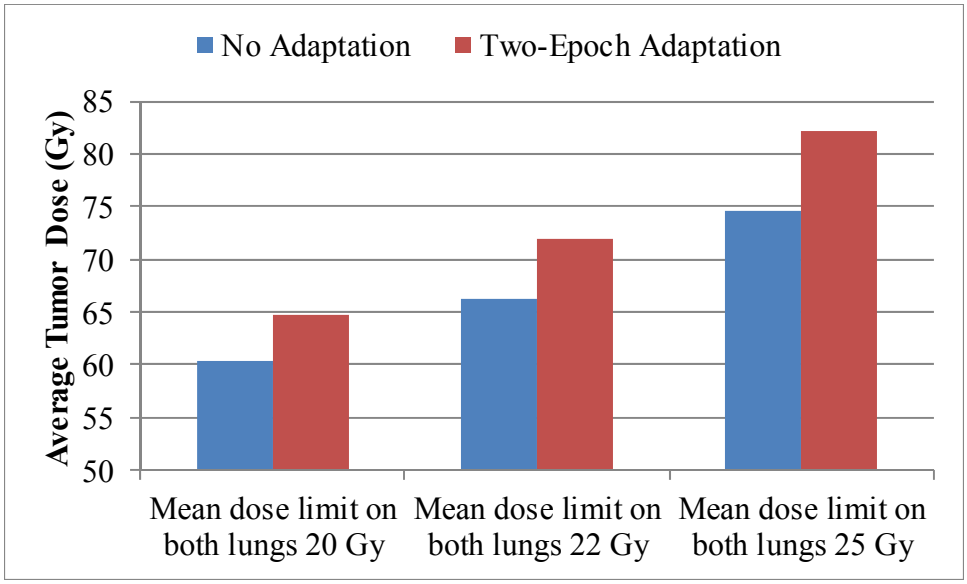

Figure 3.2: Average Tumor Doses Received by No Adaptation vs. Two-Epoch Adaptation

3.5 Discussions

Chapter 3 addresses the problem of fractionation in the adaptive planning context. As a consequence of solely taking cumulative dose objectives into account in the treatment planning

optimization, plans re-optimized in response to the changes in the geometrical conditions can provide dose distributions that do not allow the adapted plan to be divided into fractions satisfying both the minimum fraction size requirement placed on tumor (e.g. ≥1.8 Gy) and the maximum fraction size requirement placed on healthy tissues (≤2.1 Gy). In this case, the practitioners must take the approach of relaxing the fraction size dose requirements in order to achieve a least violated fractionation plan which would likely reduce the efficacy of the overall treatment plan.

Specifically, the fractionation challenge is illustrated above by using a lung test case simulating real practice. Treatment plans are re-optimized partway through treatment by incorporating the latest tumor shrinkage information. With the re-optimization in the experiments, structures Heart and Not Otherwise Specified receive more dose relative to the tumor which does not allow feasible fractionation of the adapted plan. The minimum number of fractions required for healthy tissue doses to be given in fraction sizes below 2.1 Gy is significantly higher than the maximum number of fractions that the tumor dose distribution can be given without falling below about 1.8 Gy (Table 3.4). When the adapted plans are divided, the violations of healthy tissue fraction sizes doses can be as significant as 3 Gy per fraction whereas the tumor fraction size doses can fall down to 1.47 Gy (Figure 3.1(a-c)).

The fractionation challenge investigated in this study motivates devising methodologies that simultaneously re-optimize treatment plans against both cumulative and fraction size dose limits in adaptive plans with two or more epochs. Although the gain obtained from adaptation (Figure 3.2) might reduce as the fraction size limits are explicitly enforced in the re-optimization,

simultaneous methods would allow the feasible division of the adapted plans; therefore, increasing the effectiveness of the treatment delivered.

4 Adaptive IMRT Planning Optimization with Changing Tumor Geometry and Fraction Size Limits

Adaptive planning responds to the changes in the tumor geometry throughout the treatment and demands both cumulative and fraction size limits on tissues be satisfied together. The changes in the tumor geometry between fractions known as *inter-fractional* changes happen mostly in two forms: (1) the change in the position/shape of the tumor due to inter-fraction motion, e.g. positional change of the prostate tumor due to how much the bladder/rectum is filled on the particular day (Yan and Lockman, 2001; Yan *et al.*, 2005), (2) the change in the tumor size, e.g. tumor shrinkage/growth in lung cases (Kupelian *et al*., 2005; Siker *et al.*, 2006; Ramsey *et al.*, 2006; Underberg *et al.*, 2006; Bosmans *et al.*, 2006; Haasbek *et al.*, 2007). These inter-fractional changes can be captured by the updated images acquired through the treatment and incorporated into the planning to update the remaining plan accordingly.

In this study, the change in the tumor size/shape, specifically *tumor shrinkage* information over time, is taken into account to adapt the treatment plan. This chapter develops a promising adaptive planning optimization methodology which re-optimizes the treatment plan against both cumulative and fraction size dose constraints after delivering each epoch by incorporating the latest tumor shrinkage information. In re-optimizing the treatment plan at each adaptation point, a mixed-integer linear programming (MILP) formulation is solved; therefore, a series of MILPs will be solved in the proposed methodology to adapt the plan periodically.

The adaptive treatment plans computed by the developed optimization methodology are compared with the treatment plans generated without adaptation (*non-adaptive*) by using the two

realistic Lung test cases described in Section 2.1 ("CERRLung") and Section 3.2 ("Lung1"). The prescription in Table 1.1 is used for CERRLung case whereas the prescription in Table 3.1 is used for Lung1 case. Note that the secondary target PTV2 is included in the Lung1 case with the same prescription in Table 1.1, and ≥2Gy fraction size requirement for tumor and mean dose limit of 25 Gy is used for both lungs. The non-adaptive plans in this chapter are generated by solving the uniform fractionation model presented in Section 2.5 or a non-adaptive planning optimization with boost approach explained in Section 4.4.2. The computed adaptive plans both satisfy cumulative and fraction size dose limits while improving the tumor doses.

4.1 Literature Review

The available methods used to generate radiation therapy plans optimize a single cumulative treatment plan and neglect changes in the tumor over time. Besides these non-adaptive methods, several approaches for adaptive treatment planning have been developed by operations researchers. In most of these approaches, the uncertainty in the tumor geometry caused by internal organ movements and set up-errors (random changes in the patient position) across all fractions are incorporated into the treatment planning. In order to generate IMRT plans under this uncertainty, a dynamic programming approach with practical strategies (Ferris and Voelker, 2004; Deng and Ferris, 2006), weighted power loss function approach calculating the ideal spatial dose distribution (Sir *et al.*, 2006), and a probabilistic model achieving robust optimization (Chu *et al.*, 2005) have been presented.

Recently, in the medical world, the reimaging of gross tumor boundaries over time has been introduced into the clinic. Devices now widely available allow periodic CTs to be performed on

the treatment couch (using cone beam or rail methods) and cross registered using fiducial markers against the planning CT (Wiersma *et al.*, 2007). The first image guided therapies in radiation accommodated rigid change in geometry by moving the treatment couch in space, a technique now widely implemented to "adapt" to a rigid shift of the body or target over time (Wu *et al.*, 2006). More sophisticated re-optimizations over the course of treatment based on observed change in shape have now been examined. Many set a goal of minimizing the difference between the initially intended and the final achieved dose distributions; linear programming proved desirable for its speed and promise of optimality (Wu *et al.*, 2008). A broader extension considers re-optimizations on the underlying tissue constraints rather than simply matching to the original plan when structure outlines are found to have changed (Wu *et al.*, 2002). The advent of a commercial system ("Planned Adaptive" marketed by Tomotherapy of Madison, WI) that captures physical change over the course of treatment replans using cumulative doses, and is linked to a reproducible system for delivery that has established the concept of adaptive radiation therapy in the minds of oncologists as a tool by which gains in tumor control can be achieved (Woodford *et al.*, 2007).

None of these adaptive approaches have succeeded in optimizing against both cumulative dose limits and dose limits placed on each fraction. This deficit may have slowed their adoption into regular practice, but increased use is expected as the technology becomes increasingly familiar, pitfalls are identified, and workarounds are devised to satisfy fraction size rules even at the price of diminishing the potential gains from the adaptive strategy. This chapter aims to help meet this deficit by developing an adaptive planning approach that re-optimizes the treatment plan against both cumulative dose limits and dose limits placed on each fraction simultaneously when it can

be productive to do so. A paper on the proposed adaptive planning approach has recently been accepted for publication (Saka *et al*., 2011).

4.2 Uniform and Non-Uniform Fractionation Model and Rationale

The uniform fractionation model described in Section 2.5 produces a single uniform plan across all fractions. One could propose improving the average tumor dose received from uniform fractionation by splitting the treatment plan into two stages where different plans would be used for each stage. *Stage* defines a subsequence of fractions delivered as part of a non-adaptive plan. That is, no changes in geometry are taken into account.

4.2.1 Non-Uniform Fractionation Model with Two-Stage Optimization

The non-uniform fractionation model is developed to optimize the treatment plan over two stages where new beamlet intensities for each stage are defined. Let x_j^1 and x_j^2 be intensities assigned to beamlet $j \in J$ during stage 1 and 2, respectively. The total dose delivered to point *i* during the first stage is denoted as d_i^1 and equal to $\sum_{j \in J} a_{ij} x_j^1$. Similarly, d_i^2 denotes the total dose delivered to point *i* during the second stage and equal to $\sum_{j \in J} a_{ij} x_j^2$.

Table 4.1 presents this non-uniform fractionation model for two-stage optimization. It maximizes the average dose delivered to the tumor over two stages. Constraint sets (4.1) through (4.5) are the overall treatment constraints imposed over two stages and have the same nature as the constraint sets (2.3) through (2.7) presented previously in Section 2.3.1. Constraint sets (4.6) through (4.8) impose lower dose limits on the secondary target and tumor points, and the upper

dose limits on all healthy tissue points for the N_1 fractions in the first stage. These integer fractionation constraints guarantee that the treatment plan in Stage 1 is delivered in uniform, feasible fractions. Here, N_1 is a choice for the number of equal fractions employed in the first stage. For instance, if the treatment plan is split after fraction 10, then N_1 is equal to 10.

For the plan delivered in the second stage, an integer variable N_2 defines the number of fractions given during the second stage. Constraint sets (4.9) through (4.11) impose lower dose limits on the secondary target and tumor points, and the upper dose limits on all healthy tissue points for the N_2 fractions in the first stage. These constraints guarantee that the plan delivered in second stage can be divided in N_2 uniform, feasible fractions.

Table 4.1: Non-Uniform Fractionation Model for Two-Stage Optimization

Objective and the Overall Treatment Constraints		
maximize $\left(\sum_{i\in T} d_i^1 + d_i^2\right) / \lvert T \rvert$		
$\sum_{i\in H_k} d_i^1 + d_i^2 \le \lvert H_k \rvert \mu_k$	$\forall k \in \overline{K}$	(4.1)
$d_i^1 + d_i^2 \le u_k^{total}$	$\forall k \in K, \forall i \in H_k$	(4.2)
$d_i^1 + d_i^2 \ge l_{sec}^{total}$	$\forall i \in S$	(4.3)
$d_i^1 + d_i^2 \le \frac{D_{min}}{\alpha}$	$\forall i \in S$	(4.4)
$D_{min} \le d_i^1 + d_i^2 \le \frac{D_{min}}{\alpha}$	$\forall i \in T$	(4.5)

Integer Fractionation Constraints for Stage 1			Integer Fractionation Constraints for Stage 2		
$d_i^1 \ge l_{sec}^{daily} \times N_1$	$\forall i \in S$	(4.6)	$d_i^2 \ge l_{sec}^{daily} \times N_2$	$\forall i \in S$	(4.9)
$d_i^1 \ge l_{tumor}^{daily} \times N_1$	$\forall i \in T$	(4.7)	$d_i^2 \ge l_{tumor}^{daily} \times N_2$	$\forall i \in T$	(4.10)
$d_i^1 \le u_k^{daily} \times N_1$	$\forall k \in K \cup \overline{K}, \forall i \in H_k$	(4.8)	$d_i^2 \le u_k^{daily} \times N_2$	$\forall k \in K \cup \overline{K}, \forall i \in H_k$	(4.11)

4.2.2 Rationale for Non-Uniform Fractionation in Adaptive Planning

Unless the treatment environment such as the patient geometry, the selected beam angles or the optimization parameters changes, this research found that it does not help to split the course of the treatment and deliver non-uniform fraction plans. This finding is proven by the following lemmas and stated as a theorem at the end.

Let x^1 and x^2 vectors of $|J|$ size where their components correspond to variables x_j^1 and x_j^2 for $j \in J$, respectively. Let x be a vector of $|J|$ size where its components correspond to variables x_j for $j \in J$.

Lemma 1: Any feasible solution (x^1, x^2, N_2) for non-uniform fractionation model can be mapped to a feasible solution (x, N) for uniform fractionation model by using $x \leftarrow x^1 + x^2$ and $N \leftarrow N_1 + N_2$, and their objective function values are same.

Proof: Since (x^1, x^2, N_2) is a feasible solution for non-uniform fractionation model, it satisfies the overall treatment constraint sets (4.1) through (4.5). Then, re-writing $d_i^1 + d_i^2$ in those constraint sets by using expression (4.12), $x \leftarrow x^1 + x^2$ satisfies them, and they are same as the overall treatment constraint sets (2.3) through (2.7) of the uniform fractionation model in Section 2.5. Therefore, (x, N) satisfies the overall treatment constraints in uniform fractionation model.

$$d_i^1 + d_i^2 = \sum_{j \in J} a_{ij} x_j^1 + \sum_{j \in J} a_{ij} x_j^2 = \sum_{j \in J} a_{ij} x_j^1 + a_{ij} x_j^2 = \sum_{j \in J} a_{ij} \left(x_j^1 + x_j^2 \right) = \sum_{j \in J} a_{ij} x_j = d_i \tag{4.12}$$

As part of the feasibility, (x^1, x^2, N_2) also satisfies the integer fractionation constraints for each stage. Adding integer fractionation constraint sets across two stages for each tissue and using the

same expression (4.12) to re-write those three added inequalities, $x \leftarrow x_1 + x^2$ satisfies them where $N \leftarrow N_1 + N_2$. These inequalities are the same as the fractionation constraint sets (2.16) through (2.18) in uniform fractionation model in Section 2.5. Therefore, (x, N) satisfies the fractionation constraints in uniform fractionation model.

Since (x, N) satisfies both overall treatment and integer fractionation constraints in uniform fractionation model, it is a feasible solution. Its objective function is equal to the objective function of (x^1, x^2, N_2), because re-writing the objective function of (x^1, x^2, N_2) which is $\left(\sum_{i \in T} d_i^1 + d_i^2\right) / |T|$ by using expression (4.12) , the objective function of (x, N) which is $\left(\sum_{i \in T} d_i\right) / |T|$ is obtained. ■

Lemma 2: Any feasible solution (x, N) for uniform fractionation model can be mapped to a feasible solution (x^1, x^2, N_2) for non-uniform fractionation model by using $x^1 \leftarrow \frac{N_1}{N} x, x^2 \leftarrow \frac{N_2}{N} x$ and $N_2 \leftarrow N - N_1$, and their objective function values are same.

Proof: Since (x, N) is feasible for uniform fractionation model, it satisfies the cumulative dose constraint sets (2.3) through (2.7) and integer fraction size dose constraint sets (2.16) through (2.18). When those constraints are re-written by using expression (4.13), $x^1 \leftarrow \frac{N_1}{N} x$ and $x^2 \leftarrow \frac{N_2}{N} x$ where $N_2 \leftarrow N - N_1$ satisfy those constraints which are identical to the constraints in

non-uniform fractionation model. Therefore, $\left(x^1, x^2, N_2\right)$ is a feasible solution for the non-uniform fractionation model.

$$d_i = \sum_{j \in J} a_{ij} x_j = \sum_{j \in J} a_{ij} \left(\frac{N_1}{N} x_j + \frac{N - N_1}{N} x_j \right) = \sum_{j \in J} a_{ij} \left(\frac{N_1}{N} x_j \right) + \sum_{j \in J} a_{ij} \left(\frac{N_2}{N} x_j \right) = \sum_{j \in J} a_{ij} x_j^1 + \sum_{j \in J} a_{ij} x_j^2 = d_i^1 + d_i^2 \qquad (4.13)$$

The objective function of $\left(x^1, x^2, N_2\right)$ is equal to the objective function of (x, N), because by re-writing $\left(\sum_{i \in T} d_i\right) / |T|$ using expression (4.13), the objective function $\left(\sum_{i \in T} d_i^1 + d_i^2\right) / |T|$ is received. ■

Theorem: The optimal solution values for uniform and non-uniform models are equivalent in the sense that the optimal solution to either model can be converted to a feasible solution of other with the same objective function value.

Proof: Without loss of generality, pick up the optimal solution for non-uniform fractionation model. By using Lemma 1, this optimal solution can be mapped to a feasible solution for uniform fractionation model with the same objective function value. Suppose there is a better solution for uniform fractionation model than this feasible solution. Then, by Lemma 2, it could be mapped back to a feasible solution with the same objective function value for non-uniform fractionation model which would have a higher objective function value than the optimal solution which creates a contradiction. Therefore, by contradiction, the feasible solution for uniform fractionation model mapped from the optimal solution for non-uniform fractionation model is optimal for the uniform fractionation model. ■

Note that by induction any use of non-uniform plans across multiple stages over the course of the treatment would not help the tumor doses received from delivering uniform plan across all

fractions unless something in the treatment environment changes such as the patient geometry, the selected beam angles or the optimization parameters changes. However, there is a potential value for re-optimizing the treatment plan over time and producing time-varying plans when the treatment environment changes. This justifies the idea of adapting treatment plans over the course of the treatment when the changes in the tumor geometry are observed.

4.3 Adaptive Planning Optimization Methodology

It is assumed that the beamlets of beam angles are pre-selected prior to the optimization. In the proposed approach, only a cumulative dose homogeneity requirement for tumor is considered. Epoch-based re-imaging is assumed, so the treatment plan is adapted after delivering each epoch. As previously stated, a mean dose limit is used for healthy tissues with dose-volume limits. Lastly, only the tumor is subject to geometrical change over the course of the treatment.

For the methodology, a few new notations are defined. Let T denote the set of *residual tumor* points having radiological evident disease through the treatment, and D denote the set of *removed tumor* points locating in tumor volume not currently radio graphically apparent as disease, but which was formerly occupied by tumor. The points in the set D are subject to the secondary target prescription.

4.3.1 Optimization Methodology

The process for the methodology is given below. The counter for the iterations is denoted as m. Let M denote the number of adaptation points throughout the treatment, so the treatment plan is

periodically adapted M times which indicates that there are $M+1$ epochs. $d_i^{delivered}$ denotes dose delivered at each tissue point and initially equal to 0 for all points.

For m = 0 to M

Acquire new image.

Update residual tumor volume by removing tumor points from the set T into the set D.

Revise the cumulative dose limits for the remaining plan according to the delivered plans.

Solve the *re-optimization formulation* to determine the immediate plan.

Deliver the fractions in the immediate plan. Update $d_i^{delivered}$ for each tissue point.

Next m

The methodology iterates $M+1$ times. The first iteration ($m=0$) occurs at the beginning of the treatment plan where no shrinkage is observed; therefore, the set T includes all the points in the original tumor while the set D is empty. In the rest of the iterations, tumor shrinkage is reflected by removing tumor points into the set D. In the methodology, each time the immediate plan is delivered, the time horizon is rolled forward by an epoch.

4.3.2 Re-optimization Formulation

At each adaptation point, the treatment plan is re-optimized by solving the formulation given in Figure 4.1. For the illustration purpose, this figure assumes that epochs $1 \ldots m$ has been delivered and the immediate plan for epoch $m+1$ will be determined. The re-optimization formulation optimizes the remaining plan against residual cumulative dose limit constraints and remaining plan fractionation constraints, and then the first N_1 optimal fractions are delivered for the

immediate plan which is labeled as a dashed rectangle in Figure 4.1. Here, N_1, a clinician defined parameter, represents the duration of the immediate plan. For example, if patient is re-imaged and the plan is updated bi-weekly, N_1=10.

Optimizing the remaining plan requires defining *one set of continuous variables* for the intensities of the beamlets in the remaining plan. Let x_j be the continuous variable defined for the intensity of beamlet $j \in J$ in the remaining plan. Then, dose delivered to point i in the remaining plan denoted as d_i is computed as $\sum_{j \in J} a_{ij} x_j$.

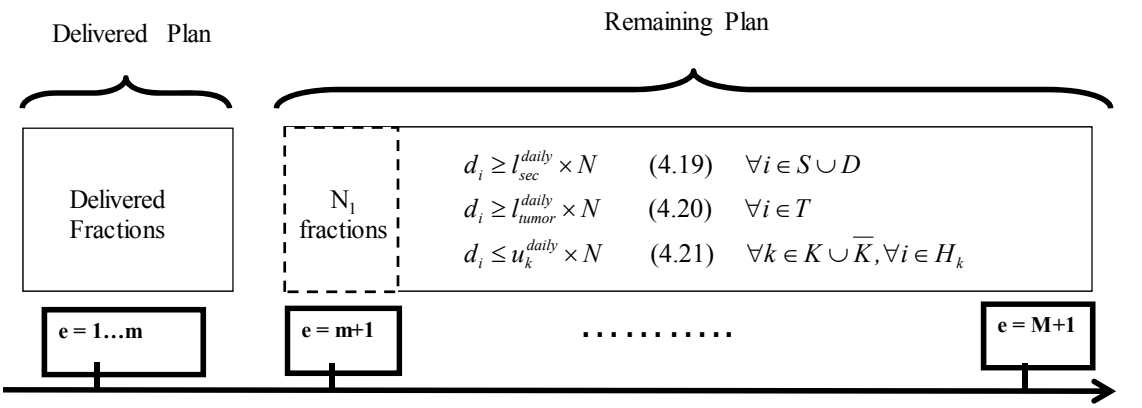

$$d_i \geq l_{sec}^{daily} \times N \quad (4.19) \quad \forall i \in S \cup D$$
$$d_i \geq l_{tumor}^{daily} \times N \quad (4.20) \quad \forall i \in T$$
$$d_i \leq u_k^{daily} \times N \quad (4.21) \quad \forall k \in K \cup \overline{K}, \forall i \in H_k$$

$$Maximize \left(\sum_{i \in T} d_i \right) / |T|$$

$$\left.\begin{array}{lll}
\sum_{i \in H_k} d_i \leq |H_k| \mu_k - \sum_{i \in H_k} d_i^{delivered} & \forall k \in \overline{K} & (4.14) \\
d_i \leq u_k^{total} - d_i^{delivered} & \forall k \in K, \forall i \in H_k & (4.15) \\
d_i \geq l_{sec}^{total} - d_i^{delivered} & \forall i \in S \cup D & (4.16) \\
d_i \leq \frac{D_{min}}{\alpha} - d_i^{delivered} & \forall i \in S \cup D & (4.17) \\
D_{min} \leq d_i + d_i^{delivered} \leq \frac{D_{min}}{\alpha} & \forall i \in T & (4.18)
\end{array}\right\} \text{Overall Treatment}$$

Figure 4.1: Re-optimization Formulation

The formulation in Figure 4.1 maximizes the average tumor dose delivered to residual tumor points $i \in T$ in the remaining plan subject to overall treatment and remaining plan fractionation

constraints. Constraint sets (4.14) through (4.18) make sure that cumulative dose limits for dose-volume healthy tissues, healthy tissues, secondary target and removed tumor points, and residual tumor points are maintained, respectively.

Constraint sets (4.19) through (4.21) impose lower dose limits on the secondary target, removed tumor and residual tumor points, and upper dose limits on healthy and dose-volume healthy tissue points for the N fractions in the remaining plan. Here, N is an integer variable and defined as the number of fractions in the remaining plan. These constraints on remaining plan ensure that the remaining plan can be delivered in N equal, feasible fractions.

At each iteration, except the last one, N_1 of these N optimal fractions are delivered in immediate plan, and the methodology moves to the next iteration. However, at the last iteration where the final adaptation occurs, all the N optimal fractions in the remaining plan are delivered in the last epoch.

In the re-optimization formulation, the immediate plan and the prospective plan (the remaining timeline after N_1 fractions) are combined into a remaining plan. It would be desired to treat them separately if the new conditions in the prospective plan were considered, e.g. further tumor shrinkage. However, this research considers the simplest case where the tumor geometry in the immediate and prospective plan is the same. It would not help the optimization results to treat them separately as a consequence of the finding stated previously. Moreover, treating them separately in this simplest case would require defining two sets of variables and two sets of fractionation constraints which would worsen the computational efficiency of the formulation.

Note that a simple relaxation of the integer variable *N* into a continuous variable may lead to infeasibility when the optimal fractional value of *N* is further rounded up or down as illustrated in Table 4.2. This motivates defining *N* as an integer variable in the re-optimization formulation.

Table 4.2: Infeasible Fractionation from Solving the LP-relaxation of the Re-optimization Formulation at the First Iteration for the Lung1 Case (Violations of fraction size requirements are in bold and highlighted.)

Structure	Dose Statistics	Cum. dose (Gy)	Fract. size dose (Gy) when *N*=34.7 is rounded down to 34	Fract. size dose (Gy) when *N*=34.7 is rounded up to 35
Tumor	Min. dose	71.3	2.10	2.04
PTV2	Min. dose	69.4	2.04	**1.98**
Right Lung	Max. dose	72.8	**2.14**	2.08
Left Lung	Max. dose	56.1	1.65	1.60
Heart	Max. dose	70.9	2.08	2.02
Esophagus	Max. dose	59.5	1.75	1.70
Not Otherwise Specified	Max. dose	72.8	**2.14**	2.08
Spinal Cord	Max. dose	45.0	1.32	1.29

Notation: N is the number of fractions the treatment plan is divided into and equal to 34.7 in the relaxation.

4.4 Computational Experiments

4.4.1 Generating Tumor Shrinkage

To test the proposed adaptive planning optimization methodology, tumor shrinkage data over time is essential. Using clinical guidance, *residual tumor volumes* on each slice that correspond to the tumor volume after delivering 25 fractions are generated. Figure 4.2 illustrates an example slice *z=0* for Lung1 case. This figure shows how the original tumor in red ("T") has shrunk to the residual tumor volume in dark blue (T*) after 25 fractions in the treatment.

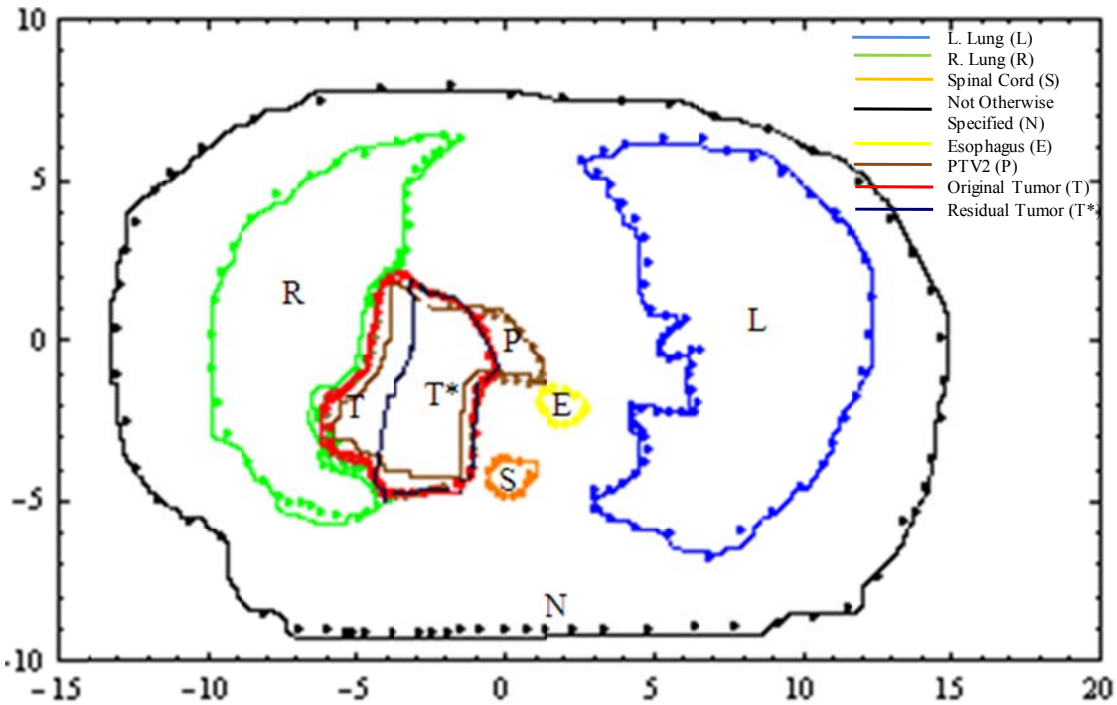

Figure 4.2: Slice z=0 for Lung1 Case

For experiments adapting the treatment plan before fraction 25, the original tumor volume is reduced with some percentage, such as 20%, 50% and 80%, to its plotted residual volume near the root of the lung. On the other hand, the residual tumor volume after fraction 25 is reduced

with some percentage, such as 10%, 30% and 50%, for the experiments where the treatment plan is adapted during the subsequent fractions after fraction 25.

4.4.2 Two-Epoch Adaptation Results

For two-epoch adaptation experiments, the treatment plans for both test cases are adapted once after fraction 25 based on the generated residual tumor volumes and compared with treatment plans generated with no adaptation (non-adaptive). When the treatment plan is adapted after fraction 25, the minimum fraction size limit constraints on the secondary target PTV2 and the removed tumor points (part of the original tumor during the first 25 fractions) are dropped from the re-optimization formulation since these points satisfy their prescribed cumulative dose limits (≥50 Gy) by receiving fraction size doses at least or greater than their required minimum limits during the first 25 fractions and there is no clinical need to deliver the minimum fraction size doses to these points during the subsequent fractions. Thus, dropping these constraints relaxes the re-optimization formulation and creates freedom.

Non-adaptive plans are first prepared by non-adaptive planning optimization without boost employed in most of the commercial products. In order to have a fuller comparison between non-adaptive and adaptive plans, a non-adaptive planning optimization with boost was also employed where the treatment plan is re-optimized after fraction 25 by dropping the fraction size limit constraints on PTV2 points without acquiring an updated image (For non-adaptive plans, "*main stage*" includes the first 25 fractions and "*boost stage*" includes fractions after re-optimization). The non-adaptive planning optimization with boost is motivated by the clinical desire to design treatments with a boosting strategy (employed in commercial systems) which uses different

uniform fractions in successive periods of treatment (Li *et al.* 2005, Popple *et al*. 2005, Dink *et al.* 2011).

Note that the uniform fractionation model presented in Section 2.5 and the ratio model with re-scaling presented in Section 2.4 are solved to prepare non-adaptive plans without boost. Adaptive plans are generated by using the proposed methodology presented in Section 4.3 where the uniform fractionation or the ratio model with re-scaling is used for re-optimization formulation. Non-adaptive plans with boost where the treatment plan is re-optimized after fraction 25 without responding to the tumor shrinkage are generated by using the same methodology. For the computational experiments presented in this chapter, all the plans for Lung1 case are computed in less than 5 minutes whereas all the plans for CERRLung case are computed in less than 30 minutes on the department's server (specifications of the machine and software are given in Section 1.4).

4.4.2.1 Using Uniform Fractionation Model in the Optimization

Table 4.3 presents results for no adaptation and two-epoch adaptation for the Lung1 and CERRLung test cases where the uniform fractionation model is solved in the optimization. Note that the tumor statistics presented throughout the computational experiments are for the whole tumor in non-adaptive plans and for the residual tumor in adaptive plans. However, due to not having adaptation, the removed tumor points are not known in the non-adaptive plans; therefore, no statistics are presented for those points.

Non-adaptive optimization without boost delivers minimum dose of 2 Gy/fraction to PTV2 points over the course of the treatment. By non-adaptive optimization with boost, the PTV2 points receive minimum dose of 0.9 Gy/fraction for Lung1 Case and minimum dose of 0.91 Gy/fraction for CERRLung case during the boost stage since the fraction size limit (≥2 Gy) on PTV2 points are not imposed in the re-optimization after fraction 25. This freedom created in non-adaptive optimization with boost improves the average tumor dose achieved in the boost epoch by 0.5 Gy for Lung1 case, so the average cumulative dose achieved by non-adaptive optimization without boost increased from 72.9 Gy to 73.4 Gy. The effect of the freedom on the optimization results is more significant in CERRLung case. Re-optimizing the treatment plan better spares the right lung by delivering average dose of 0.35 Gy/fraction after fraction 25 compared to the average dose of 0.47 Gy/fraction by non-adaptive optimization without boost. The reduction in the average dose that right lung receives allows adding 4 more fractions to the boost epoch and boosts the cumulative dose from 76.2 Gy to 84.9 Gy.

When the treatment is adapted to the tumor shrinkage after fraction 25, the right lung is better spared during the second epoch by receiving average dose of 0.6 Gy/fraction in Lung1 case and 0.31 Gy/fraction in CERRLung case compared to the 0.71 Gy/fraction and 0.35 Gy/fraction received from non-adaptive optimization with boost for both test cases, respectively. Better sparing the right lung is achieved by taking advantage of the extra freedom created in the re-optimization formulation by dropping the minimum fraction size limit constraints on the removed tumor points. The removed tumor points receive minimum dose of 0.53 Gy/fraction during the second epoch (with boost) for Lung1 case and minimum dose of 0.65 Gy/fraction for CERRLung case. However, same points are required to receive 2 Gy/fraction in non-adaptive

plans. The reduction in the average dose/fraction that the right lung receives during the second epoch allows increasing the number of fractions delivered in the second epoch from 10 to 12 for Lung1 case and from 15 to 17 for CERRLung case.

Table 4.3: No Adaptation and Two-Epoch Adaptation Results for Lung1 and CERRLung Test Cases (The uniform fractionation model is solved in optimization, bold and highlighting signifies numbers referenced in the text.)

Case Name	Structure	Statistics	No Adaptation (No Boost)		No Adaptation (with Boost)					Two-Epoch Adaptation				
			Total		Main Stage		Boost Stage		Total	Epoch 1		Epoch 2 (with Boost)		Total
			Cum. dose (Gy)	Fract. size dose (Gy)	Cum. dose (Gy)	Fract. size dose (Gy)	Cum. dose (Gy)	Fract. size dose (Gy)	Cum. dose (Gy)	Cum. dose (Gy)	Fract. size dose (Gy)	Cum. dose (Gy)	Fract. size dose (Gy)	Cum. dose (Gy)
Lung1 Case	Tumor	Max. Dose	75.0	2.14	53.6	2.14	24.3	2.43	75.3	53.6	2.14	29.6	2.47	80.5
		Min. Dose	71.3	2.04	50.9	2.04	20.0	2.00	71.6	50.9	2.04	24.0	2.00	76.5
		Avg. Dose	**72.9**	2.08	52.1	2.08	21.3	2.13	**73.4**	52.1	2.08	26.6	2.22	**78.7**
	Removed Tumor Points	Min. Dose	-	-	-	-	-	-	-	-	-	6.4	**0.53**	57.8
	PTV2	Min. Dose	70.0	**2.00**	50.0	2.00	9.0	**0.90**	59.1	50.0	2.00	6.4	0.53	56.6
	Right Lung	Avg. Dose	25.0	**0.71**	17.9	0.71	7.1	**0.71**	25.0	17.9	0.71	7.1	**0.60**	25.0
	Number of fractions given		**35**		25		**10**		**35**	25		**12**		**37**
CERRLung Case	Tumor	Max. Dose	78.2	2.17	54.3	2.17	34.9	2.33	86.9	54.3	2.17	39.0	2.30	91.0
		Min. Dose	74.3	2.06	51.6	2.06	30.0	2.0	82.5	51.6	2.06	34.0	2.0	86.4
		Avg. Dose	**76.2**	2.12	52.9	2.12	31.9	2.13	**84.9**	52.9	2.12	36.0	2.12	**88.9**
	Removed Tumor Points	Min. Dose	-	-	-	-	-	-	-	-	-	11.1	**0.65**	64.5
	PTV2	Min. Dose	72.0	**2.00**	50.0	2.00	13.7	**0.91**	63.7	50.0	2.00	4.2	0.25	54.2
	Right Lung	Avg. Dose	17.0	**0.47**	11.8	0.47	5.2	**0.35**	17.0	11.8	0.47	5.2	**0.31**	17.0
	Number of fractions given		**36**		25		**15**		**40**	25		**17**		**42**

The overall tumor dose statistics received from no adaptation and two-epoch adaptation for Lung1 case are summarized in Figure 4.3(a). Adapting the treatment plan improves the overall tumor doses significantly. It adds 2 more fractions to the overall treatment and increases the average tumor dose by 5.3 to 5.8 Gy. This corresponds to over 7% boost in the average tumor dose. Figure 4.3(b) illustrates the improvement in the overall tumor doses achieved by adaptation for CERRLung case. Compared to non-adaptive optimization without boost, 6 more fractions are delivered in the treatment plan and average dose of 12.7 Gy (17%) gain is achieved by adapting the treatment plan once. Although re-optimizing the non-adaptive plan after fraction 25 improves non-adaptive planning results significantly, two-epoch adaptation still performs superior to no adaptation. In this case, the average tumor dose is boosted from 84.9 Gy to 88.9 Gy corresponding to a 4 Gy (4.7%) increase and 2 more fractions are delivered in the treatment plan.

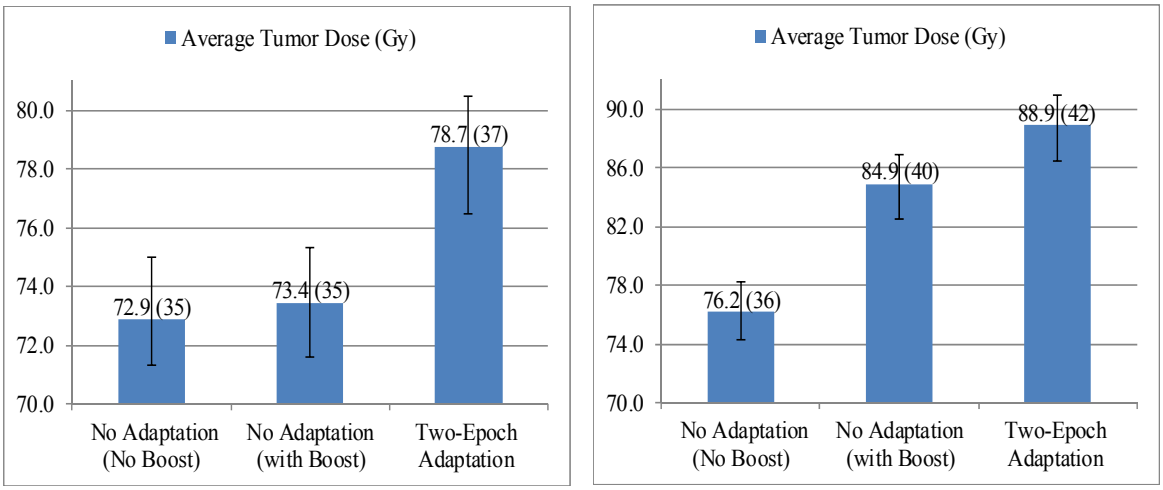

(a) Lung1 Case (b) CERRLung Case

Figure 4.3: Comparison of Overall Tumor Dose Statistics Received by No Adaptation and Two-Epoch Adaptation (Number of fractions delivered in the overall treatment given in the parenthesis, the lower and upper bar on each column showing the minimum and maximum cumulative tumor dose achieved, respectively.)

Increasing the delivered number of fractions by re-optimization in the non-adaptive plan with boost and adaptive plans may create very high hot-spots within the tumor. However, a homogeneity dose constraint is enforced in the re-optimization (constraint set (4.18) in Figure 4.1) which should prevent having very low cold-spots as well as very high hot-spots at the end of the treatment. For example, as Table 4.3 shows, two-epoch adaptation plan for CERRLung case delivers minimum and maximum tumor doses of 86.4 Gy and 91.0 Gy, respectively, which satisfies the prescribed tumor homogeneity dose limit (86.4/91.0≥0.95). As a result, enforcing tumor homogeneity dose constraint in the re-optimization imposes homogeneous tumor dose distribution to be delivered over the course of the treatment. Furthermore, an upper dose limit constraint on the removed tumor points is enforced in the re-optimization which would prevent

having very high hot-spots among the removed tumor points by ensuring that their cumulative doses do not exceed the maximum cumulative dose achieved in the tumor.

It could be desired to bound the increase in the number of fractions by re-optimization due to clinical reasons, e.g. considering adjuvant therapies, such as chemotherapy. This could be easily done in the developed methodology by adding the following constraint $N+N_{delivered} \leq U$ to the re-optimization formulation given in Figure 4.1 where $N_{delivered}$ defines the number of fractions given in the delivered plan, and U is the clinician-defined parameter for the upper bound on the number of fractions delivered in the overall treatment. Nevertheless, adding this constraint might reduce the gains in average tumor dose achieved by adaptation.

The detailed results for the computed plans on CERRLung test case given in Table 4.3 are shown in Table 4.4. Table 4.4 presents cumulative and fraction size dose statistics for each structure over each stage/epoch and the overall treatment as well as the number of fractions delivered in each time period in non-adaptive plans without or with boost and two-epoch adaptive plan. The dose statistics in Table 4.4 indicate that both cumulative and fraction size dose limits placed on each healthy tissue are satisfied in the non-adaptive and adaptive plans. For example, the right lung receives a mean dose of 17.0 Gy (≤17 Gy) in mean fraction size doses of 0.47 during 36 fractions in the non-adaptive plan without boost. During each of these fractions, the maximum dose that the right lung receives is 2.1 Gy which is in accordance with its maximum fraction size limit (≤2.1 Gy). Furthermore, the other healthy tissues satisfy their cumulative dose limits being that the mean dose that the left lung receives is 9.7 Gy (<17 Gy), the heart receives 4.2 Gy (<35 Gy), and the esophagus receives 16.8 Gy (<35 Gy). The maximum dose the not otherwise

specified tissue receives is 75.6 Gy (<100 Gy) and the spinal cord receives is 9.5 Gy (<45 Gy). These healthy tissues under interest receive fraction size doses less than or equal to their maximum fraction size limit during each fraction. Satisfaction of both the cumulative and the fraction size limits for each tissue carries over to the non-adaptive plan with boost and adaptive plans as Table 4.4 demonstrates.

Since the developed re-optimization approach is to maximize dose delivered to the tumor within cumulative and fraction size tolerance levels of healthy tissues, rather than meeting a specific prescription for the tumor, some healthy tissues are dosed to its cumulative limit (e.g. Right lung receives average cumulative dose of 17 Gy in CERRLung case). However, this approach is in accordance with clinical studies on dose escalation (c.f. van Baardwijk et al., 2008; van Baardwijk et al., 2010) and the prescribed cumulative dose limits on healthy tissues are respected in the computed adaptive plans.

The detailed dose statistics for Lung1 case are given in Appendix A. The results show that all cumulative dose limits for the overall treatment and fraction size dose limits for each stage/epoch fraction are satisfied in both non-adaptive and adaptive plans.

Table 4.4: No Adaptation vs. Two-Epoch Adaptation Results for the CERRLung Test Case (The uniform fractionation model is solved in the optimization.)

Structure	Dose Statistics (Gy)	No Adaptation (No Boost)	No Adaptation (with Boost)			Two-Epoch Adaptation		
		Total	Main Stage	Boost Stage	Total	Epoch 1	Epoch 2 (with Boost)	Total
Tumor	Max. Dose	78.2 [2.17]	54.3 [2.17]	34.9 [2.33]	86.9	54.3 [2.17]	39.0 [2.30]	91.0
	Min. Dose	74.3 [2.06]	51.6 [2.06]	30.0 [2.00]	82.5	51.6 [2.06]	34.0 [2.00]	86.4
	Mean Dose	76.2 [2.12]	52.9 [2.12]	31.9 [2.13]	84.9	52.9 [2.12]	36.0 [2.12]	88.9
Removed Tumor Points	Max. Dose	-	-	-	-	-	37.7 [2.22]	91.0
	Min. Dose	-	-	-	-	-	11.1 [0.65]	64.5
	Mean Dose	-	-	-	-	-	32.0 [1.88]	84.9
PTV2	Max. Dose	78.2 [2.17]	54.3 [2.17]	35.9 [2.39]	86.9	54.3 [2.17]	40.0 [2.35]	91.0
	Min. Dose	72.0 [2.00]	50 [2.00]	13.7 [0.91]	63.7	50 [2.00]	4.2 [0.25]	54.2
	Mean Dose	75.3 [2.09]	52.3 [2.09]	29.4 [1.96]	81.6	52.3 [2.09]	30.9 [1.81]	83.1
Right Lung	Max. Dose	75.6 [2.10]	52.5 [2.10]	31.5 [2.10]	84.0	52.5 [2.10]	35.7 [2.10]	88.2
	Mean Dose	17.0 [0.47]	11.8 [0.47]	5.2 [0.35]	17.0	11.8 [0.47]	5.2 [0.31]	17.0
Left Lung	Max. Dose	75.6 [2.10]	52.5 [2.10]	31.5 [2.10]	82.0	52.5 [2.10]	32.3 [1.90]	81.7
	Mean Dose	9.7 [0.27]	6.7 [0.27]	2.8 [0.19]	9.6	6.7 [0.27]	2.6 [0.16]	9.4
Heart	Max. Dose	72.3 [2.01]	50.2 [2.01]	25.4 [1.69]	75.6	50.2 [2.01]	20.6 [1.21]	69.7
	Mean Dose	4.2 [0.12]	2.9 [0.12]	1.0 [0.06]	3.9	2.9 [0.12]	1.0 [0.06]	4.0
Esophagus	Max. Dose	75.6 [2.10]	52.5 [2.10]	24.8 [1.65]	77.3	52.5 [2.1]	22.0 [1.29]	74.5
	Mean Dose	16.8 [0.47]	11.7 [0.47]	3.5 [0.23]	15.2	11.7 [0.47]	3.0 [0.18]	14.7
Not Otherwise Specified	Max. Dose	75.6 [2.10]	52.5 [2.10]	31.5 [2.10]	84.0	52.5 [2.10]	35.7 [2.10]	88.2
	Mean Dose	7.5 [0.21]	5.2 [0.21]	2.4 [0.16]	7.6	5.2 [0.21]	2.4 [0.14]	7.6
Spinal Cord	Max. Dose	9.5 [0.26]	6.6 [0.26]	4.5 [0.30]	10.6	6.6 [0.26]	7.2 [0.42]	12.0
	Mean Dose	1.7 [0.05]	1.2 [0.05]	0.7 [0.05]	1.9	1.2 [0.05]	0.5 [0.03]	1.7
# of Fractions Given		36	25	15	40	25	17	42

Note: The fraction size doses are given in brackets below the cumulative doses. PTV2 represents the secondary target.

4.4.2.2 Using the Ratio Model in the Optimization

Non-adaptive and adaptive treatment plans for both test cases are also generated where the ratio model is solved in the re-optimization and the results are re-scaled if necessary (Table 4.5). Note that, the freedom generated by non-adaptive planning optimization with boost over optimization without boost, and the extra freedom created by adaptation in the re-optimization, which has been explained through the results in Table 4.3, apply to the results in Table 4.5 too. For Lung1 case, doses received from the optimization in the beginning of the treatment are re-scaled down by 2% and the treatment plan is divided into 34 feasible fractions. After delivering 25 of those 34 fractions in the main stage, the re-optimization for non-adaptive planning optimization with boost allows dividing the remaining plan into at most 10 fractions to satisfy the minimum fraction size limit on the tumor and at least 11 fractions to satisfy the maximum fraction size limit on healthy tissues. The doses for the remaining plan are re-scaled down by 0.5% and the boost epoch is delivered in 10 feasible fractions. For adaptive planning optimization, the tumor volume is updated after fraction 25 and the re-optimization allows dividing the remaining treatment plan into at most 12 fractions to satisfy the minimum fraction size limit on the residual tumor and at least 13 fractions to satisfy the maximum healthy tissue fraction size limit. The doses for the remaining plan are re-scaled down by 3.7% and the second epoch is delivered in 12 feasible fractions in the adaptive planning optimization.

For CERRLung case, the doses received from the optimization in the beginning of the treatment are re-scaled down by 0.5% and the treatment plan is divided into 36 feasible fractions. In the main stage, 25 of those 36 fractions are delivered. Then, the treatment plan is re-optimized after fraction 25 for non-adaptive planning optimization with boost, and the computed doses allow

dividing the remaining plan into at most 15 and at least 16 fractions in order to satisfy the minimum and the maximum fraction size limits, respectively. These doses are re-scaled down by 5% and the remaining treatment plan is delivered in 15 feasible fractions. For the adaptive planning optimization, the doses received from the re-optimization allow dividing the remaining plan into at most 17 and at least 18 fractions. These doses are re-scaled down by 2% and 17 feasible fractions are delivered in the second epoch.

Table 4.5: No Adaptation vs. Two-Epoch Adaptation Results for Lung1 and CERRLung Test Case (Ratio model is solved in the optimization and the results are rescaled if necessary, bold and highlighting signifies numbers referenced in the text.)

Case Name	Structure	Statistics	No Adaptation (No Boost)		No Adaptation (with Boost)					Two-Epoch Adaptation				
			Total		Main Stage		Boost Stage		Total	Epoch 1		Epoch 2 (with Boost)		Total
			Cum. dose (Gy)	Fract. size dose (Gy)	Cum. dose (Gy)	Fract. size dose (Gy)	Cum. dose (Gy)	Fract. size dose (Gy)	Cum. dose (Gy)	Cum. dose (Gy)	Fract. size dose (Gy)	Cum. dose (Gy)	Fract. size dose (Gy)	Cum. dose (Gy)
Lung1 Case	Tumor	Max. Dose	73.6	2.17	54.1	2.17	22.1	2.21	75.3	54.1	2.17	28.9	2.41	80.4
		Min. Dose	69.9	2.06	51.4	2.06	20.0	2.00	71.5	51.4	2.06	24.0	2.00	76.4
		Avg. Dose	**71.6**	2.11	52.7	2.11	20.7	2.07	**73.4**	52.7	2.11	25.6	2.13	**78.3**
	Removed Tumor Points	Min. Dose	-	-	-	-	-	-	-	-	-	6.0	0.50	57.7
	PTV2	Min. Dose	68.0	2.00	50.0	2.00	9.7	0.97	59.7	50.0	2.00	6.0	0.50	56.0
	Right Lung	Avg. Dose	24.5	0.72	18.0	0.72	6.9	0.69	25.0	18.0	0.72	6.7	0.56	24.7
	Number of fractions given		**34**		25		**10**		**35**	25		**12**		**37**
CERRLung Case	Tumor	Max. Dose	78.0	2.17	54.1	2.17	34.4	2.29	86.2	54.1	2.17	38.7	2.28	90.6
		Min. Dose	74.1	2.06	51.4	2.06	30.0	2.00	81.9	51.4	2.06	34.0	2.00	86.0
		Avg. Dose	**75.9**	2.11	52.7	2.11	31.5	2.10	**84.2**	52.7	2.11	35.8	2.10	**88.5**
	Removed Tumor Points	Min. Dose	-	-	-	-	-	-	-	-	-	10.5	0.62	62.5
	PTV2	Min. Dose	72.0	2.0	50.0	2.00	12.7	0.84	62.7	50.0	2.00	3.6	0.21	53.6
	Right Lung	Avg. Dose	16.9	0.47	11.7	0.47	5.0	0.33	16.7	11.7	0.47	5.1	0.30	16.9
	Number of fractions given		**36**		25		**15**		**40**	25		**17**		**42**

Figure 4.4 compares the average tumor dose and the number of fractions delivered in non-adaptive and adaptive plans for both test cases. For Lung1 case, Figure 4.4(a) shows that adapting the treatment plan once adds 3 more fractions to the overall treatment received by optimization without boost and boosts the average tumor dose from 71.6 Gy to 78.3 Gy which corresponds to a 6.7 Gy (9.4%) increase. Compared to the non-adaptive planning optimization with boost, adaptation improves the average tumor dose from 73.4 Gy to 78.3 Gy corresponding to a 4.9 Gy (6.7%) gain while adding 2 more fractions to the overall treatment. The improvement in the treatment outcomes by adaptation is illustrated by the CERRLung case results presented in Figure 4.4(b). Adapting the treatment plan once adds 2 more fractions to the overall treatment received by non-adaptive planning optimization with boost and boosts the average tumor dose from 84.2 Gy to 88.5 Gy corresponding to a 4.3 Gy increase (5.1% gain). This gain gets significantly bigger when the adaptive planning results are compared to the optimization without boost results where the average tumor dose is boosted by 12.6 Gy (16.6%) and the number of fractions given in the treatment increased by 6.

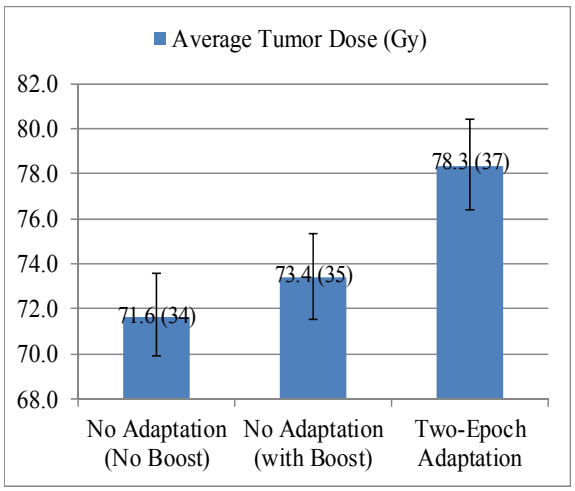

(a) Lung1 Case

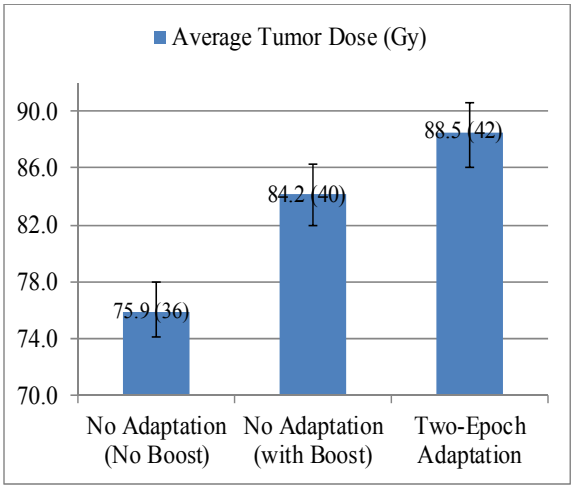

(b) CERRLung Case

Figure 4.4: Comparison of Treatment Outcomes When the Ratio Model is solved in the Optimization

The detailed dose statistics for each structure in non-adaptive and adaptive plans for Lung1 and CERRLung case are presented in Appendix B and C, respectively. The results show that both cumulative and fraction size dose limits for all structures are satisfied in the computed plans.

4.4.3 Three-Epoch Adaptation Results

It is an interesting question to investigate whether the tumor doses received from two-epoch adaptation would improve by acquiring another image of the patient and adapting the plan at some point during the first 25 fractions. In addition, the extended time in second epoch (i.e. the second epoch includes 12 and 17 fractions for Lung1 and CERRLung case, respectively, as Table 4.3 indicates) allows additional adaptation before the treatment ends.

4.4.3.1 Adapting after Fraction 10 and 25 (Earlier Re-Imaging)

Three-epoch adaptation results for Lung1 case where the treatment plan is adapted after delivering fractions 10 and 25 are summarized in Figure 4.5(a). This figure displays both the average tumor dose achieved at the end of the treatment and the number of fractions given in the treatment when the original tumor shrinks with different rates during the first 10 fractions towards the residual tumor. For the purpose of comparison, two-epoch adaptation results are given too.

Adapting the plan twice in case of 80% tumor shrinkage during the first 10 fractions only improves the two-epoch adaptation results by 0.6 Gy while the number of fractions given in the treatment does not change. This small gain diminishes when tumor shrinks with a lower rate in the first 10 fractions. As a result, adapting the treatment plan during the first 25 fractions does not improve the two-epoch adaptation results considerably and is not sensitive to the rate of tumor shrinkage.

The same conclusion is reached from three-epoch adaptation results for CERRLung case given in Figure 4.5(b). The average tumor dose achieved from two-epoch adaptation increases slightly from 88.9 Gy to 89.0 Gy under 50% and 80% shrinkage during the first 10 fractions while the number of fractions given in the treatment does not change.

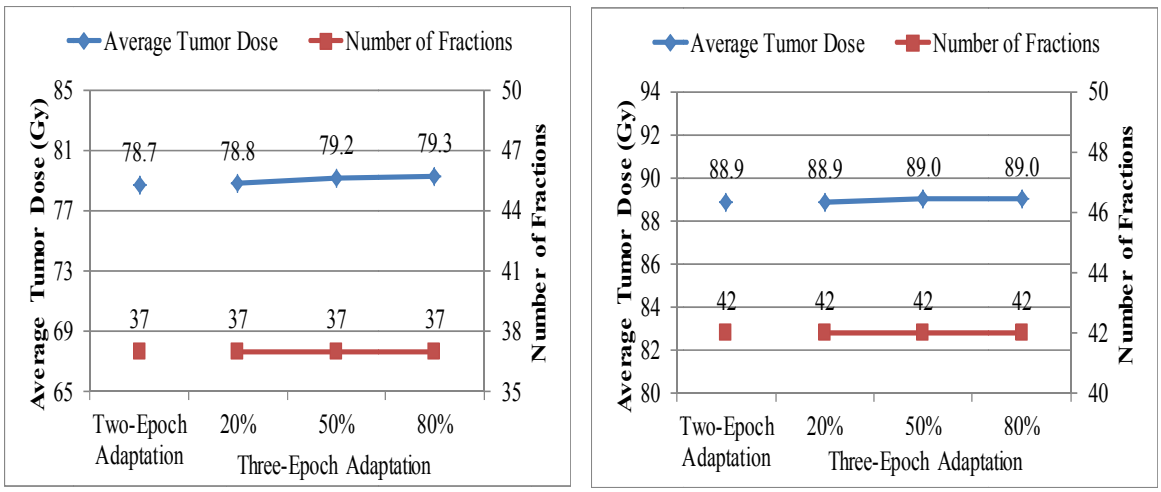

(a) Lung1 Case (b) CERRLung Case

Figure 4.5: Two-Epoch Adaptation (Adapting after Fraction 25) vs. Three-Epoch Adaptation (Adapting after Fraction 10 and 25) when the Original Tumor Shrinks with Different Rates (%) during the first 10 Fractions towards the Residual Tumor after Fraction 25 (Uniform fractionation model is solved in the re-optimization.)

The details of the experiments summarized in Figure 4.5 can be found in Appendix D and E for Lung1 and CERRLung case, respectively, which demonstrate that the targets and healthy tissues satisfy their cumulative limits for the overall treatment and fraction size limits during each fraction delivered in epoch 1, 2, and 3.

4.4.3.2 Adapting after Fraction 25 and 30 (Later Re-Imaging)

In contrast to the earlier adaptation, later adaptation performed after fraction 30 for both Lung1 and CERRLung cases improves two-epoch adaptation results significantly. Appendix F and G present the details of these experiments indicating both cumulative and fraction size dose limits are satisfied in the computed plans. Figure 4.6(a) summarizes results from adapting the plan

twice after fraction 25 and 30 for Lung1 case where the residual tumor shrinks with different rates after fraction 25. The average tumor dose achieved from two-epoch adaptation improves by 1.5 Gy and 2.2 Gy with 10% and 30% tumor shrinkage rates, respectively. For these cases, the number of fractions delivered in the treatment increased by 1. With residual tumor shrinking 50%, 3 more fractions are added to the treatment, and the average tumor dose is boosted from 78.7 Gy to 84.2 Gy indicating a boost of 5.5 Gy. Moreover, compared to 73.4 Gy received from non-adaptive planning optimization with boost, this corresponds to a 15% gain. The results in Figure 4.6(a) illustrate that the amount of gain obtained from adapting the plan after fraction 30 is sensitive to the rate the residual tumor shrinks after fraction 25.

Figure 4.6(b) draws the same conclusions from the results on adapting the treatment plan after fraction 25 and 30 for CERRLung case. With 50% shrinkage, the average tumor dose achieved is enhanced from 88.9 Gy to 93.6 Gy corresponding to a 4.7 Gy increase while two additional fractions are delivered in the treatment. Compared to the 84.9 Gy received from non-adaptive planning optimization with boost, a 10.2% gain is accomplished by adapting the plan after fraction 30.

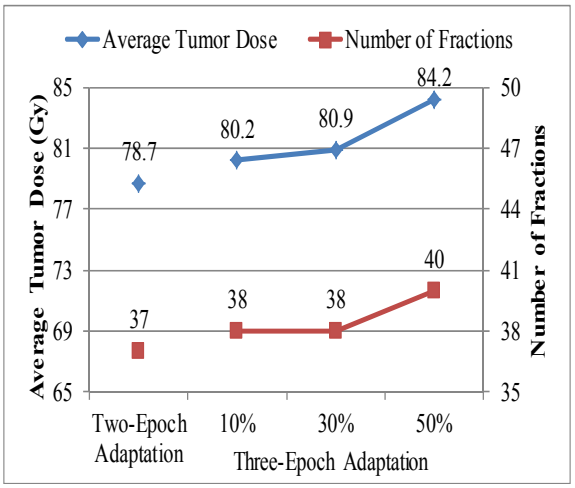

(a) Lung1 Case

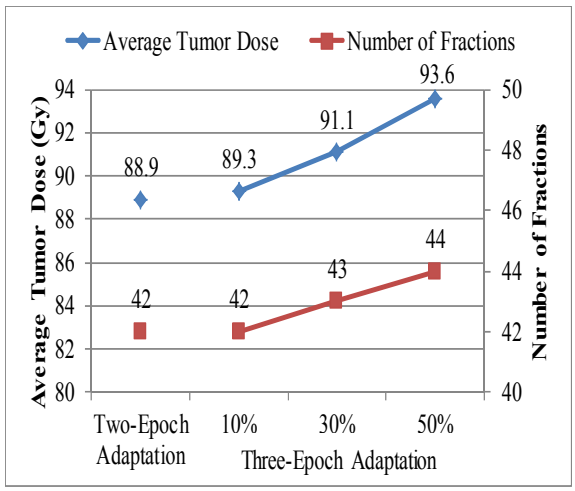

(b) CERRLung Case

Figure 4.6: Two-Epoch Adaptation (Adapting after Fraction 25) vs. Three-Epoch Adaptation (Adapting after Fraction 25 and 30) with Residual Tumor after Fraction 25 Shrinking with Different Rates (%) (Uniform fractionation model is solved in the re-optimization.)

The reason behind the improvement by later adaptation is related to the extra freedom created in the re-optimization. When more tumor points are removed from the residual tumor after fraction 30 for both test cases, the minimum fraction size limit constraints on those points are dropped from the re-optimization formulation because the cumulative limits on those points have already been fulfilled. This relaxes the optimization model and creates more freedom to take advantage of in the rest of the plan. In contrast, with the earlier adaptation, fractionation constraints on those points are not dropped from the re-optimization since they have not received their minimum cumulative dose by that time. Therefore, this prevents relaxing the model and does not create necessary freedom for achieving significant improvement by adapting the plan early. Note that re-planning the treatment plan at later stages of the treatment (e.g. during the subsequent fractions after fraction 25) is always feasible due to the fact that the re-optimization

formulation solved at later adaptation points does not include any minimum cumulative dose constraint on the secondary target and removed tumor points. For example, one feasible solution for re-optimization after fraction 25 would be the solution with 0 beamlet intensity values and *N=0* since this solution preserves the homogeneous tumor dose distribution achieved during the first 25 fractions and satisfies the residual cumulative dose constraints on healthy tissues and fraction size dose constraints on all tissues.

However, for the re-optimization formulation solved at a later adaptation point after fraction 30, the same solution (*0 beamlet intensities and N=0*) might not be feasible for the re-optimization because the delivered dose to the tumor by fraction 30 could be inhomogeneous in spite of maintaining tumor dose homogeneity over the course of the treatment (constraint set (4.18) in Figure 4.1). Although this is the case, there still exists a feasible solution defined as the remaining part of the plan after fraction 30 determined by the re-optimization after fraction 25 (e.g. the plan for the last 12 of the 17 fractions in Epoch 2 computed by the re-optimization after fraction 25 is feasible for the re-optimization formulation solved after fraction 30 for CERRLung case). Note that this feasible solution may result in higher tumor cumulative dose homogeneity than the prescribed level (> 0.95), because some of the points from the residual tumor after fraction 25 are removed due to the tumor shrinkage after fraction 30. As a result, due to existence of at least one feasible solution for the re-optimization after fraction 25 or 30, the potential infeasibility of the subsequent optimization problems at later epochs of re-planning is not an issue in the proposed methodology.

4.4.4 Three-Epoch Cases Using the Ratio Model in the Re-Optimization

Three-epoch adaptation experiments for the more interesting case of adapting after fraction 25 and 30 by solving the ratio model (rescaling results if necessary) in the re-optimization are also performed. The results for Lung1 and CERRLung case are summarized in Figure 4.7(a) and (b), respectively. The details of these results are given in Appendix H and I demonstrating that both cumulative and fraction size dose limits for all structures are satisfied in the twice adapted plans. When the residual tumor shrinks with 10% and 30% for Lung1 case, the average tumor dose received by two-epoch adaptation is boosted by 2 Gy while an additional fraction is given in the overall treatment. With 50% shrinkage, 4.3 Gy increase is achieved whereas 2 more fractions are added to the overall treatment. In addition to these results, three-epoch adaptation results for CERRLung case show a similar improvement in one time adaptation results in Figure 4.7(b). With 50% shrinkage, the average tumor dose received from two-epoch adaptation increased from 88.5 Gy to 94.9 Gy corresponding to a 6.4 Gy increase whereas 3 fractions are added to the overall treatment.

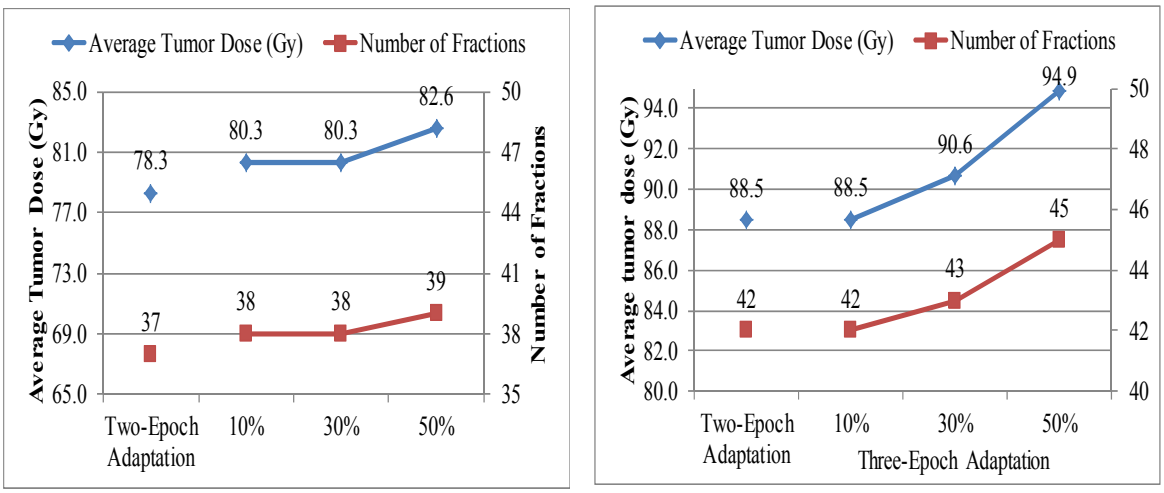

(a) Lung1 Case

(b) CERRLung Case

Figure 4.7: Two-Epoch Adaptation (Adapting after Fraction 25) vs. Three-Epoch Adaptation (Adapting after Fraction 25 and 30) with Residual Tumor after Fraction 25 Shrinking with Different Rates (%)(The ratio model is solved (the results are rescaled if necessary) in the re-optimization.)

5 Biologically Guided IMRT Optimization with Fraction Constraints

5.1 Background and Significance

Adaptive radiation therapy based only on geometric changes in the tumor does not exploit modern imaging science fully. The frontier of treatment now is generating radiation therapy plans that can act on the information acquired on tumor biology (Kim and Tome, 2006; Ling and Li, 2005). The initial tumor biological information and the changes in the tumor biology over the course of the treatment can be demonstrated using modern methods of physical, functional and molecular imaging (Titz and Jeraj, 2008; Stewart and Li, 2007).

Historically, the internal structure (biology) of a tumor in the individual was unknown, leading to guidelines that recommend homogeneous dose distributions of doses across target (ICRU Report #62, Goitein 1986). However, recent pathologic analysis of tumor specimens from surgery and physiologic studies of animal models reveal a complicated tumor structure where the biological elements, e.g. hypoxia, proliferation or drug concentration, are not distributed homogeneously across the tumor (Levin-Plotnik and Hamilton, 2004; Sovik *et al*., 2007; Chen *et al*., 2007). These biological elements are related to the *tumor point sensitivity* defined as the biological responses (sensitivity) of the points to radiation.

Tumor hypoxia (low oxygenation) is a well-known biological cause of resistance to radiation and can be quantified by using recent molecular and functional images. Hypoxic (low-oxygenated) tumor regions are resistant to radiation whereas well-oxygenated tumor regions are sensitive to radiation. Identifying the resistant and sensitive tumor regions based on their oxygenation levels motivates designing *Biologically Guided Radiation Therapy (BGRT)* plans that realign the

radiation delivered across the tumor with the new information on tumor biology in order to yield more effective plans achieving higher tumor control.

In BGRT, the dose at each tumor point can be classified as follows.

- *Tumor physical dose* is the dose deposited from all beamlets to each tumor point
- *Tumor biological dose* is the effective dose received at each tumor point due to the tumor point sensitivity (Note that, the tumor biological dose can be at most as great as the tumor physical dose)

Figure 5.1 demonstrates the effective biological dose received at tumor points across conditions of different oxygenation given the same physical dose. As illustrated, as the oxygenation level decreases (extreme hypoxia), the resistance to the radiation increases; therefore, the biological dose received at tumor points reduces significantly. This motivates BGRT plans to deliver higher dose to the hypoxic tumor points in order to prevent cold spots (under-dosed regions) in tumor.

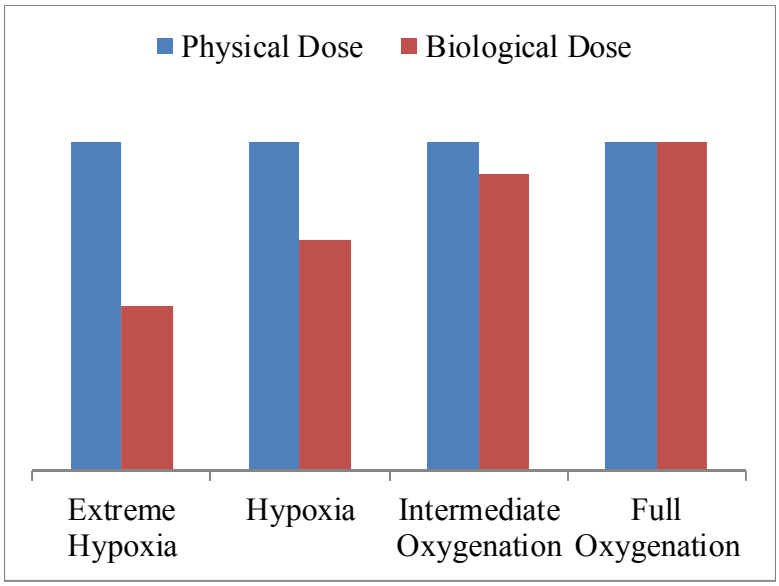

Figure 5.1: Tumor Physical Dose vs. Tumor Biological Dose across Conditions of Different Oxygenation

This research develops optimization models that take biological information, e.g. tumor hypoxia, into account in the treatment planning optimization. Developing mathematical models and testing them is a challenging problem since BGRT is a new area. Quantification of biological data is new and still in development and not much known on modeling issues. Also, there are no known, openly available datasets on tumor biology outside of the clinical institutions yet. This dissertation research is one of the first attempts that deal with modeling and testing biological optimization concepts without losing significant relevancy to clinical practice.

5.2 Biological Optimization Models

5.2.1 Modeling Notation and Assumptions

The previous notation introduced for secondary targets in Chapter 2 is modified in order to handle multiple secondary targets. Let V denote the set of secondary targets. Let l_v^{total} and l_v^{daily}

represent the minimum cumulative and fraction size dose limit for all the points in secondary target $v \in V$, respectively.

Up to this point, all the tumor doses computed in Chapter 2 through Chapter 4 were physical doses where no information was known on the biology. In this chapter, the tumor dose will be specifically classified as tumor physical or tumor biological dose.

Note that, the equation (1) in Section 2.2 presented the physical dose computation for each tumor point $i \in T$ as $d_i = \sum_{j \in J} a_{ij} x_j$. The physical tumor dose d_i for each tumor point i will be adjusted by its tumor point sensitivity in order to compute the actual biological dose received at that point. Tumor point sensitivity can represented as:

λ_i: adjustment factor due to the loss of effect with hypoxia for each point $i \in T$ ($0 < \lambda_i \leq 1$)

Then let d_i^b be biological dose received at tumor point $i \in T$ computed by multiplying tumor point i's sensitivity (λ_i) by the physical dose deposited to point i (d_i) as follows (Titz and Jeraj 2008).

$$d_i^b = \sum_{j \in J} \left(\lambda_i a_{ij}\right) x_j = \lambda_i \sum_{j \in J} a_{ij} x_j = \lambda_i d_i \quad \forall i \in T \tag{5.1}$$

It is assumed that sensitivity needs to be accounted for only on tumor points and the tumor point sensitivities (λ) do not change over the course of the treatment in static (non-adaptive) plans.

5.2.2 Biological Uniform Fractionation Model

The biological uniform fractionation model developed is a variant of the uniform fractionation model presented in Section 2.5. The model maximizes average tumor biological dose (5.2) over non-negative d_i^b subject to cumulative average and upper dose limit constraint sets (5.3) through (5.4) on healthy tissues, cumulative minimum dose limit constraint set (5.5) on secondary targets, tumor dose homogeneity limit (5.6), dose consistency constraint (5.7) and the integer fraction size dose constraint sets (5.8) through (5.10). In the rest of this section, the major differences between the uniform fractionation model of Section 2.5 and the biological uniform fractionation will be highlighted.

$$\text{maximize} \quad \left(\sum_{i \in T} d_i^b\right) / |T| \tag{5.2}$$

$$\sum_{i \in H_k} d_i \le |H_k| \mu_k \qquad \forall k \in \overline{K} \tag{5.3}$$

$$d_i \le u_k^{total} \qquad \forall k \in K, \forall i \in H_k \tag{5.4}$$

$$d_i \ge l_v^{total} \qquad \forall v \in V, \forall i \in S_v \tag{5.5}$$

$$D_{min} \le d_i \le \frac{D_{min}}{\alpha} \qquad \forall i \in T \tag{5.6}$$

$$d_i \le \frac{D_{min}}{\alpha} \qquad \forall v \in V, \forall i \in S_v \tag{5.7}$$

$$d_i \ge l_v^{daily} \times N \qquad \forall v \in V, \forall i \in S_v \tag{5.8}$$

$$d_i^b \ge l_{tumor}^{daily} \times N \qquad \forall i \in T \tag{5.9}$$

$$d_i \le u_k^{daily} \times N \qquad \forall k \in K \cup \overline{K}, \forall i \in H_k \tag{5.10}$$

Biological objective function

The objective function of the optimization model (5.2) maximizes average biological dose across the tumor in contrast to the previous objective of maximizing average tumor physical dose in the uniform fractionation model.

Tumor physical dose homogeneity

One of the open questions in biological optimization is whether homogeneity limits should be enforced on tumor physical or biological doses. In the case of enforcing a homogeneity limit on tumor physical doses, the constraint set (5.6) would remain the same. In addition, that constraint set would allow capturing the maximum tumor physical dose (D_{min}/α) which then would be used as the right hand side of the dose consistency constraint set (5.7) (Recall that, the dose consistency constraint ensures that the maximum dose received at secondary targets does not exceed the maximum tumor physical dose).

Furthermore, in order to effectively react to the more severe hypoxia in tumor, one could choose lower homogeneity value (e.g $\alpha = 0.8$) which would give freedom to the model in optimizing tumor physical dose distribution.

Tumor biological dose homogeneity

If one desires to impose a homogeneity limit on tumor biological doses rather than tumor physical doses, constraint set (5.6) would be replaced with constraint set (5.11) in the optimization model, where D^b_{min} is a continuous variable defining the minimum tumor biological dose.

$$D_{min}^{b} \le d_i^b \le \frac{D_{min}^{b}}{\alpha} \qquad \forall i \in T \tag{5.11}$$

Enforcing constraint set (5.11) captures the maximum tumor biological dose but not the maximum tumor physical dose which makes the dose consistency constraint harder to model. Exact modeling of this constraint requires introducing binary variables resulting in a much more computationally expensive optimization model. To avoid this, an approximate method is used to estimate the maximum tumor physical dose by dividing the maximum biological dose by hypoxic adjustment factor λ of the second most insensitive region value. By using this estimation, the dose consistency constraint (5.7) is replaced with the following dose consistency constraint set (5.12) where $\hat{\lambda}$ denotes the hypoxic adjustment factor of the second most insensitive tumor region value.

$$d_i \le \frac{D_{min}^{b} / \alpha}{\hat{\lambda}} \qquad \forall v \in V, \forall i \in S_v \tag{5.12}$$

Tumor fraction size requirement

Lastly, the tumor fraction size dose constraint set (5.9) is stated in terms of biological dose in the optimization model. This imposes a lower dose requirement on tumor biological doses per fraction rather than tumor physical doses per fraction. Controlling the minimum biological dose achieved per fraction would increase the probability of cure.

In summary, the biological uniform fractionation model is a single integer variable mixed-integer linear programming model producing uniform plans over N fractions. The integer variable N in the fraction size dose constraint sets guarantees that the cumulative plan can be divided into

integer number of fractions where all the fraction size dose limits on healthy tissues and secondary targets, and biological fraction size dose limit on all tumor points are satisfied.

5.2.3 Biological Adaptive Planning Optimization Methodology

An adaptive planning optimization methodology is also developed that re-plans treatment plans in response to the changes in the tumor point sensitivities (λ). This methodology follows the same steps summarized in Section 4.3. Although the adaptive planning optimization methodology given in Section 4.3 considers adapting the treatment plan M times, here only two-epoch adaptation ($M=1$) would be investigated. The major reasons behind this choice are two-epoch adaptation in Chapter 4 gave excellent results (lessening the need to adapt more than once) and adapting more than once to the changes in the sensitivities would require more data generation for testing which could not have been done realistically since little is known on quantifying the sensitivity change.

In the proposed adaptive approach, the treatment plan is adapted after delivering a sequence of fractions by incorporating the latest tumor point sensitivity information (λ) in order to achieve the best IMRT design for the overall treatment and for each fraction. The treatment plan is first optimized against both cumulative and fraction size dose limits based on the biological image at the beginning of the treatment by solving the biological uniform fractionation model presented in the previous section. The optimized treatment plan is divided into N fractions and the first N_1 are delivered in Epoch 1.

After delivering the first epoch, a new biological image showing the latest hypoxia information is acquired and the tumor point sensitivities (λ) are updated. In addition to this, the residual cumulative dose limits for all tissue points (right hand side of the constraints in the previous section) are updated by subtracting the dose delivered from against their cumulative dose limits in Epoch 1. Then, the remaining treatment plan is *re-optimized* against residual cumulative and fraction size dose limits by solving the model in the previous section (with integer variable N_2) to compute N_2 fractions to be delivered in Epoch 2. The steps taken in this adaptive approach are summarized with a flow chart in Figure 5.2.

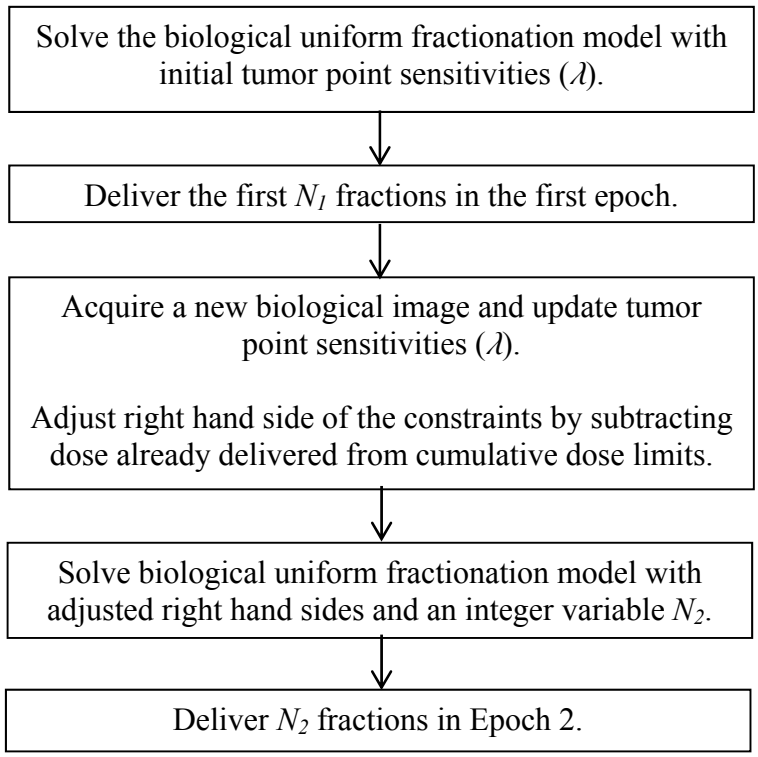

Figure 5.2: Summary of Biological Adaptive Optimization Approach

5.2.4 Tumor Control Probability: Measure of Effectiveness

In the previous chapters, the effectiveness of the computed plans is measured by the tumor dose statistics such as maximum, minimum and average tumor physical doses. With the tumor point sensitivity information (λ), it is not possible to compute tumor biological dose statistics and use them instead to evaluate treatment plans. A further step to more accurately measure the biological effectiveness of plans would be to convert the tumor physical dose distributions with the tumor point sensitivity information (λ) into a commonly used biological objective in the literature as *Tumor Control Probability (TCP)* (Ruggieri *et al*., 2010; Yang and Xing, 2005).

TCP is defined as the probability that all the cells in tumor are inactivated after a course of treatment; therefore, it estimates the success of the treatment. Using *TCP* provides a fair comparison between plans since it is impacted by both average and the minimum biological doses. For example, although a treatment plan achieving a higher average biological dose seems to be a more effective plan, it could result in being a less successful treatment due to under-dosed points with a smaller minimum biological dose. However, the effect of both achieved average biological dose and the minimum biological dose is captured in *TCP* calculation; therefore, allows a fair comparison between treatment plans.

Equation (5.13) computes *TCP* by multiplying TCP_i across all tumor voxels. TCP_i represents the probability that all the cells in voxel i are inactivated for $\forall i \in T$.

$$TCP = \prod_{i=1}^{|T|} TCP_i \tag{5.13}$$

TCP_i is a function of initial number of cells in each tumor voxel, denoted as n, and the surviving fraction of cells at voxel i ($S_N(d_i)$) after d_i physical dose is delivered over N fractions. The effect of hypoxia is included in the surviving fraction formula in (5.15). Here, n is equal to tumor voxel size (mm^3) times tumor cell density ($cells/mm^3$). TCP_i is computed in equation (5.14) as follows.

$$TCP_i = exp\{-nS_N(d_i)\} \qquad \forall i \in T \tag{5.14}$$

The $S_N(d_i)$ at each tumor voxel i is computed by the equation (5.14) (Ruggieri *et al*., 2010). The first term of the exponential function is the cell killing effect over N fractions whereas the second term is the re-population effect (i.e. tendency of tumor cells to regrow over the course of the treatment) over N fractions. Here, re-population parameters are denoted as following: Δt is the inter-fractional time interval, T_{eff} is effective clonogenic doubling time, T_d is delay time in clonogenic accelerated repopulation.

$$S_N(d_i) = exp\left\{-d_i\left(\alpha_i + \beta_i \frac{d_i}{N}\right) + \frac{ln\,2}{T_{eff}}\left[(N-1)\Delta t - T_d\right]\right\} \qquad \forall i \in T \tag{5.15}$$

The tumor hypoxia at each voxel i is included in equation (5.15) by the radiosensitivity parameters α_i and β_i. Here, $\alpha_i = \alpha_o * \lambda_i$ and $\beta_i = \beta_o * (\lambda_i)^2$ are used (Titz and Jeraj, 2008) where α_o and β_o are radiosensitivity parameters at well-oxygenated state.

The formula given in equation (5.15) computes surviving fraction assuming same tumor point sensitivity over N uniform fractions. There is a need to use a slightly modified formula in case of tumor point sensitivity change. Equation (5.16) computes the overall surviving fraction for tumor

voxel i after d_i^1 physical dose is delivered over N_1 fractions in the first epoch taking into account initial hypoxia and d_i^2 physical dose is delivered over N_2 fractions in the second epoch taking into account updated hypoxia. Since the tumor point sensitivity (λ_i) changes between first and second epoch, radiosensitivity parameters $\left(\alpha_i^1, \beta_i^1\right)$ and $\left(\alpha_i^2, \beta_i^2\right)$ are defined for the first and second epoch, respectively. The first and second term of the exponential function in equation (5.16) is the cell killing effects over the first and second epoch, respectively, whereas the last term incorporates the repopulation effect into the formula.

$$S_{(N_1,N_2)}\left(d_i^1, d_i^2\right) = exp\left\{-d_i^1\left(\alpha_i^1 + \beta_i^1 \frac{d_i^1}{N_1}\right) - d_i^2\left(\alpha_i^2 + \beta_i^2 \frac{d_i^2}{N_2}\right) + \frac{ln2}{T_{eff}}\left[(N_1 + N_2 - 1)\Delta t - T_d\right]\right\} \tag{5.16}$$

5.3 Generating a Test Case

5.3.1 The Need

Testing biological optimization models requires cases where the tumor hypoxia information is known. Unfortunately, such desired test cases are not publicly available, because clinical studies on hypoxia imaging are new and not many institutions have performed these studies. In addition, it is always challenging to get datasets from research institutions due to their very strict rules on sharing patient data.

One way to obtain the tumor hypoxia information might be randomly generating the tumor point sensitivities (λ) across the tumor. However, this approach would not have much clinical validity and would conflict with this dissertation research's efforts on testing optimization models with cases simulating real practice. In order to maintain clinical relevancy as much as possible, the approach (Section 5.3.3) of inserting artificial hypoxia information based on a published test case

extracted from CERR website ("CERR: A Computational Environment for Radiotherapy Research") was adopted.

5.3.2 Description of the CERR Head and Neck Test Case

An anonymized head and neck case presented on CERR website is used as a basis for the test case. Figure 5.3 displays an example slice outlining structures under interest. With clinical guidance, it was decided to treat Target1, Target2, and Target3 as secondary targets and insert an artificial primary target (tumor) inside Target1 (shown as dashed circle). Note that, the artificial primary target is stretched in z-direction (±) to have a 3-dimensional, more realistic tumor shape of a prolate sperhoid (i.e. shape of a football).

Table 5.1 shows the number of sampling points used for the optimization and the influence matrix density for each structure in the head and neck test case along with the selected beam angles. The number of sampling points for each structure is determined after doing experimentation with different sampling densities. During experimentation, the dose-volume histograms (DVHs) using all possible points are created from the optimization results based on different sampling densities, and a sampling density that creates acceptable DVHs was selected for each structure. The influence matrix for this test case is generated using radiation therapy software system CERR.

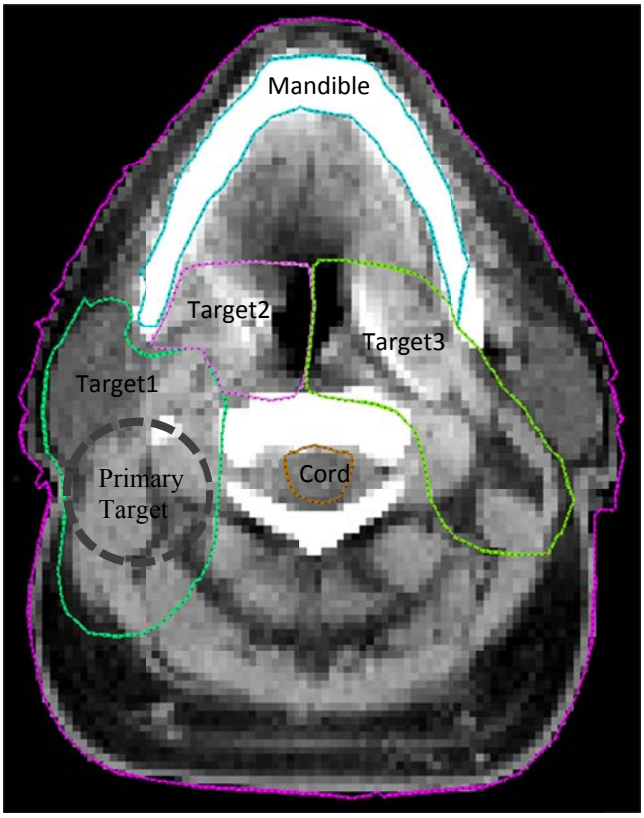

Figure 5.3: Example Head and Neck Case Slice

Table 5.1: Head and Neck Test Case Description

Structure	Structure Description	Head and Neck Case	
		Point Count	Matrix Density
Tumor	Primary Target	2,528	86%
Target1	Secondary Target	1,314	85%
Target2	Secondary Target	2,412	91%
Target3	Secondary Target	1,465	84%
Mandible	Healthy Tissue	681	78%
Brainstem	Healthy Tissue	671	82%
Not Otherwise Specified Tissue	Healthy Tissue	8,489	52%
Spinal Cord	Healthy Tissue	2,198	72%
Beam Angles: 0 40 80 120 160 200 240 280 320 (1,393 beamlets)			

Table 5.2 shows the prescription used in the computational experiments with the head and neck test case. The table presents both cumulative dose objectives and fraction size dose limits for the

primary target, secondary targets and healthy tissues. All of the points in each structure are subject to its corresponding fraction size limit.

Table 5.2: Prescription for the Head and Neck Test Case ("pDose" refers to tumor physical dose, "bDose" refers to tumor biological dose)

Structure	Structure Description	Head and Neck Case	
		Cumulative Dose Objective/Limit (Gy)	Fraction Size Dose Limit (Gy)
Tumor	Primary Target	Maximize avg. pDose/bDose	≥ 1.80
		$\frac{\text{min. tumor p(b)Dose}}{\text{max. tumor p(b)Dose}} \geq 0.9$	
Target1	Secondary Target	$100\% \geq 60$	≥ 1.80
Target2	Secondary Target	$100\% \geq 60$	≥ 1.80
Target3	Secondary Target	$100\% \geq 54$	≥ 1.65
Mandible	Healthy Tissue	Avg. dose ≤ 40 $100\% \leq 72$	≤ 2.10
Brainstem	Healthy Tissue	$100\% \leq 58$	≤ 2.10
Not Otherwise Specified Tissue	Healthy Tissue	$100\% \leq 80$	≤ 2.10
Spinal Cord	Healthy Tissue	$100\% \leq 50$	≤ 2.10

5.3.3 Calibrating Tumor Point Sensitivities (λ)

An human PET image acquired prior to the treatment and the mathematical relationships from a recent study (Titz and Jeraj, 2008) are used in order to generate λ's in the simulated tumor. Figure 5.4(a) shows the PET image with tumor hypoxia information (in color) where different colors indicate different hypoxia levels. As Figure 5.4(b) illustrates, the hypoxia distribution of the inserted artificial primary target on a single slice (the example slice in Figure 5.3) is approximated with the help of the hypoxia map on the PET image given in Figure 5.4(a) where

the primary target is divided into five different hypoxic regions represented by a different color: Red, Green, Yellow, Light Blue, and Dark Blue. All tumor regions are stretched in z-direction (±) proportional to their x-y radius which take the final form of prolate spheroids within each other.

Different colors are quantified by using the color code for standardized uptake value (*SUV*) presented in in Figure 5.4(c). Higher *SUV* values indicate more hypoxia while lower *SUV* values indicate well-oxygenation. For example, the color red corresponding to *SUV* values close to 7 illustrate hypoxic region whereas the color dark blue taking *SUV* values close to 0 illustrate well-oxygenated region in Figure 5.4(b).

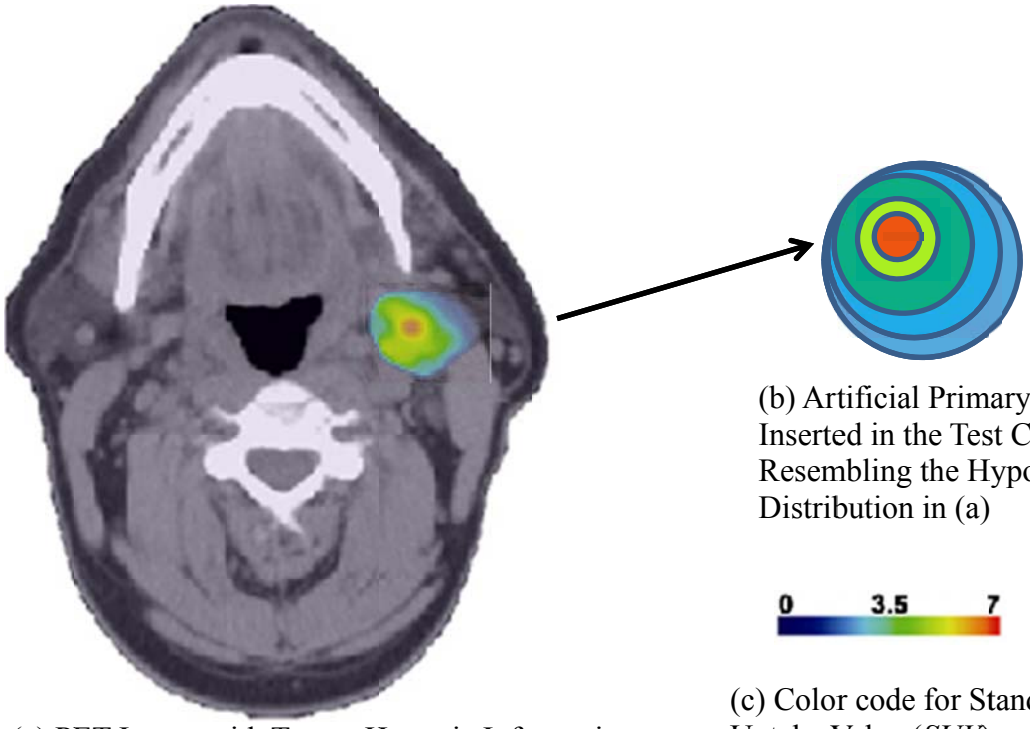

(a) PET Image with Tumor Hypoxia Information

(b) Artificial Primary Target Inserted in the Test Case Resembling the Hypoxia Distribution in (a)

(c) Color code for Standardized Uptake Value (*SUV*)

Figure 5.4: PET Image Used to Generate Tumor Hypoxia in the Test Case[1]

[1] Figure 5.4(a) and (c) are taken from a published study (Titz and Jeraj, 2008).

Once the *SUV* values for tumor regions are quantified, they are then converted into oxygen tension pO_2 (mmHg) by using the sigmoid relationship presented in Figure 5.5(a). Next, the pO_2 values are matched to oxygen-enhanced ratio (*OER*) values and oxygen modification factor (*OMF*) values by using the dependence demonstrated in Figure 5.5(b). The mathematical function used to map pO_2 values to *OER* values is given in equation (5.17) where m denotes the maximum *OER* value and K is the pO_2 value at $OER=(m+1)/2$. In this study, m value of 3 and K value of 3 mmHg are used based on Titz and Jeraj's paper (2008).

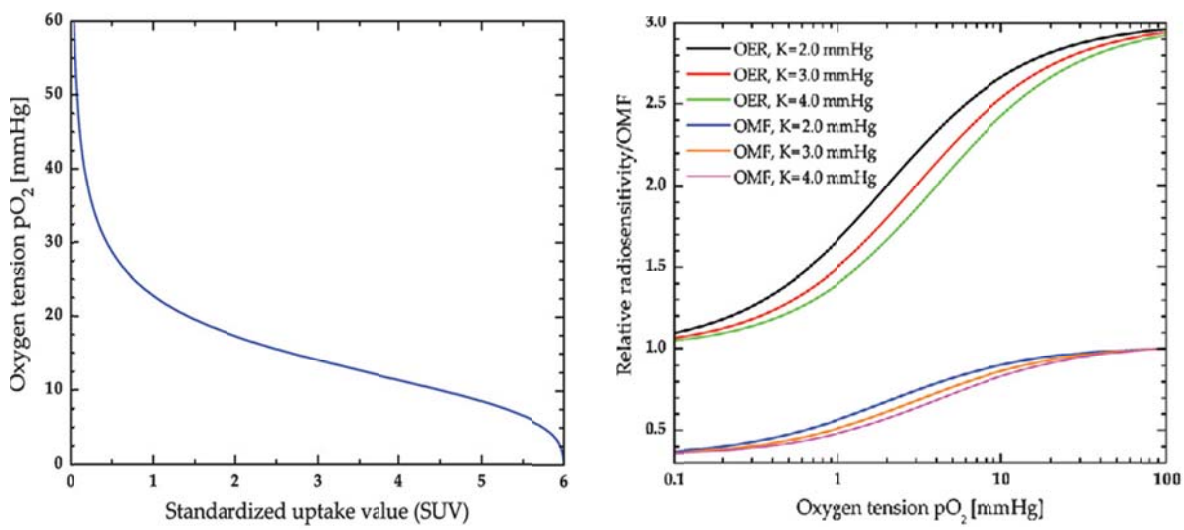

(a) Illustration of the sigmoid relationship between the oxygen partial pressure (pO_2) and the standardized uptake value (*SUV*)

(b) Dependence of the relative radio-sensitivity (expressed through oxygen-enhanced ratio (*OER*)) and the oxygen-modification factor (*OMF*) as a function of the pO_2.

Figure 5.5: Mathematical Relationships Used to Derive Tumor Point Sensitivities[2]

$$OER(pO_2) = \frac{m \cdot pO_2 + K}{pO_2 + K} \tag{5.17}$$

[2] Figure 5.5(a) and (b) are taken from published study (Titz and Jeraj 2008).

The *OMF* values in Figure 5.5(b) are actually equal to rescaled *OER* to [0-1] range. These *OMF* values are used as tumor point sensitivities (λ) in the biological optimization.

The *OMF* values (λ) for each tumor region used in the computational experiments are summarized in Table 5.3. The details including the approximate *SUV* range for each tumor region, the selected *SUV* values and their pO_2 values corresponding to the *OMF* values in each base case are given in Appendix J. As Table 5.3 demonstrates, only the hypoxia level in red region differs between two base cases, where the red region is more hypoxic in the second base case with a lower OMF value (*OMF*=0.77 vs. *OMF*=0.82). Besides the *OMF* values, the table presents the point count and matrix density for each tumor region.

Table 5.3: Two Base Cases Used in the Experiments (*OMF*=Oxygen-Modification Factor, λ=Tumor Point Sensitivities)

Tumor Regions	First Base Case	Second Base Case	Point Count	Matrix Density
	OMF=λ	*OMF*=λ		
Red	**0.82**	**0.77**	94	85%
Yellow	0.88	0.88	186	85%
Green	0.91	0.91	749	85%
Light Blue	0.92	0.92	710	86%
Dark Blue	0.98	0.98	789	87%

5.3.4 Generating Biological Change in Tumor Point Sensitivity (λ)

The initial λ values presented in Table 5.3 may change as the treatment evolves. However, how to quantify this change as a function of delivered dose is unknown, and more clinical research is required to understand how tumor point sensitivities change throughout the treatment. Currently, there are published studies in the literature giving insight on the direction of the change

(Eschmann *et al*., 2007; Popple *et al*., 2002; Titz and Jeraj, 2008; Lee *et al*., 2009; Rischin *et al*., 2001; Hall, 1994). These papers indicate that the hypoxic cells can absorb oxygen and change their state to oxygenated. This phenomenon is known as re-oxygenation of tumor cells.

Following the re-oxygenation phenomenon, the tumor regions in the generated test case are expected to get more oxygenated; therefore, the λ values (=*OMF*) in Table 5.3 are likely to increase over the course of the treatment and get closer to 1.0 (*OMF* value for well-oxygenated state). Since the rate of the re-oxygenation is not known, it is assumed that the all tumor regions will close their gap by a fraction β at a specific point in time, referred as *adaptation/re-optimization point*, denoted as *R.* For example, assuming all tumor regions are one quarter re-oxygenated after delivering R=25 fractions, β would be equal to 0.25. The following formula computes the updated λ, denoted as λ_u, at the adaptation point.

$$\lambda_u = \lambda + (1-\lambda)*\beta \tag{5.18}$$

5.4 Computational Experiments

Computational experiments on biological optimization compared various approaches by testing on the cases presented above. Section 5.4.1 will present physically and biologically optimized plans computed for the datasets above to assess the benefit of taking the initial tumor point sensitivity (λ) information into account in the treatment planning optimization. To illustrate the importance of modeling fractionation constraints explicitly in the optimization, Section 5.4.2 will compare plans optimized against cumulative dose constraints alone and plans optimized against both cumulative and fraction size dose constraints. Furthermore, Section 5.4.3 will show results from re-planning the treatment plans to the changes in the tumor point sensitivity to realize if

gains in the treatment outcomes can be achieved. All these plans are computed with two different tumor hypoxia scenarios summarized in Table 5.3.

For the *TCP* computation throughout the computational experiments, the following parameters are used based on a published paper (Ruggieri *et al*., 2010): Δt=1 day, T_{eff}=3 days, T_d=0 days, α_o=0.35Gy^{-1} and β_o=0.035Gy^{-2}. The number of cells in each tumor voxel (n) is equal to 1,200,000 (voxel size (12 mm^3)*cell density (10^5 cells/mm^3)) where the used cell density of 10^5 cells/mm^3 is an acceptable value between 10^4 cells/mm^3 (Ruggieri *et al*., 2010) and 10^6 cells/mm^3 (Titz and Jeraj, 2008). The *TCP* calculation for the plans presented in Section 5.4.1 and Section 5.4.2 uses the surviving fraction equation (5.15) whereas the *TCP* calculation for the plans given in Section 5.4.3 uses the surviving fraction equation (5.16).

5.4.1 Physically Optimized Plan Results vs. Biologically Optimized Plan Results

Physically and biologically optimized plans can be defined as follows.

- *Physically optimized plans*: Plans computed ignoring tumor biology in the optimization, but biologically scored after optimization using the tumor point sensitivity (λ)
- *Biologically optimized plans*: Plans computed considering tumor biology in the optimization

Physically optimized plans are generated by solving the uniform fractionation model presented in Section 2.5. Biologically optimized plans are generated by solving the biological uniform fractionation model presented in Section 5.2.2. All the physical and biological plans were

computed in less than a day on the server employed (specifications of the machine are given in Section 1.4).

5.4.1.1 First Base Case Results (Red Hypoxia Lower, Homogeneity=0.9)

Figure 5.6 summarizes the results obtained from physically and biologically optimized plans with 0.9 tumor dose homogeneity. Figure 5.6(a) presents physical and biological tumor dose statistics whereas Figure 5.6(b) shows the number of fractions delivered and the achieved *TCP* at the end of the treatment across all plans. The biologically optimized plans are computed considering either tumor biological dose homogeneity requirement, referred as *biological homogeneity*, or tumor physical dose homogeneity requirement, referred as *physical* homogeneity. All these computed plans satisfy their cumulative and fraction size dose constraints on all targets and healthy tissues (for details on dose statistics for each structure, see Appendix K).

As Figure 5.6(a) exhibits, although the biologically optimized plan with physical homogeneity provides similar tumor physical dose statistics as physically optimized plan does, the biological plan increases the minimum tumor biological dose from 66.9 Gy to 68.4 Gy corresponding to a 1.5 Gy increase. In addition, using the number of fractions delivered from Figure 5.6(b), the minimum tumor biological fraction size dose delivered in physically optimized plan is 1.72 Gy (66.9 Gy/39) compared to the minimum tumor biological fraction size dose of 1.80 Gy in the biologically optimized plan with physical homogeneity (68.4 Gy/38). Delivering at least 1.80 Gy biological dose per fraction to tumor points is ensured by the enforced biological fraction size requirement in the optimization. As a result, the increase in both the minimum biological

cumulative and fraction size dose achieved by biologically optimized plan with physical homogeneity raises the *TCP* value by 0.08 (0.66 vs. 0.74).

By contrast, enforcing biological homogeneity in biologically optimized plan reduces average tumor physical and biological dose substantially (Figure 5.6(a)). Comparing against the physically optimized plan, the average biological dose decreased by 4.4 Gy (78.9 Gy vs. 74.5 Gy). The main reason behind the significant reduction in average biological dose is the optimization keeps the maximum biological dose lower in order to maintain tumor biological dose homogeneity. The restriction of the average biological dose in biologically optimized plan with biological homogeneity reduced the *TCP* significantly from 0.66 to 0.47 corresponding to a 0.19 decrease (Figure 5.6(b)).

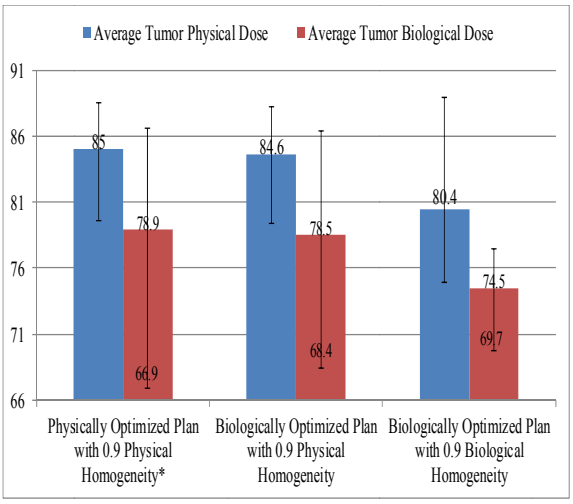

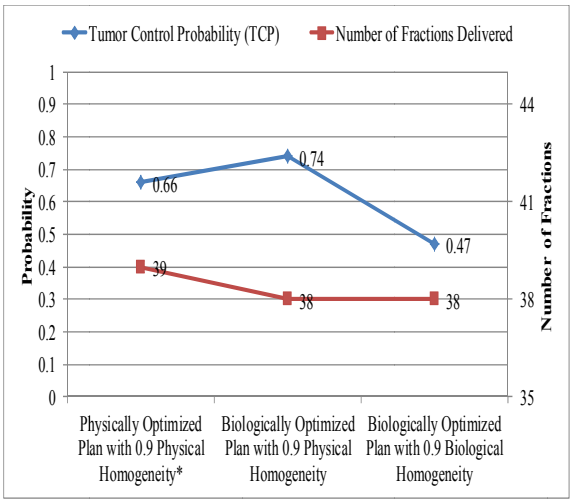

per
ıd

ity
:actions

Figure 5.6: Summary of Physically Optimized Plans vs. Biologically Optimized Plans at Lower Red Hypoxia and 0.9 Tumor Dose Homogeneity (*Physically optimized plans are biologically scored using initial tumor point sensitivities.)

5.4.1.2 Second Base Case Results (Red Hypoxia Higher, Homogeneity=0.8)

Due to the more severe hypoxia in red region in the second base, the biological fraction size requirement (≥1.80) on red region points is replaced with the same physical fraction size requirement (relaxing the model to maintain feasibility) and maximizing biological dose in red region objective is used instead for biologically optimized plans. Figure 5.7(a) and (b) summarize all the results received from physically optimized and biologically optimized plans with 0.8 tumor dose homogeneity. Both the cumulative and fraction size dose constraints are satisfied in all computed plans (for details on dose statistics for each structure, see Appendix L). Similar to the first base case results, biologically optimized plan with physical homogeneity improves the *TCP* obtained by the physically optimized plan. Considering the results in Figure

5.7(a) and (b), although the biological plan achieves less average tumor dose (81.6 Gy vs. 78.8 Gy), it increases the minimum tumor biological dose from 63.5 Gy to 64.8 Gy and the minimum tumor biological fraction size dose from 1.67 Gy (63.5 Gy/38 fractions) to 1.71 Gy (64.8 Gy/38 fractions). Since *TCP* is very sensitive to the increase in the minimum biological dose, these increases in both biological cumulative and fraction size dose were reflected in 0.07 raise in *TCP* (0.63 vs. 0.70).

As the results in Figure 5.7(a) and (b) illustrate, biologically optimized plan with biological homogeneity again lowers the *TCP* obtained by physically optimized plan significantly which is in line with the first base case results. The biological optimization keeps the maximum tumor biological dose lower due to the homogeneity requirement on tumor biological doses. This restricts the average tumor biological dose over 6 Gy (81.6 Gy vs. 75.2 Gy). This significant decrease in average tumor biological dose reduced the *TCP* value from 0.63 to 0.27.

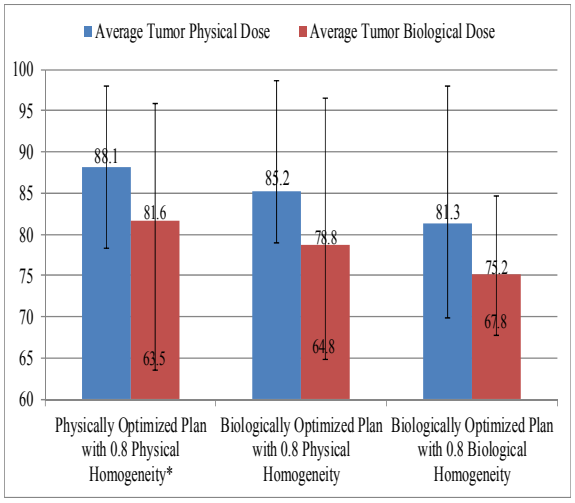

(a) Tumor Physical and Biological Dose Statistics across All Plans (Lower and upper bar on each column indicate minimum and maximum doses.)

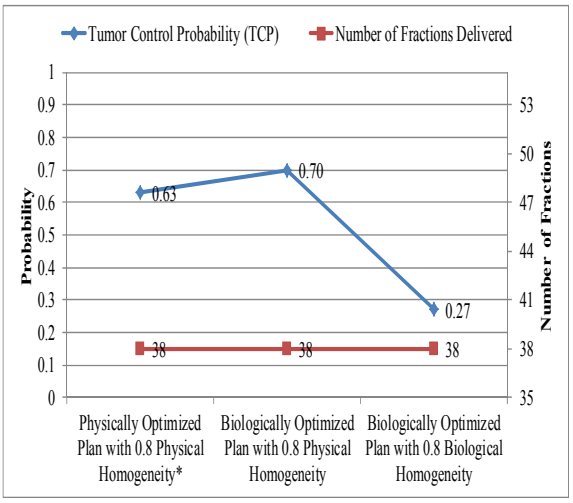

(b) Tumor Control Probability Achieved and Number of Fractions Delivered across All Plans

Figure 5.7: Summary of Physically Optimized Plans vs. Biologically Optimized Plans at Higher Red Hypoxia and 0.8 Tumor Dose Homogeneity (*Physically optimized plans are biologically scored with initial tumor point sensitivities.)

The results presented on both cases in Section 5.4.1.1 and 5.4.1.2 demonstrate the potential benefit of incorporating biological information into the treatment planning optimization, and therefore, prove the concept of possible clinically significant gains that might be achieved by biological optimization. Furthermore, the importance of deciding whether to enforce homogeneity requirement on tumor physical or biological doses is demonstrated by the results, and enforcing tumor physical dose homogeneity in the optimization is preferred throughout the computational experiments due to allowing better plans.

It is noteworthy to state that although *TCP* is a good measure of biological effectiveness, it was discovered during the computational experiments that it could be volatile for some instances. This volatility is further illustrated in Appendix M.

5.4.2 Illustrating the Need to Include Fractionation Constraints Explicitly in the Optimization

In addition to the improvement in *TCP* obtained by biological optimization, satisfying fraction size requirements on secondary targets in the computed plans helps achieve better cure for these structures. Figure 5.8(a) and (b) illustrates the importance of explicitly including integer fractionation constraints into both physical and biological optimization. The physically or biologically optimized feasibly fractionated plans already presented in Section 5.4.1.1 and 5.4.1.2 were optimized against both cumulative and fraction size dose constraints. For comparison purposes, physically optimized cumulative plans are generated by solving the LP formulation in Section 2.3.1 and biologically optimized cumulative plans are generated by solving the biological uniform fractionation model in Section 5.2.2 ignoring fraction size constraints. Note that, both physical and biological cumulative plans are optimized against cumulative dose constraints alone.

The graphs in Figure 5.8(a) and (b) show the control probabilities for the secondary targets including Target1, Target2, and Target 3 as well as the primary target across all computed plans. The cumulative plans are divided into integer number of fractions satisfying all the healthy tissue maximum fraction size requirements (e.g. cumulative plans are delivered over 39 fractions). Satisfying the healthy tissue fraction size limits come at the expense of violating the minimum

fraction size requirements on secondary targets in cumulative plans. This is reflected by computing control probabilities for secondary targets by using the same calculations in Section 5.2.4. Lower cell density (10^3cells/mm^3) is used for secondary target control probability computations (Strigari *et al.*, 2008).

As Figure 5.8(a) and (b) show, although the tumor control probabilities are very close to each other between cumulative and feasibly fractionated plans, the secondary target control probabilities are clinically significantly lower in cumulative plans (e.g. 0.07 vs. 0.92 Target2 control probabilities for base case 1 and 0.07 vs. 0.95 Target2 control probabilities for base case 2 achieved in biologically optimized cumulative and feasibly fractionated plans, respectively). The reason behind achieving better secondary target control probabilities in feasibly fractionated plans is imposing minimum fraction size requirement on secondary targets in the optimization. Explicitly including constraints on this requirement ensures higher control probability values for secondary targets without sacrificing the tumor control probability values.

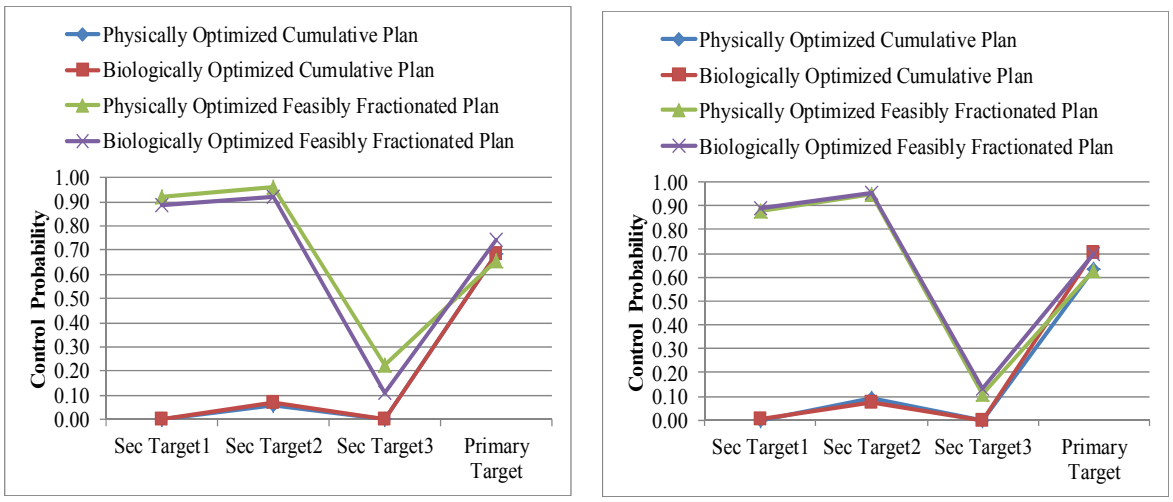

(a) First Base Case (b) Second Base Case

Figure 5.8: Illustrating the Importance of Including Fractionation Constraints in the Optimization ("Cumulative" refers to plans optimized against cumulative dose constraints alone, "Feasibly Fractionated" refers to plans optimized against both cumulative and fraction size dose constraints.)

5.4.3 Results from Re-planning the Biologically Optimized Plans to the Changes in Tumor Point Sensitivity (λ)

Treatment plans are adapted to the changes in the tumor point sensitivity (λ) by using the biological adaptive optimization methodology presented in Section 5.2.3. The initial λ values used in the adaptive methodology are as same as the λ values presented in Table 5.3. For the computational experiments in this section, initial λ values are assumed to one quarter and one half re-oxygenate, closing their gap by β=0.25 and β=0.50, respectively. The updated λ values are calculated by using equation (5.18). The re-optimization (adaptation) point, denoted as R, correspond to after fraction 25 or fraction 30 in the experiments.

The adaptive plans computed in this section are compared against the physically optimized plans and biologically optimized plans presented in Section 5.4.1. Note that before, the plans from Section 5.4.1 did not take into account the changes in λ both in planning and scoring; therefore, they can be referred as *non-adaptive plans*. Now, all these non-adaptive plans are re-scored in later fractions using updated λ_u in order to have fair comparison. The plans considered in this section can be summarized as follows.

- *Non-adaptive physically optimized plans*: Physically optimized plans from Section 5.4.1, but biologically scored after optimization using original λ for the first R fractions and updated λ_u in later fractions
- *Non-adaptive biologically optimized plans*: Biologically optimized plans from Section 5.4.1, but later fractions after R are biologically re-scored after optimization with updated λ_u
- *Biologically optimized adaptive plans:* Biologically optimized plans re-optimized with updated λ_u after delivering R fractions

5.4.3.1 First Base Case Results (Red Hypoxia Lower, Homogeneity=0.9)

Figure 5.9 compares non-adaptive physically optimized plans, non-adaptive biologically optimized plans, and biologically optimized adaptive plans across various scenarios where plans are adapted at different re-optimization points (R) with respect to different re-oxygenation rates (β). The biological dose statistics, including maximum, average, and minimum doses, as well as the achieved *TCP* for each plan and the number of fractions delivered in each plan are displayed in the Figure. Note that, with biological re-scoring, only the cumulative biological doses received at tumor increases in non-adaptive plans without changing the doses on other structures;

therefore, the plans still satisfy all their cumulative and fraction size dose limits. In addition, both cumulative and fraction size dose limits are maintained in computed adaptive plans since the related constraints are explicitly enforced in the optimization.

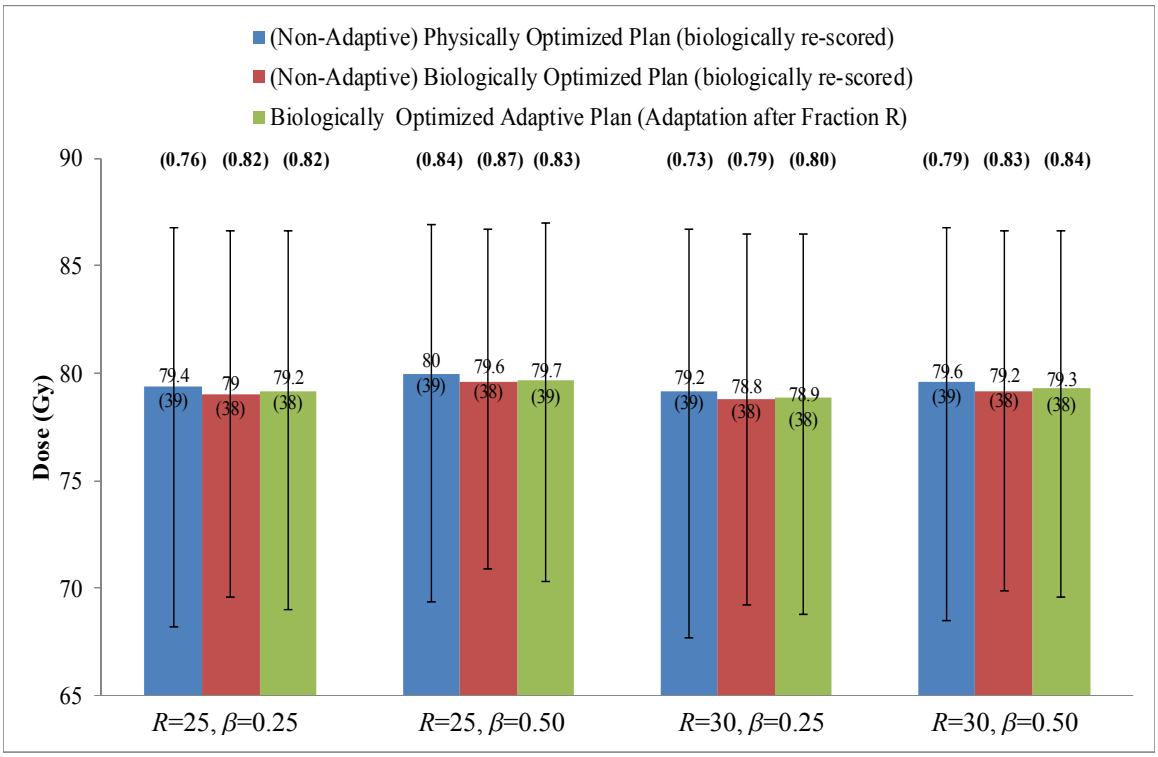

Figure 5.9: Comparison of Treatment Plans across Various Scenarios of Different Re-optimization Point (R) and Re-oxygenation rate (β) on First Base Case (Each column shows the average biological dose with its upper and lower bar indicating the minimum and maximum biological doses achieved, respectively. The numbers in bold show *TCP* values for each plan whereas the numbers in parenthesis below average doses indicate the number of fractions delivered in each plan.)

Although biological re-scoring due to re-oxygenation helps non-adaptive physically optimized plans, non-adaptive biologically optimized plans still do better in terms of *TCP* as Figure 5.9

illustrates. In case of quarter re-oxygenation acquired by a biological image after fraction 25 (R=25, β=0.25), the biologically optimized plan improves the *TCP* by 0.06 (0.76 vs. 0.82). For a different scenario with halfway re-oxygenation after fraction 30 (R=30, β=0.50), the increase in *TCP* is equal to 0.04 (0.79 vs. 0.83). These increases in *TCP* by biologically optimized plans are achieved by due to the significant raises in the minimum biological doses of the physically optimized plans as illustrated in Figure 5.9.

Furthermore, re-optimizing the treatment plan to the changes in the tumor point sensitivity (λ) produces further gains in *TCP*. The biological plan is re-optimized in response to quarter re-oxygenation acquired by an image after fraction 30 (R=30, β=0.25) and improves the *TCP* by 0.01 (0.79 vs. 0.80) due to the small increase in average tumor biological dose (78.8 Gy vs. 78.9 Gy). Similar improvement (0.83 vs. 0.84) is achieved by biologically optimized adaptive plan in case of halfway re-oxygenation after fraction 30 (R=30, β=0.50) due to the small increase in average tumor biological dose (79.2 Gy vs. 79.3 Gy). As a result, these small improvements in *TCP* obtained by adaptive plans increase the *TCP* gain over physically optimized plans (0.73 vs. 0.80 for (R=30, β=0.25), 0.79 vs. 0.84 for (R=30, β=0.50)).

One last note on the results presented in Figure 5.9 is related to the number of fractions delivered in each plan. As demonstrated in the Figure, except for (R=25, β=0.50), the number of fractions delivered in adaptive plans does not change by re-optimization (i.e. 38 fractions are delivered at those scenarios). However, for the specified case, the re-optimization adds a single fraction to the treatment resulting in 39 fractions. The increase in the number of fractions lowers the per-fraction biological effect resulting in a lower *TCP* of 0.83.

5.4.3.2 Second Base Case Results (Red Hypoxia Higher, Homogeneity=0.8)

Results obtained from non-adaptive and adaptive plans computed for the second base case are summarized in Figure 5.10. In re-optimizing the adaptive plans, the objective of maximizing average biological dose over all tumor regions is used with enforcing biological fraction size requirement on all tumor regions in contrast to using the objective of maximizing average biological dose only in red region with physical fraction size requirement on red region (biological fraction requirement elsewhere) in the first epoch optimization. This change was possible due to re-oxygenation of red region avoiding the violation of the biological fraction size requirement caused by higher hypoxia. Lastly, all the adaptive plans computed in this section satisfy both prescribed cumulative and fraction size dose limits.

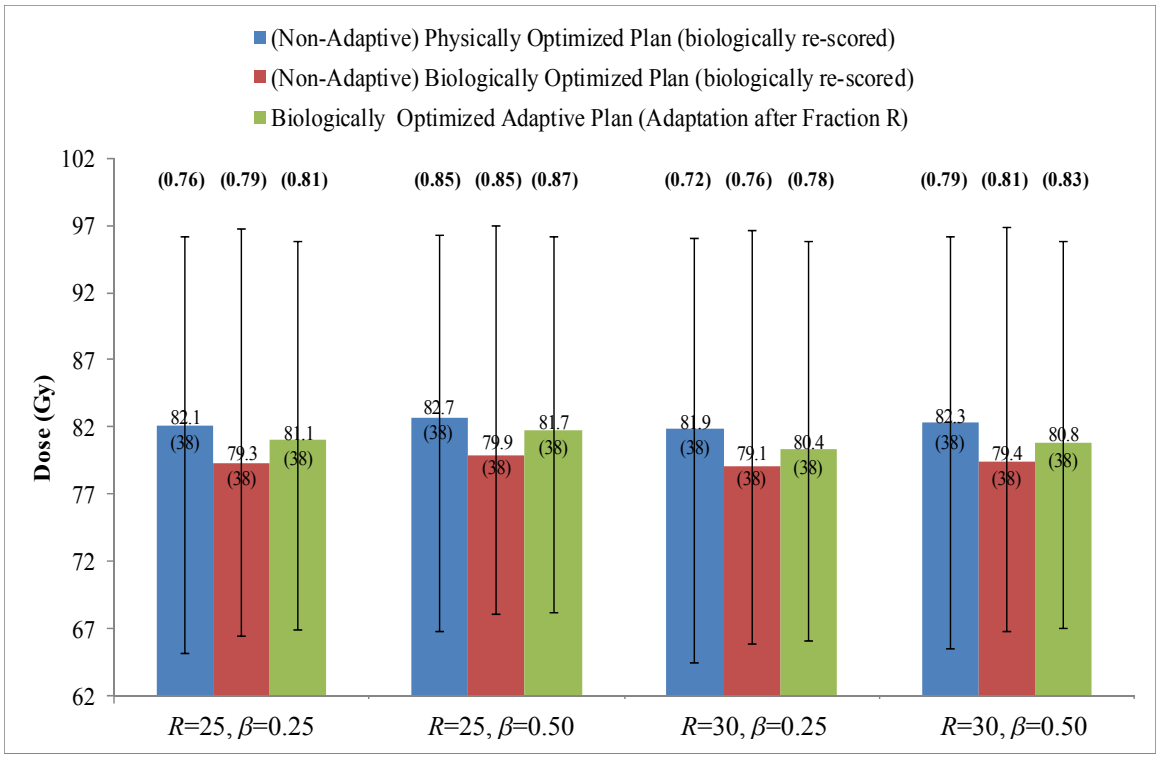

Figure 5.10: Comparison of Treatment Plans across Various Scenarios of Different Re-optimization Point (R) and Re-oxygenation rate (β) on Second Base Case (Each column shows the average biological dose with its upper and lower bar indicating the minimum and maximum biological doses achieved, respectively. The numbers in bold show *TCP* values for each plan whereas the numbers in parenthesis below average doses indicate the number of fractions delivered in each plan.)

Similar to the first base case results presented in the previous section, non-adaptive biologically optimized plans improve over non-adaptive physically optimized plans in case of re-oxygenation as illustrated in Figure 5.10. In case of the quarter re-oxygenation that occurs at the end fraction 25 (R=25, β=0.25), the biological plan improves the *TCP* by 0.03 (0.76 vs. 0.79). For the case of halfway re-oxygenation by the end of fraction 30 (R=30, β=0.50), *TCP* improves from 0.79 to

0.81 corresponding to a 0.02 gain. The improvements in *TCP* are achieved due to the significant increases in the minimum tumor biological doses of the physical plans.

As Figure 5.10 demonstrates, biologically optimized adaptive plans raise *TCP* for all these higher red hypoxia (lower OMF) scenarios by a higher magnitude than the improvements seen in the previous section. It is also important to note that the average tumor biological doses achieved in non-adaptive biologically optimized plans increase by significant amount with the help of re-optimization in adaptive plans. When an acquired biological image after fraction 25 shows quarter re-oxygenation (R=25, β=0.25), re-optimizing the treatment plan to this change improves the average tumor biological dose by 1.8 Gy (79.3 Gy vs. 81.1 Gy) resulting in a 0.02 gain in *TCP* (0.79 vs. 0.81). Similarly, re-optimizing the treatment plan after fraction 25 in response to the halfway re-oxygenation (R=25, β=0.50) improves the average tumor biological dose by 1.8 Gy (79.9 Gy vs. 81.7 Gy) and improves the *TCP* from 0.85 to 0.87. For the scenario considering (R=30, β=0.25), the biological adaptive plan improves the average tumor biological dose obtained from non-adaptive biological plan by 1.3 Gy (79.1 Gy 80.4 Gy) resulting in a 0.02 increase in *TCP* (0.76 vs. 0.78). Lastly, for (R=30, β=0.50), the average tumor biological dose increases by 1.4 Gy (79.4 Gy 80.8 Gy) and the *TCP* rises from 0.81 to 0.83 corresponding to a 0.02 gain.

These gains produced by biologically optimized adaptive plans help achieving more significant improvements over the physically optimized plans. For example, in case of quarter re-oxygenation after fraction 25 (R=25, β=0.25), adaptive plan improves *TCP* of physical plan by 0.05 (0.76 vs. 0.81). In addition, for (R=30, β=0.25), *TCP* increases by 0.06 (0.72 vs. 0.78).

The results presented in Figure 5.9 and 5.10 demonstrate the importance of when to re-optimize (R) and how fast the re-oxygenation occurs (β) for the improvements in *TCP* obtained by biologically optimized adaptive plan. For both first and second base cases, the improvement gets its highest values (0.07 for the first base case and 0.06 for the second base case) at a later re-optimization point (R=30) with lower re-oxygenation rate (β=0.25). The lower re-oxygenation rate acquired by a late image in the treatment leaves a longer period of time where the initial hypoxia values are used in scoring the physical plans which worsens the results. However, a longer period of time with initial hypoxia values favors biologically optimized plans since the initial biology information is dealt with in the optimization allowing the opportunity for the biological plans to show their superiority. In contrast, higher re-oxygenation rate imaged earlier in the treatment (R=25, β=0.50) reduces the *TCP* gain by helping physical plans significantly and removing opportunities for biologically optimized plans by reducing the period of time that more severe hypoxia applies.

Overall, the results presented in Section 5.4.3.1 and 5.4.3.2 show that re-planning the biological plans in response to the changes in the tumor point sensitivity (λ) provides mathematical gains that are enough to be clinically significant. These gains demonstrate the potential benefit of adapting the biological plans to the changing tumor biology, and therefore, prove the concept of achieving higher *TCP* by biologically adaptive planning optimization.

6 Conclusions and Future Research

This research investigates the opportunities that could be created in IMRT planning by incorporating the changes in the tumor geometry and the initial and changing tumor biology into the optimization. Adaptive optimization methodologies were developed that re-optimized the treatment plans in response to the changes in the tumor geometry acquired from updated images against both cumulative and fraction size dose constraints in order to determine the best design for each fraction and the overall treatment.

Using the tumor biology information prior to the treatment, biological optimization models were developed that adjusted the radiation delivered across tumor to the sensitivity of tumor points. Furthermore, biologically optimized plans were designed which were adaptive to the changes in tumor point sensitivity over the course of the treatment.

All the optimization models developed in this research were based on mixed-integer linear programming formulations of the problem with single non-negative integer variable for the number of fractions. Throughout the research, significant attention was given to the feasible fractionation of the treatment plans by explicitly including cumulative and fraction size dose constraints in the formulations.

The contributions of this dissertation research are listed as follows. This research:

- Developed and tested a ratio model with re-scaling approach to deal with fractionation of treatment plans

- Demonstrated the challenge of fractionating adaptive plans re-optimized against only cumulative dose limits using a lung test case simulating real practice
- Showed clinically significant improvements in tumor doses with re-optimizing treatment plans in response to the changes in the tumor geometry over the course of the treatment using two lung test cases simulating real practice (Both cumulative and fraction size dose limits are satisfied in computed adaptive plans.)
- Demonstrated significant improvements in tumor control by including initial tumor hypoxia information into the optimization on a synthetic head and neck test case
- Illustrated the need to explicitly enforce integer fraction size dose constraints in such biological optimization
- Showed mathematical gains in tumor control and average tumor doses that are enough to be clinically important by adapting treatment plans to the changes in the tumor hypoxia throughout the treatment (Both cumulative and fraction size dose limits are satisfied in computed adaptive plans.)
- Displayed the volatility of tumor control probability to the changes in the tumor hypoxia values

For future research on adaptive planning optimization with changes in the tumor geometry, the currently used tumor homogeneity dose requirement over the course of the treatment can be extended by introducing tumor dose homogeneity limit for each epoch which will make the computed plans clinically more applicable. Modeling this requirement in the re-optimization formulation will make sure that all regions of the tumor receive a homogeneous dose distribution not only over the entire treatment but also over each epoch. Another extension of this study

might be on improving the quality of the updated plans received from re-optimization. At present, the treatment plan is re-optimized based on the latest tumor geometry, so no future changes on the tumor geometry are predicted. Information on the future tumor geometry received by using a predictive modeling can be incorporated into the re-optimization formulation which might improve the plan delivered after adaptation. Lastly, although incorporating dose-volume constraints into the optimization increases the computational complexity of the models (Lee *et al*., 2006; Tuncel *et al*. 2010), the trade-off between the quality of the adaptive plans with dose-volume constraints and the computational time to generate them should be investigated.

Research on biologically guided radiation therapy planning optimization can be extended in several ways. As more test cases with tumor hypoxia information become available in the future, the biological optimization models developed in this research can be further tested and the improvements in the tumor control can be evaluated. In addition, in parallel to the clinical research on quantifying change in the hypoxia with respect to dose, more reliable adaptive scenarios could be generated and the proposed adaptive planning optimization methodology could be tested with multiple scenarios.

7 References

Acosta, R., Brick, W., Hanna, A., Holder, A., Lara, D., McQuilen, G., Nevin, D., Uhlig, P. and Salter, B. (2009) Radiotherapy optimAl Design: An academic radiotherapy treatment design system in *Operations Research and Cyber-Infrastructure*, *vol. 47*, Chinneck, J.W., Kristjansson, B. and Saltman, M.J. (eds), Springer, NY, pp 401-425.

American Cancer Society, Cancer Facts & Figures, 2011.

Blanco, A.I. and Chao, K.S.C. (2002) Intensity-modulated radiation therapy and protection of normal tissue function in head and neck cancer in *Principles and Practice of Radiation Oncology Updates*, *vol. 3*, Perez, C. A. and Brady. L.W. (eds), Lippincott Williams & Wilkins Healthcare, NY, pp. 2-12.

Bortfeld, T., Chan, T.C.Y, Trofimov, A. and Tsitsiklis, J.N. (2008) Robust management of motion uncertainty in intensity-modulated radiation therapy. *Operations Research*, **56**, 1461-1473.

Bosmans, G., Van Baardwijk, A., Dekker, A., Ollers, M., Boersma, L., Minken, A., Lambin, P. and De Ruysscher, D. (2006) Intra-patient variability of tumor volume and tumor motion during conventionally fractionated radiotherapy for locally advanced non-small-cell lung cancer: A prospective study. *International Journal of Radiation Oncology Biology Physics*, **66**, 748-753.

Bradley, J.D., Hope, A., El Naqa, I., Apte, A., Lindsay, P.E., Bosch, W., Matthews, J., Sause, W., Graham, M.V. and Deasy, J.O. (2007) A normogram to predict radiation pneumonitis derived from a combined analysis of RTOG 9311 and institutional data. *International Journal of Radiation Oncology Biology Physics*, **69**, 985-992.

CERR: A Computational Environment for Radiotherapy Research. Washington University in St. Louis. http://radium.wustl.edu/cerr

Chen, G.P., Ahunbay, .E, Schultz, C. and Li, X.A. (2007) Development of an inverse optimization package to plan nonuniform dose distributions based on spatially inhomogeneous radiosensitivity extracted from biological images. *Medical Physics*, **34**, 1198-1205.

Cho, P.S., Lee, S., Marks, R.J., Oh, S., Sutlief, S.G. and Phillips, M.H. (1998) Optimization of intensity modulated beams with volume constraints using two methods: Cost function minimization and projections onto convex sets. *Medical Physics*, **25**, 435-443.

Chu, M., Zinchenko, Y., Henderson, S.H. and Sharpe, M.B. (2005) Robust optimization for intensity modulated radiation therapy treatment planning under uncertainty. *Physics in Medicine and Biology*, **50**, 5463-5477.

Deng, G. and Ferris, M.C. (2008) Neuro-dynamic programming for fractionated radiotherapy planning. *Optimization in Medicine*, **12**, 47-70.

Dink, D. (2005) *Ph.D. Dissertation: Approaches to 4-D Intensity Modulated Radiation Therapy Planning with Fraction Constraints*. School of Industrial Engineering, Purdue University.

Dink, D., Langer, M., Orcun, S., Pekny, J., Rardin, R., Reklaitis, G. and Saka, B. (2011) IMRT optimization with both fractionation and cumulative constraints. Accepted by *American Journal of Operations Research*.

Eschmann, S.M., Paulsen, F., Bedeshem, C., Machulla, H., Hehr, T., Bamberg, M. and Bares, R. (2007) Hypoxia-imaging with ^{18}F-Misanidazole and PET: Changes of kinetics during radiotherapy of head-and-neck cancer. *Radiotherapy and Oncology*, **83**, 406-410.

Ezzel. G.A. (1996) Genetic and geometric optimization of three-dimensional radiation therapy treatment planning. *Medical Physics*, **23**, 293-305.

Ferris, M.C. and Voelker, M.M. (2004) Fractionation in radiation treatment planning. *Mathematical Programming*, **101**, 387-413.

Goitein, M. (1986) Causes and consequences of inhomogeneous dose distributions in radiation therapy. *International Journal of Radiation Oncology Biology Physics*, **12**,701-704.

GRATIS. Sherouse Systems Inc. http://www.gwsherouse.com

Haasbek, C.J.A., Lagerwaard, F.J., Cuijpers, J.P., Slotman, B.J. and Senan, S. (2007) Is adaptive treatment planning required for stereotactic radiotherapy of stage I non-small-cell lung cancer? *International Journal of Radiation Oncology Biology Physics*, **67**, 1370-1374.

Hall, E. Radiobiology for the radiologist. 4th ed. Philadelphia: JB Lippincott; 1994.

Hristov, D.H. and Fallone, B.G. (1998) A continuous penalty function method for inverse treatment planning. *Medical Physics*, **25**, 208-223.

ICRU-50: (1993) Prescribing, recording and reporting photon beam therapy: International Commission on Radiation Units and Measurements, Bethesda, MD.

ICRU-62: (1999) Prescribing and reporting photon beam therapy (supplement to ICRU report 50): International Commission on Radiation Units and Measurements, Bethesda,MD.

Kim, Y. and Tome, W. (2006) Risk-adaptive optimization: Selective boosting of high-risk tumor subvolumes. *International Journal of Radiation Oncology Biology Physics*, **66**, 1528-42.

Kupelian, P.A., Ramsey, C., Meeks, S.L., Willoughby, T.R., Forbes, A., Wagner, T.H. and Langen, K.M. (2005) Serial megavoltage CT imaging during external beam radiotherapy for non-small cell lung cancer: Observations on tumor regression during treatment. *International Journal of Radiation Oncology Biology Physics*, **63**, 1024-1028.

Kwa, S.L., Lebesque, J.V., Theuws, J.C., Marks, L.B., Munley, M.T., Bentel, G., Oetzel, D., Spahn, U., Graham, M.V., Drzymala, R.E., Purdy, J.A., Lichter, A.S., Martel, M.K. and Ten

Haken, R.K. (1998) Radiation pneumonitis as a function of mean dose: An analysis of pooled data of 540 patients. *International Journal of Radiation Oncology Biology Physics*, **42**, 1–9.

Langer, M., Brown, R., Urie, M., Leong, J., Stracher, M. and Shapiro, J. (1990) Large scale optimization of beam weights under dose-volume restrictions. *International Journal of Radiation Oncology Biology Physics*, **18**, 887–993.

Langer, M., Kijewski, P., Brown, R. and Ha, C. (1991) The effect on minimum tumor dose of restricting target-dose inhomogeneity in optimized three-dimensional treatment of lung cancer. *Radiotherapy and Oncology*, **21**, 245–256.

Langer, M., Lee, E.K., Deasy, J.O., Rardin R.L. and Deye, J.A. (2003) Operations research applied to radiotherapy, An NCI-NSF-Sponsored Workshop. *International Journal of Radiation Oncology Biology Physics*, **57**, 762-768.

Langer, M., Morrill, S., Brown, R., Lee, O. and Lane, R. (1996) A comparison of mixed-integer programming and fast simulated annealing for optimizing beam weights in radiation therapy. *Medical Physics*, **23**, 957–964.

Langer, M., Morrill, S., Brown, R., Lee, O. and Lane, R. (1996) A genetic algorithm for generating beam weights. *Medical Physics*, **23**, 965-971.

Lee, E.K, Fox, T. and Crocker, I. (2003) Integer programming applied to intensity-modulated radiation treatment planning. *Annals of Operations Research*, **119**, 165-181.

Lee, E.K., Fox, T. and Crocker, I. (2006) Simultaneous beam geometry and intensity map optimization in intensity-modulated radiation therapy. *International Journal of Radiation Oncology Biology Physics*, **64**, 301-320.

Lee, N., Nehmeh, S., Schoder, H., Fury, M., Chan, K., Ling, C.C. and Humm J. (2009) Prospective trial incorporating pre-/mid-treatment [^{18}F]-Misonidazole positron emission tomography for head-and-neck cancer patients undergoing concurrent chemoradiotherapy. *International Journal of Radiation Oncology Biology Physics*, **75**, 101-108.

Levin-Plotnik, D. and Hamilton, R.J. (2004) Optimization of tumor control probability for heterogeneous tumors in fractionated radiaotherapy. *Physics in Medicine and Biology*, **49**, 407-424.

Li, X. A., Wang, J. Z., Jursinic, P. A., Lawton, C. A. and Wang, D. (2005) Dosimetric advantages of IMRT simultaneous integrated boost for high-risk prostate cancer. *International Journal of Radiation Oncology Biology Physics,* **61,** 1251–1257.

Ling, C.C. and Li, X. (2005) Over the next decade the success of radiation treatment planning will be judged by the immediate biological response of tumor cells rather than by surrogate measures such as dose maximization and uniformity. *Medical Physics*, **32**, 2189-2192.

Lu, X.Q. and Chin, L.M. (1993) Sampling techniques for the evaluation of treatment plans. *Medical Physics*, **20**, 151-161.

Mageras, G.S. and Mohan, R. (1993) Application of fast simulated annealing to optimization of conformal radiation treatments. *Medical Physics*, **20**, 639-647.

Morril, S.M., Lane, R.G. and Rosen, I.I. (1990) Constrained simulated annealing for optimized radiation therapy. *Computer Methods and Programs in Biomedicine*, **33**,135-144.

Morrill, S.M., Rosen, I.I., Lane, R.G. and Belli, J.A. (1990) The influence of dose constraint point placement on optimized radiation therapy treatment planning. *International Journal of Radiation Oncology Biology Physics,* **19**, 129-141.

Niemierko, A. and Goitein, M. (1990) Random sampling for evaluating treatment plans. *Medical Physics*, **17**, 753-762.

Niemierko, A. and Goitein, M. (1993) Comments on "Sampling techniques for the evaluation of treatment plans". *Medical Physics*, **20**, 1377-1380.

Popple, R.A., Prellop, P.B., Spencer, S.A., De Los Santos, J.F., Duan, J., Fiveash, J.B. and Brezovich, I. A. (2005) Simultaneous optimization of sequential IMRT plans. *Medical Physics,* **32,** 3257-3266.

Popple, R.A., Ove, R. and Shen, S. (2002) Tumor control probability for selective boosting of hypoxic subvolumes, including the effect of reoxygenation. *International Journal of Radiation Oncology Biology Physics*, **54**, 921-927.

Preciado-Walters, F., Rardin, R.L., Langer, M.P. and Thai, V. (2004) A coupled column generation, mixed integer approach to optimal planning of intensity modulated radiation therapy for cancer. *Mathematical Programming*, **101**, 319-338.

Preciado-Walters, F., Langer, M.P., Rardin, R.L. and Thai, V. (2006) Column generation for IMRT cancer therapy optimization with implementable segments. *Annals of Operations Research*, **148**, 65-79.

Ramsey, C.R., Langen, K.M., Kupelian, P.A., Scaperoth, D.D., Meeks, S.L., Mahan, S.L. and Seibert, R.M. (2006) A technique for adaptive image-guided helical tomotherapy for lung cancer. *International Journal of Radiation Oncology Biology Physics*, **64**, 1237-1244.

Rischin, D., Peters, L., Hicks, R., Hughes, P., Fisher, R., Hart, R., Sexton, M., D'Costa L. and von Roemeling R. (2001) Phase I trial of concurrent tirapazamine, cisplatin, and radiotherapy in patients with advanced head and neck cancer. *Journal of Clinical Oncology*, **19**, 535-542.

Romeijn, H.E., Ahuja, R.K., Dempsey, J.F., Kumar, A. and Li, J.G. (2003) A novel linear programming approach to fluence map optimization for intensity modulated radiation treatment planning. *Physics in Medicine and Biology*, **48**, 3521-3542.

Romeijn, H.E, Ahuja, R.K. and Dempsey, J.F. (2006) A new linear programming approach to radiation therapy treatment planning problems. *Operations Research*, **54**, 201-216.

Romeijn, H.E., Ahuja, R.K., Dempsey, J.F. and Kumar, A. (2005) A column generation approach to radiation therapy treatment planning using aperture modulation. *SIAM Journal on Optimization*, **15**, 838-862.

Ruggieri, R., Naccarato, S. and Nahum, A.E. (2010) Severe hypofractionation: Non-homogeneous tumour dose delivery can counteract tumour hypoxia. *Acta Oncologica*, **49**, 1304-1314.

Saka, B., Rardin, R. and Langer, M. (2010) The fractionation challenge in adaptive intensity modulated radiation therapy planning. In revision.

Saka, B., Rardin, R., Langer, M. and Dink, D. (2011) Adaptive intensity modulated radiation therapy planning optimization with changing tumor geometry and fraction size limits. Accepted by *IIE Transactions on Healthcare Systems Engineering*.

Siker, M.L., Tome, W.A. and Mehta, M.P. (2006) Tumor volume changes on serial imaging with megavoltage CT for non-small lung cancer during intensity-modulated radiotherapy: How reliable, consistent, and meaningful is the effect? *International Journal of Radiation Oncology Biology Physics*, **66**, 135-141.

Sir, M.Y., Pollock, S.M., Epelman, M.A., Lam, K.L. and Ten Haken, R.K. (2006) Ideal spatial radiotherapy dose distributions subject to positional uncertainties. *Physics in Medicine and Biology*, **51**, 6329-6347.

Sovik, A., Malinen, E., Skogmo, H.K., Bentzen, S.M., Bruland, O.S. and Olsen, D.R. (2007) Radiotherapy adapted to spatial and temporal variability in tumor hypoxia. *International Journal of Radiation Oncology Biology Physics*, **68**, 1496-1504.

Spirou, S.V. and Chui, C.S. (1998) A gradient inverse planning algorithm with dose-volume constraints. *Medical Physics*, **25**, 321-333.

Stewart, R.D. and Li, X.A. (2007) BGRT: Biologically guided radiation therapy-The future is fast approaching. *Medical Physics*, **34**, 3739-3751.

Strigari, L., D'Andrea, M., Abate, A. and Benassi, M. (2008) A heterogeneous dose distribution in simultaneous integrated boost: the role of the clonogenic cell density on the tumor control probability. *Physics in Medicine and Biology*, **53**, 5257-5273.

Titz, B. and Jeraj, B. (2008) An imaging-based tumor growth and treatment response model: Investigating the effect of tumor oxygenation on radiation therapy response. *Physics in Medicine and Biology,* **53**, 4471-4488.

Tuncel, A., Preciado-Walters F., Rardin R.L., Langer, M. and Richard, J-P.P. (2010) Strong valid inequalities for fluence map optimization problem under dose-volume restrictions. *Annals of Operations Research,* DOI: 10.1007/s10479-010-0759-1.

Underberg, R.W.M., Lagerwaard, F.J., Van Tinteren, H., Cuijpers, J.P., Slotman, B.J. and Senan, S. (2006) Time trends in target volumes for stage I non-small-cell lung cancer after

stereotactic radiotherapy. *International Journal of Radiation Oncology Biology Physics*, **64**, 1221-1228.

Van Baardwijk, A., Bosmans, G., Boersma, L., Wanders, S., Dekker, A., Dingemans, A.M.C., Bootsma, G., Geraedts, W., Pitz, C., Simons, J., Lambin, P. and De Ruysscher, D. (2008) Individualized radical radiotherapy of non-small-cell lung cancer based on normal tissue dose constraints: a feasibility study. *International Journal of Radiation Oncology Biology Physics*, **71**, 1394-1401.

Van Baardwijk, A., Wanders, S., Boersma, L., Borger, J., Ollers, M., Dingemans, A.M.C., Bootsma, G., Geraedts, W., Pitz, C., Lunde, R., Lambin, P. and De Ruysscher, D. (2010) Mature results of an individualized radiation dose prescription study based on normal tissue constraints in stages I to III non-small-cell lung cancer. *Journal of Clinical Oncology*, **28**, 1380-1386.

Webb, S. (2003) Historical perspective on IMRT in *Intensity-Modulated Radiation Therapy-The State of the Art*, Palta, J.R. and Mackie, T.R. (eds) Medical Physics Publishing, Madison, WI, pp. 1-23.

Webb S. (1991) Optimization by simulated annealing of three-dimensional conformal treatment planning for radiation fields defined by a multileaf collimator. *Physics in Medicine and Biology*, **34**, 1201-1226.

Wiersma, R.D., Mao, W. and Xing, L. (2008) Combined kV and MV imaging for real time tracking of implanted fiducial markers. *Medical Physics*, **35**, 1191-1198.

Woodford, C., Yartsev, S., Dar, A.R., Bauman, G. and Van Dyk, J. (2007) Adaptive radiotherapy planning on decreasing gross tumor volumes as seen on megavoltage computed tomographic images. *International Journal of Radiation Oncology Biology Physics*, **69**, 1316–1322.

Wu, Q., Manning, M., Schmidt-Ulrich, R. and Mohan, R. (2000) The potential for sparing of parotids and escalation of biologically effective dose with intensity-modulated radiation treatments of head and neck cancers: a treatment design study, *International Journal of Radiation Oncology Biology Physics,* **46**, 195-205.

Wu, Q, and Mohan, R. (2000) Algorithms and functionality of an intensity modulated radiotherapy optimization system. *Medical Physics*, **27**, 701-771.

Wu, X., Zhu, Y., Dai, J. and Wang, Z. (2000) Selection and determination of beam weights based on genetic algorithms for conformal radiotherapy treatment planning. *Physics in Medicine and Biology*, **45**, 2547-2558.

Wu, C., Jeraj, R., Olivera, G.H. and Mackie, T.R. (2002) Re-optimization in adaptive radiotherapy. *Physics in Medicine and Biology*, **47**, 3181-3195.

Wu, Q., Ivaldi, G., Liang, J., Lockman, D., Yan, D. and Martinez, A. (2006) Geometric and dosimetric evaluations of an online image guidance strategy for 3D-CRT of prostate cancer. *International Journal of Radiation Oncology Biology Physics*, **64**, 1596-1609.

Wu, Q.J., Thongphiew, D., Wang, Z., Mathayomchan, B., Chankong, V., Yoo, S., Lee, W.R. and Yin, F. (2008) On-line reoptimization of prostate IMRT plans for adaptive radiation therapy. *Physics in Medicine and Biology*, **53**, 673-691.

Yan, D. and Lockman, D. (2001) Organ/patient geometric variation in external beam radiotherapy and its effects. *Medical Physics,* **28**, 593-602.

Yan, D., Lockman, D., Martinez, A., Wong, J., Brabbins, D., Vicini, F., Liang, J. and Kestin, L. (2005) Computed tomography guided management of interfractional patient variation. *Seminars in Radiation Oncology*, **15**, 168-179.

Yang, Y. and Xing, L. (2005) Towards biologically conformal radiation therapy (BCRT): Selective IMRT dose escalation under the guidance of spatial biology distribution. *Medical Physics*, **32**, 1473-1484.

APPENDICES

Appendix A[3]: No Adaptation vs. Two-Epoch Adaptation Results for the Lung1 Test Case (The uniform fractionation model solved in the optimization)

Structure	Dose Statistics (Gy)	No Adaptation (No Boost)	No Adaptation (with Boost)			Two-Epoch Adaptation		
		Total	Main Stage	Boost Stage	Total	Epoch 1	Epoch 2 (with Boost)	Total
Tumor	Max. Dose	75.0 [2.14]	53.6 [2.14]	24.3 [2.43]	75.3	53.6 [2.14]	29.6 [2.47]	80.5
	Min. Dose	71.3 [2.04]	50.9 [2.04]	20.0 [2.00]	71.6	50.9 [2.04]	24.0 [2.00]	76.5
	Avg. Dose	72.9 [2.08]	52.1 [2.08]	21.3 [2.13]	73.4	52.1 [2.08]	26.6 [2.22]	78.7
Removed Tumor Points	Max. Dose	-	-	-	-	-	27.2 [2.26]	80.5
	Min. Dose	-	-	-	-	-	6.4 [0.53]	57.8
	Avg. Dose	-	-	-	-	-	16.1 [1.34]	68.2
PTV2	Max. Dose	75.0 [2.14]	53.6 [2.14]	23.4 [2.34]	75.3	53.6 [2.14]	29.8 [2.48]	80.5
	Min. Dose	70.0 [2.00]	50.0 [2.00]	9.0 [0.9]	59.1	50.0 [2.00]	6.4 [0.53]	56.6
	Avg. Dose	72.7 [2.08]	51.9 [2.08]	21.0 [2.10]	72.9	51.9 [2.08]	22.5 [1.87]	74.4
Right Lung	Max. Dose	73.2 [2.09]	52.3 [2.09]	21.0 [2.10]	73.3	52.3 [2.09]	24.2 [2.02]	75.6
	Avg. Dose	25.0 [0.71]	17.9 [0.71]	7.1 [0.71]	25.0	17.9 [0.71]	7.1 [0.60]	25.0
Left Lung	Max. Dose	62.8 [1.79]	44.8 [1.79]	16.1 [1.61]	58.3	44.8 [1.79]	16.6 [1.38]	55.7
	Avg. Dose	22.8 [0.65]	16.3 [0.65]	6.7 [0.67]	23.0	16.3 [0.65]	7.1 [0.59]	23.4
Heart	Max. Dose	70.2 [2.01]	50.2 [2.01]	18.9 [1.89]	69.1	50.2 [2.01]	25.2 [2.10]	75.2
	Avg. Dose	24.2 [0.69]	17.3 [0.69]	7.1 [0.71]	24.4	17.3 [0.69]	7.3 [0.61]	24.6
Esophagus	Max. Dose	60.6 [1.73]	43.3 [1.73]	17.2 [1.72]	60.4	43.3 [1.73]	20.4 [1.70]	61.1
	Avg. Dose	27.6 [0.79]	19.7 [0.79]	7.7 [0.77]	27.4	19.7 [0.79]	8.9 [0.74]	28.6
Not Otherwise Specified	Max. Dose	73.5 [2.10]	52.5 [2.10]	21.0 [2.10]	73.5	52.5 [2.10]	25.2 [2.10]	77.7
	Avg. Dose	24.6 [0.70]	17.5 [0.70]	7.1 [0.71]	24.6	17.5 [0.70]	7.6 [0.63]	25.2
Spinal Cord	Max. Dose	45.0 [1.29]	32.1 [1.29]	15.5 [1.55]	45.0	32.1 [1.29]	17.7 [1.48]	45.0
	Avg. Dose	23.9 [0.68]	17.1 [0.68]	6.92 [0.69]	24.0	17.1 [0.68]	7.77 [0.65]	24.9
# of Fractions Given		35	25	10	35	25	12	37

[3] The fraction size doses are given in brackets below the cumulative doses. PTV2 represents the secondary target.

Appendix B[4]: No Adaptation vs. Two-Epoch Adaptation Results for the Lung1 Test Case (The ratio model solved in the optimization and the optimized doses rescaled if necessary)

Structure	Dose Statistics (Gy)	No Adaptation (No Boost)	No Adaptation (with Boost)			Two-Epoch Adaptation		
		Total	Main Stage	Boost Stage	Total	Epoch 1	Epoch 2 (with Boost)	Total
Tumor	Max. Dose	73.6 [2.17]	54.1 [2.17]	22.1 [2.21]	75.3	54.1 [2.17]	28.9 [2.41]	80.4
	Min. Dose	69.9 [2.06]	51.4 [2.06]	20.0 [2.00]	71.5	51.4 [2.06]	24.0 [2.00]	76.4
	Avg. Dose	71.6 [2.11]	52.7 [2.11]	20.7 [2.07]	73.4	52.7 [2.11]	25.6 [2.13]	78.3
Removed Tumor Points	Max. Dose	-	-	-	-	-	26.7 [2.22]	80.4
	Min. Dose	-	-	-	-	-	6.0 [0.50]	57.7
	Avg. Dose	-	-	-	-	-	14.8 [1.24]	67.5
PTV2	Max. Dose	73.6 [2.17]	54.1 [2.17]	22.2 [2.22]	75.3	54.1 [2.17]	28.9 [2.41]	80.4
	Min. Dose	68.0 [2.00]	50 [2.00]	9.7 [0.97]	59.7	50.0 [2.00]	6.0 [0.50]	56.0
	Avg. Dose	71.3 [2.10]	52.4 [2.10]	20.4 [2.04]	72.9	52.4 [2.10]	21.6 [1.80]	74.0
Right Lung	Max. Dose	71.4 [2.10]	52.5 [2.10]	21.0 [2.10]	73.5	52.5 [2.10]	23.2 [1.93]	75.1
	Avg. Dose	24.5 [0.72]	18.0 [0.72]	6.9 [0.69]	25.0	18.0 [0.72]	6.7 [0.56]	24.7
Left Lung	Max. Dose	55.0 [1.62]	40.4 [1.62]	15.3 [1.53]	55.7	40.4 [1.62]	14.8 [1.24]	52.8
	Avg. Dose	22.5 [0.66]	16.5 [0.66]	6.5 [0.65]	23.0	16.5 [0.66]	6.5 [0.54]	23.0
Heart	Max. Dose	69.5 [2.04]	51.1 [2.04]	19.7 [1.97]	70.6	51.1 [2.04]	25.2 [2.10]	76.1
	Avg. Dose	23.7 [0.70]	17.5 [0.70]	7.0 [0.70]	24.4	17.5 [0.70]	7.0 [0.58]	24.4
Esophagus	Max. Dose	58.3 [1.72]	42.9 [1.72]	16.1 [1.61]	58.9	42.9 [1.72]	19.0 [1.58]	60.0
	Avg. Dose	27.3 [0.8]	20.1 [0.80]	7.5 [0.75]	27.6	20.1 [0.80]	7.8 [0.65]	27.8
Not Otherwise Specified	Max. Dose	71.4 [2.10]	52.5 [2.10]	21.0 [2.10]	73.5	52.5 [2.10]	25.2 [2.10]	77.7
	Avg. Dose	24.2 [0.71]	17.8 [0.71]	6.9 [0.69]	24.7	17.8 [0.71]	7.2 [0.60]	25.0
Spinal Cord	Max. Dose	44.1 [1.30]	32.4 [1.30]	15.3 [1.53]	44.9	32.4 [1.30]	15.0 [1.25]	44.5
	Avg. Dose	23.4 [0.69]	17.2 [0.69]	6.8 [0.68]	24.0	17.2 [0.69]	7.0 [0.59]	24.2
# of Fractions Given		34	25	10	35	25	12	37

[4] The fraction size doses are given in brackets below the cumulative doses. PTV2 represents the secondary target.

Appendix C[5]: No Adaptation vs. Two-Epoch Adaptation Results for the CERRLung Test Case (The ratio model solved in the optimization and the optimized doses rescaled if necessary)

Structure	Dose Statistics (Gy)	No Adaptation (No Boost)	No Adaptation (with Boost)			Two-Epoch Adaptation		
		Total	Main Stage	Boost Stage	Total	Epoch 1	Epoch 2 (with Boost)	Total
Tumor	Max. Dose	78.0 [2.17]	54.1 [2.17]	34.4 [2.29]	86.2	54.1 [2.17]	38.7 [2.28]	90.6
	Min. Dose	74.1 [2.06]	51.4 [2.06]	30 [2.0]	81.9	51.4 [2.06]	34 [2.0]	86.0
	Avg. Dose	75.9 [2.11]	52.7 [2.11]	31.5 [2.1]	84.2	52.7 [2.11]	35.8 [2.1]	88.5
Removed Tumor Points	Max. Dose	-	-	-	-	-	37.7 [2.22]	90.6
	Min. Dose	-	-	-	-	-	10.5 [0.62]	62.5
	Avg. Dose	-	-	-	-	-	31.7 [1.87]	84.5
PTV2	Max. Dose	78.0 [2.17]	54.1 [2.17]	34.9 [2.33]	86.2	54.1 [2.17]	39.3 [2.31]	90.6
	Min. Dose	72.0 [2.0]	50 [2.0]	12.7 [0.84]	62.7	50 [2.0]	3.6 [0.21]	53.6
	Avg. Dose	75.1 [2.09]	52.1 [2.09]	28.7 [1.91]	80.9	52.1 [2.09]	30.6 [1.8]	82.7
Right Lung	Max. Dose	75.6 [2.1]	52.5 [2.1]	31.5 [2.1]	84.0	52.5 [2.1]	35.7 [2.1]	88.2
	Avg. Dose	16.9 [0.47]	11.7 [0.47]	5 [0.33]	16.7	11.7 [0.47]	5.1 [0.3]	16.9
Left Lung	Max. Dose	75.6 [2.1]	52.5 [2.1]	31.5 [2.1]	82.5	52.5 [2.1]	33.2 [1.95]	82.0
	Avg. Dose	9.7 [0.27]	6.7 [0.27]	2.7 [0.18]	9.5	6.7 [0.27]	2.6 [0.15]	9.3
Heart	Max. Dose	72.7 [2.02]	50.5 [2.02]	17.1 [1.14]	67.6	50.5 [2.02]	20.7 [1.22]	68.2
	Avg. Dose	4.2 [0.12]	2.9 [0.12]	0.9 [0.06]	3.9	2.9 [0.12]	1 [0.06]	4.0
Esophagus	Max. Dose	75.6 [2.1]	52.5 [2.1]	22.9 [1.53]	75.3	52.5 [2.1]	20.3 [1.19]	72.7
	Avg. Dose	16.6 [0.46]	11.5 [0.46]	3.2 [0.21]	14.7	11.5 [0.46]	3 [0.17]	14.5
Not Otherwise Specified	Max. Dose	75.6 [2.1]	52.5 [2.1]	31.5 [2.1]	84.0	52.5 [2.1]	35.7 [2.1]	88.2
	Avg. Dose	7.5 [0.21]	5.2 [0.21]	2.3 [0.15]	7.5	5.2 [0.21]	2.4 [0.14]	7.6
Spinal Cord	Max. Dose	10.4 [0.29]	7.2 [0.29]	6.8 [0.45]	10.4	7.2 [0.29]	7.7 [0.45]	11.3
	Avg. Dose	1.6 [0.04]	1.1 [0.04]	0.6 [0.04]	1.7	1.1 [0.04]	0.5 [0.03]	1.6
# of Fractions Given		36	25	15	40	25	17	42

[5] The fraction size doses are given in brackets below the cumulative doses. PTV2 represents the secondary target.

Appendix D[6]: Three-Epoch Adaptation Results for the Lung1 Case (Adapted after fraction 10 and 25, the uniform fractionation model solved in the re-optimization)

Structure	Dose Statistics (Gy)	Same plan is delivered for the first epoch	The original tumor shrinks 20% towards the residual tumor after fraction 25 during the first 10 fractions			The original tumor shrinks 50% towards the residual tumor after fraction 25 during the first 10 fractions			The original tumor shrinks 80% towards the residual tumor after fraction 25 during the first 10 fractions		
		Epoch 1	Epoch 2	Epoch 3 (with Boost)	Total	Epoch 2	Epoch 3 (with Boost)	Total	Epoch 2	Epoch 3 (with Boost)	Total
Tumor	Max. Dose	21.4 [2.14]	32.3 [2.15]	29.6 [2.47]	80.6	32.8 [2.19]	29.5 [2.46]	81.0	33.5 [2.23]	29.4 [2.45]	81.2
	Min. Dose	20.4 [2.04]	30.5 [2.03]	24.0 [2.00]	76.5	30.6 [2.04]	24 [2]	76.9	31 [2.06]	24.0 [2.00]	77.1
	Avg. Dose	20.8 [2.08]	31.4 [2.09]	26.6 [2.22]	78.8	31.7 [2.11]	26.6 [2.22]	79.2	32 [2.13]	26.5 [2.21]	79.3
Removed Tumor Points	Max. Dose	-	32.2 [2.15]	27.1 [2.26]	80.6	32.7 [2.18]	27.2 [2.27]	81.0	33.4 [2.22]	27.3 [2.28]	81.2
	Min. Dose	-	30.0 [2.00]	6.5 [0.55]	57.2	30.0 [2.00]	6.5 [0.54]	57.2	30.0 [2.00]	6.5 [0.55]	57.2
	Avg. Dose	-	31.0 [2.07]	16.2 [1.35]	68.3	31.2 [2.08]	16.2 [1.35]	68.5	31.2 [2.08]	16.2 [1.35]	68.4
PTV2	Max. Dose	21.4 [2.14	32.3 [2.15]	29.9 [2.49]	80.6	32.9 [2.19]	29.7 [2.47]	81.0	33.2 [2.22]	29.6 [2.47]	81.2
	Min. Dose	20.0 [2.00]	30.0 [2.00]	6.5 [0.54]	56.6	30.0 [2.00]	6.4 [0.54]	56.5	30.0 [2.00]	6.5 [0.54]	56.6
	Avg. Dose	20.8 [2.08]	31.2 [2.08]	22.5 [1.88]	74.5	31.5 [2.1]	22.6 [1.88]	74.8	31.6 [2.11]	22.5 [1.87]	74.8
Right Lung	Max. Dose	20.9 [2.09]	31.4 [2.10]	24.2 [2.02]	75.5	31.3 [2.08]	24.7 [2.06]	76.0	31.4 [2.1]	24.6 [2.05]	76.3
	Avg. Dose	7.1 [0.71]	10.7 [0.71]	7.1 [0.6]	25.0	10.7 [0.71]	7.1 [0.6]	25.0	10.7 [0.71]	7.1 [0.6]	25.0
Left Lung	Max. Dose	17.9 [1.79]	25.9 [1.73]	16.7 [1.39]	54.1	24.7 [1.64]	16.2 [1.35]	52.3	23.4 [1.56]	16.4 [1.36]	51.9
	Avg. Dose	6.5 [0.65]	9.8 [0.65]	7.2 [0.6]	23.5	9.8 [0.66]	7.1 [0.59]	23.5	9.8 [0.65]	7.1 [0.59]	23.4
Heart	Max. Dose	20.1 [2.01]	30.4 [2.03]	25.2 [2.1]	75.5	31.2 [2.08]	25.2 [2.1]	76.4	31.4 [2.09]	25.2 [2.1]	76.6
	Avg. Dose	6.9 [0.69]	10.4 [0.69]	7.3 [0.61]	24.6	10.4 [0.69]	7.3 [0.61]	24.7	10.4 [0.69]	7.3 [0.61]	24.6
Esoph.	Max. Dose	17.3 [1.73]	25.8 [1.72]	20.5 [1.71]	61.2	25.6 [1.71]	20.6 [1.72]	61.6	27.3 [1.82]	20.4 [1.7]	61.4
	Avg. Dose	7.9 [0.79]	11.9 [0.79]	9 [0.75]	28.7	12.1 [0.81]	8.9 [0.74]	28.9	12.2 [0.82]	9.0 [0.75]	29.1
N.O.S.	Max. Dose	21.0 [2.10]	31.5 [2.10]	25.2 [2.1]	77.7	31.5 [2.1]	25.2 [2.1]	77.7	31.5 [2.1]	25.2 [2.1]	77.7
	Avg. Dose	7.0 [0.70]	10.5 [0.70]	7.6 [0.64]	25.2	10.6 [0.71]	7.6 [0.63]	25.2	10.6 [0.71]	7.6 [0.63]	25.2
Spinal Cord	Max. Dose	12.9 [1.29]	19.3 [1.29]	18.1 [1.51]	45.0	19.3 [1.29]	17.4 [1.45]	45.0	19.3 [1.29]	16.7 [1.39]	45.0
	Avg. Dose	6.8 [0.68]	10.3 [0.68]	7.8 [0.65]	24.9	10.3 [0.68]	7.7 [0.64]	24.8	10.2 [0.68]	7.6 [0.64]	24.7
# of Fractions Given		10	15	12	37	15	12	37	15	12	37

[6] The fraction size doses are given in brackets below the cumulative doses. PTV2 represents the secondary target. "N.O.S" is abbreviation of "Not Otherwise Specified" tissue.

Appendix E[7]: Three-Epoch Adaptation Results for the CERRLung Case (Adapted after fraction 10 and 25, the uniform fractionation model solved in the re-optimization)

Structure	Dose Statistics (Gy)	Same plan is delivered for the first epoch	The original tumor shrinks 20% towards the residual tumor after fraction 25 during the first 10 fractions			The original tumor shrinks 50% towards the residual tumor after fraction 25 during the first 10 fractions			The original tumor shrinks 80% towards the residual tumor after fraction 25 during the first 10 fractions		
		Epoch 1	Epoch 2	Epoch 3 (with Boost)	Total	Epoch 2	Epoch 3 (with Boost)	Total	Epoch 2	Epoch 3 (with Boost)	Total
Tumor	Max. Dose	21.7 [2.17]	32.7 [2.18]	39.0 [2.3]	91.0	32.9 [2.19]	39.1 [2.3]	91.0	32.9 [2.19]	39.0 [2.29]	91.0
	Min. Dose	20.6 [2.06]	30.8 [2.05]	34.0 [2.00]	86.5	30.9 [2.06]	34.0 [2.00]	86.5	31.0 [2.06]	34.0 [2.00]	86.5
	Avg. Dose	21.2 [2.12]	31.8 [2.12]	36.0 [2.12]	88.9	31.9 [2.12]	35.9 [2.11]	89.0	31.9 [2.13]	35.9 [2.11]	89.0
Removed Tumor Voxels	Max. Dose	-	32.6 [2.17]	37.7 [2.22]	91.0	32.7 [2.18]	37.4 [2.2]	91.0	32.7 [2.18]	30.9 [1.82]	91.0
	Min. Dose	-	30.0 [2.00]	10.8 [0.64]	63.5	30.0 [2.00]	11.0 [0.65]	63.5	30.0 [2.00]	37.5 [2.21]	64.0
	Avg. Dose	-	31.3 [2.08]	31.9 [1.88]	84.8	31.3 [2.09]	32.1 [1.89]	84.8	31.3 [2.09]	11.0 [0.65]	84.7
PTV2	Max. Dose	21.7 [2.17]	32.8 [2.19]	39.6 [2.33]	91.0	33.0 [2.20]	40.6 [2.39]	91.0	33.1 [2.21]	40.0 [2.35]	91.0
	Min. Dose	20.0 [2.00]	30.0 [2.00]	4.3 [0.25]	54.3	30[2]	3.9 [0.23]	53.9	30.0 [2.00]	4.1 [0.24]	54.1
	Avg. Dose	20.9 [2.09]	31.4 [2.09]	30.8 [1.81]	83.1	31.4 [2.09]	30.9 [1.82]	83.2	31.4 [2.09]	30.9 [1.82]	83.2
Right Lung	Max. Dose	21.0 [2.10]	31.5 [2.10]	35.7 [2.10]	88.2	31.5 [2.10]	35.7 [2.10]	88.2	31.5 [2.10]	35.7 [2.10]	84.7
	Avg. Dose	4.7 [0.47]	7.1 [0.47]	5.2 [0.31]	17.0	7.1 [0.47]	5.2 [0.31]	17.0	7.1 [0.47]	5.2 [0.31]	17.0
Left Lung	Max. Dose	21.0 [2.10]	31.5 [2.1]	32.3 [1.9]	81.6	31.5 [2.1]	32.5 [1.91]	81.8	31.5 [2.10]	33.5 [1.97]	82.2
	Avg. Dose	2.7 [0.27]	4.0 [0.27]	2.6 [0.15]	9.3	3.9 [0.26]	2.6 [0.15]	9.2	4.0 [0.27]	2.6 [0.15]	9.3
Heart	Max. Dose	20.1 [2.01]	30.7 [2.04]	20.8 [1.23]	70.8	31.1 [2.07]	21.2 [1.25]	71.3	31.3 [2.09]	21.9 [1.29]	72.3
	Avg. Dose	1.2 [0.12]	1.8 [0.12]	1.0 [0.06]	4.0	1.8 [0.12]	1.0 [0.06]	4.0	1.8 [0.12]	1.1 [0.06]	4.0
Esoph.	Max. Dose	21.0 [2.1]	31.5 [2.1]	22.4 [1.32]	74.8	31.5 [2.1]	20 [1.18]	72.4	31.5 [2.1]	21.6 [1.27]	74.0
	Avg. Dose	4.7 [0.47]	7.0 [0.47]	3.1 [0.18]	14.8	7.1 [0.47]	2.8 [0.17]	14.6	7.2 [0.48]	3 [0.18]	14.8
N.O.S.	Max. Dose	21.0 [2.10]	31.5 [2.1]	35.7 [2.1]	88.2	31.5 [2.1]	35.7 [2.1]	88.2	31.5 [2.10]	35.7 [2.10]	88.2
	Avg. Dose	2.1 [0.21]	3.1 [0.21]	2.4 [0.14]	7.6	3.1 [0.21]	2.4 [0.14]	7.6	3.1 [0.21]	2.4 [0.14]	7.6
Spinal Cord	Max. Dose	2.6 [0.26]	5.4 [0.36]	7.0 [0.41]	12.1	5.3 [0.35]	7.4 [0.43]	13.8	4.8 [0.32]	8.4 [0.49]	13.2
	Avg. Dose	0.5 [0.05]	0.8 [0.05]	0.5 [0.03]	1.8	0.9 [0.06]	0.5 [0.03]	1.9	0.8 [0.05]	0.5 [0.03]	1.8
# of Fractions Given		10	15	17	42	15	17	42	15	17	42

[7] The fraction size doses are given in brackets below the cumulative doses. PTV2 represents the secondary target. "N.O.S" is abbreviation of "Not Otherwise Specified" tissue.

Appendix F[8]: Three-Epoch Adaptation Results for the Lung1 Case (Adapted after fraction 25 and 30, the uniform fractionation model solved in the re-optimization)

Structure	Dose Statistics (Gy)	Same plan is delivered for the first two epochs		The residual tumor after fraction 25 shrinks 10%		The residual tumor after fraction 25 shrinks 30%		The residual tumor after fraction 25 shrinks 50%	
		Epoch 1	Epoch 2 (with Boost)	Epoch 3 (with Boost)	Total	Epoch 3 (with Boost)	Total	Epoch 3 (with Boost)	Total
Tumor	Max. Dose	53.6 [2.14]	12.3 [2.47]	19.5 [2.43]	82.3	19.7 [2.46]	82.8	23.5 [2.35]	86.7
	Min. Dose	50.9 [2.04]	10.0 [2.00]	16.0 [2.00]	78.2	16.0 [2.00]	78.6	20.0 [2.00]	82.4
	Avg. Dose	52.1 [2.08]	11.1 [2.22]	17.0 [2.12]	80.2	17.7 [2.22]	80.9	21.1 [2.11]	84.2
Removed Tumor Points	Max. Dose	-	11.3 [2.26]	17.5 [2.19]	81.9	18.3 [2.29]	82.8	22.0 [2.20]	86.4
	Min. Dose	-	2.7 [0.53]	3.8 [0.47]	57.8	3.6 [0.45]	57.6	3.7 [0.37]	57.6
	Avg. Dose	-	6.7 [1.34]	9.0 [1.12]	68.3	9.5 [1.18]	69.8	9.1 [0.91]	70.0
PTV2	Max. Dose	53.6 [2.14]	12.4 [2.48]	19.5 [2.44]	82.3	19.9 [2.49]	82.8	23.5 [2.35]	86.7
	Min. Dose	50.0 [2.00]	2.6 [0.53]	3.8 [0.48]	56.5	3.6 [0.45]	57.3	3.7 [0.37]	57.2
	Avg. Dose	51.9 [2.08]	9.4 [1.87]	13.6 [1.7]	74.9	13.2 [1.65]	74.5	13.2 [1.32]	74.5
Right Lung	Max. Dose	52.3 [2.09]	10.1 [2.02]	14.8 [1.86]	76.3	15.5 [1.94]	77.0	16.1 [1.61]	72.1
	Avg. Dose	17.9 [0.71]	3.0 [0.6]	4.2 [0.52]	25.0	4.2 [0.52]	25.0	4.2 [0.42]	25.0
Left Lung	Max. Dose	44.8 [1.79]	6.9 [1.38]	10.5 [1.31]	57.1	11.8 [1.47]	56.6	13.3 [1.33]	55.7
	Avg. Dose	16.3 [0.65]	3.0 [0.59]	4.1 [0.51]	23.4	4.4 [0.55]	23.7	4.2 [0.42]	23.5
Heart	Max. Dose	50.2 [2.01]	10.5 [2.1]	15.8 [1.97]	76.3	16.8 [2.1]	77.3	18.7 [1.87]	79.3
	Avg. Dose	17.3 [0.69]	3.0 [0.61]	4.3 [0.53]	24.6	4.4 [0.55]	24.7	4.5 [0.45]	24.9
Esoph.	Max. Dose	43.3 [1.73]	8.5 [1.7]	13.1 [1.63]	62.2	15 [1.87]	64.2	16.9 [1.69]	66.0
	Avg. Dose	19.7 [0.79]	3.7 [0.74]	4.9 [0.61]	28.3	5.7 [0.72]	29.2	5.4 [0.54]	28.9
N.O.S.	Max. Dose	52.5 [2.10]	10.5 [2.1]	16.8 [2.1]	79.8	16.8 [2.1]	79.8	21.0 [2.10]	84.0
	Avg. Dose	17.5 [0.70]	3.2 [0.63]	4.6 [0.58]	25.3	4.7 [0.58]	25.4	4.8 [0.48]	25.5
Spinal Cord	Max. Dose	32.1 [1.29]	7.4 [1.48]	9.7 [1.21]	45.0	16.5 [2.06]	45.0	12.6 [1.26]	45.0
	Avg. Dose	17.1 [0.68]	3.2 [0.65]	4.6 [0.57]	24.9	5 [0.63]	25.4	4.8 [0.48]	25.1
# of Fractions Given		25	5	8	38	8	38	10	40

[8] The fraction size doses are given in brackets below the cumulative doses. PTV2 represents the secondary target. "N.O.S" is abbreviation of "Not Otherwise Specified" tissue.

Appendix G[9]: Three-Epoch Adaptation Results for the CERRLung Case (Adapted after fraction 25 and 30, the uniform fractionation model solved in the re-optimization)

Structure	Dose Statistics (Gy)	Same plan is delivered for the first two epochs		The residual tumor after fraction 25 shrinks 10%		The residual tumor after fraction 25 shrinks 30%		The residual tumor after fraction 25 shrinks 50%	
		Epoch 1	Epoch 2 (with Boost)	Epoch 3 (with Boost)	Total	Epoch 3 (with Boost)	Total	Epoch 3 (with Boost)	Total
Tumor	Max. Dose	54.3 [2.17]	11.5 [2.3]	28.0 [2.33]	91.4	30.2 [2.32]	93.4	32.9 [2.35]	95.9
	Min. Dose	51.6 [2.06]	10 [2]	24.0 [2]	86.8	26 [2]	88.8	28.0 [2.0]	91.1
	Avg. Dose	52.9 [2.12]	10.6 [2.12]	25.8 [2.15]	89.3	27.7 [2.13]	91.1	30.2 [2.16]	93.6
Removed Tumor Points	Max. Dose	-	11.1 [2.22]	27.7 [2.31]	91.4	30.1 [2.31]	93.4	32.4 [2.31]	95.9
	Min. Dose	-	3.3 [0.65]	4.2 [0.35]	60.6	3.4 [0.26]	60.6	2.4 [0.17]	59.8
	Avg. Dose	-	9.4 [1.88]	21.6 [1.8]	84.0	21.9 [1.69]	84.6	22.7 [1.62]	85.6
PTV2	Max. Dose	54.3 [2.17]	11.8 [2.35]	29.0 [2.42]	91.4	30.1 [2.32]	93.4	33.3 [2.38]	95.9
	Min. Dose	50 [2.0]	1.2 [0.25]	2.0 [0.16]	53.2	2.1 [0.16]	53.3	1.5 [0.1]	53.0
	Avg. Dose	52.3 [2.09]	9.1 [1.81]	21.6 [1.8]	82.9	21.8 [1.68]	83.2	22.5 [1.61]	83.8
Right Lung	Max. Dose	52.5 [2.1]	10.5 [2.1]	25.2 [2.1]	88.2	27.3 [2.1]	90.3	29.4 [2.1]	92.4
	Avg. Dose	11.8 [0.47]	1.5 [0.31]	3.7 [0.31]	17.0	3.7 [0.28]	17.0	3.7 [0.26]	17.0
Left Lung	Max. Dose	52.5 [2.1]	9.5 [1.9]	24.8 [2.06]	83.5	23.6 [1.82]	73.5	29.3 [2.09]	84.3
	Avg. Dose	6.7 [0.27]	0.8 [0.16]	1.8 [0.15]	9.3	1.6 [0.12]	9.1	1.8 [0.13]	9.3
Heart	Max. Dose	50.2 [2.01]	6.1 [1.21]	15.7 [1.31]	69.3	15.4 [1.18]	65.4	16.7 [1.2]	61.6
	Avg. Dose	2.9 [0.12]	0.3 [0.06]	0.7 [0.06]	4.0	0.6 [0.05]	3.9	0.6 [0.04]	3.9
Esoph.	Max. Dose	52.5 [2.1]	6.5 [1.29]	15.3 [1.28]	74.3	13.0 [1.0]	71.7	9.6 [0.69]	68.4
	Avg. Dose	11.7 [0.47]	0.9 [0.18]	1.9 [0.15]	14.4	1.7 [0.13]	14.3	1.4 [0.1]	14.0
N.O.S.	Max. Dose	52.5 [2.1]	10.5 [2.1]	25.2 [2.1]	88.2	27.3 [2.1]	90.3	29.4 [2.1]	92.4
	Avg. Dose	5.2 [0.21]	0.7 [0.14]	1.6 [0.14]	7.6	1.6 [0.13]	7.6	1.7 [0.12]	7.6
Spinal Cord	Max. Dose	6.6 [0.26]	2.1 [0.42]	1.4 [0.12]	7.6	2.6 [0.2]	9.2	4.4 [0.31]	10.4
	Avg. Dose	1.2 [0.05]	0.2 [0.03]	0.3 [0.02]	1.6	0.5 [0.04]	1.8	0.5 [0.04]	1.8
# of Fractions Given		25	5	12	42	13	43	14	44

[9] The fraction size doses are given in brackets below the cumulative doses. PTV2 represents the secondary target. "N.O.S." is abbreviation of "Not Otherwise Specified" tissue.

Appendix H[10]: Three-Epoch Adaptation Results for the Lung1 Case (Adapted after fraction 25 and 30, the ratio model is solved in the re-optimization and the re-optimized doses rescaled if necessary)

Structure	Dose Statistics (Gy)	Same plan is delivered for the first two epochs		The residual tumor after fraction 25 shrinks 10%		The residual tumor after fraction 25 shrinks 30%		The residual tumor after fraction 25 shrinks 50%	
		Epoch 1	Epoch 2 (with Boost)	Epoch 3 (with Boost)	Total	Epoch 3 (with Boost)	Total	Epoch 3 (with Boost)	Total
Tumor	Max. Dose	54.1 [2.17]	12.1 [2.41]	19.0 [2.38]	82.5	18.7 [2.34]	82.7	21.9 [2.43]	85.0
	Min. Dose	51.4 [2.06]	10.0 [2.00]	16.0 [2.00]	78.4	16.0 [2.00]	78.5	18 [2]	80.7
	Avg. Dose	52.7 [2.11]	10.7 [2.13]	16.9 [2.12]	80.3	17.0 [2.13]	80.3	19.3 [2.14]	82.6
Removed Tumor Points	Max. Dose	-	11.1 [2.22]	17.4 [2.18]	82.2	17.8 [2.22]	82.7	20 [2.22]	84.1
	Min. Dose	-	2.5 [0.50]	3.8 [0.47]	58.4	3.4 [0.42]	57.5	3.3 [0.37]	57.5
	Avg. Dose	-	6.2 [1.24]	8.9 [1.11]	68.4	8.4 [1.05]	68.8	8.3 [0.92]	69.2
PTV2	Max. Dose	54.1 [2.17]	12.1 [2.41]	19.0 [2.38]	82.5	18.8 [2.35]	82.7	21.3 [2.37]	85.0
	Min. Dose	50.0 [2.00]	2.5 [0.5]	3.8 [0.47]	56.3	3.4 [0.42]	56.2	3.3 [0.37]	57.1
	Avg. Dose	52.4 [2.1]	9.0 [1.80]	13.6 [1.7]	75.0	12.4 [1.55]	73.8	12.0 [1.33]	73.4
Right Lung	Max. Dose	52.5 [2.1]	9.7 [1.93]	15.2 [1.89]	76.7	14.6 [1.83]	76.2	14.3 [1.59]	70.4
	Avg. Dose	18.0 [0.72]	2.8 [0.56]	4.2 [0.52]	25.0	3.8 [0.47]	24.6	3.8 [0.42]	24.6
Left Lung	Max. Dose	40.4 [1.62]	6.2 [1.24]	9.8 [1.22]	53.1	13.1 [1.64]	52.1	10.7 [1.19]	50.0
	Avg. Dose	16.5 [0.66]	2.7 [0.54]	4.1 [0.51]	23.3	3.8 [0.47]	23.0	3.9 [0.43]	23.1
Heart	Max. Dose	51.1 [2.04]	10.5 [2.1]	14.5 [1.81]	75.9	16.8 [2.1]	78.2	17.2 [1.91]	78.4
	Avg. Dose	17.5 [0.7]	2.9 [0.58]	4.2 [0.53]	24.6	4.0 [0.51]	24.4	4.2 [0.47]	24.6
Esoph.	Max. Dose	42.9 [1.72]	7.9 [1.58]	13.1 [1.63]	62.0	13.1 [1.63]	62.0	14.9 [1.65]	63.8
	Avg. Dose	20.1 [0.8]	3.2 [0.65]	4.9 [0.61]	28.2	4.7 [0.59]	28.1	5.0 [0.56]	28.3
N.O.S.	Max. Dose	52.5 [2.1]	10.5 [2.1]	16.8 [2.1]	79.8	16.8 [2.1]	79.8	18.9 [2.1]	81.9
	Avg. Dose	17.8 [0.71]	3.0 [0.6]	4.6 [0.57]	25.4	4.3 [0.54]	25.1	4.4 [0.48]	25.1
Spinal Cord	Max. Dose	32.4 [1.3]	6.3 [1.25]	9.2 [1.15]	45.0	9.3 [1.16]	44.3	13.1 [1.45]	44.3
	Avg. Dose	17.2 [0.69]	2.9 [0.59]	4.5 [0.57]	24.7	4.2 [0.53]	24.4	4.4 [0.49]	24.6
# of Fractions Given		25	5	8	38	8	38	9	39

[10] The fraction size doses are given in brackets below the cumulative doses. PTV2 represents the secondary target. "N.O.S." is abbreviation of "Not Otherwise Specified" tissue.

Appendix I[11]: Three-Epoch Adaptation Results for the CERRLung Case (Adapted after fraction 25 and 30, the ratio model solved in the re-optimization and the re-optimized doses rescaled if necessary)

Structure	Dose Statistics (Gy)	Same plan is delivered for the first two epochs		The residual tumor after fraction 25 shrinks 10%		The residual tumor after fraction 25 shrinks 30%		The residual tumor after fraction 25 shrinks 50%	
		Epoch 1	Epoch 2 (with Boost)	Epoch 3 (with Boost)	Total	Epoch 3 (with Boost)	Total	Epoch 3 (with Boost)	Total
Tumor	Max. Dose	54.1 [2.17]	11.4 [2.28]	27.5 [2.29]	90.6	29.7 [2.28]	92.9	34.4 [2.3]	97.5
	Min. Dose	51.4 [2.06]	10 [2.0]	24.0 [2.0]	86.1	26.0 [2.0]	88.3	30.0 [2.0]	92.6
	Avg. Dose	52.7 [2.11]	10.5 [2.1]	25.3 [2.11]	88.5	27.5 [2.11]	90.6	31.8 [2.12]	94.9
Removed Tumor Points	Max. Dose	-	11.1 [2.22]	27.0 [2.25]	90.6	29.7 [2.28]	92.9	33.9 [2.26]	97.5
	Min. Dose	-	3.1 [0.62]	4.0 [0.34]	59.8	3.6 [0.28]	59.9	2.0 [0.13]	58.9
	Avg. Dose	-	9.3 [1.87]	21.4 [1.78]	83.6	22.1 [1.7]	84.5	23.6 [1.58]	86.2
PTV2	Max. Dose	54.1 [2.17]	11.6 [2.31]	27.8 [2.31]	90.6	29.6 [2.28]	92.9	35.8 [2.39]	97.5
	Min. Dose	50 [2.0]	1.1 [0.21]	2.0 [0.17]	53.1	2.0 [0.15]	53.1	1.5 [0.1]	52.7
	Avg. Dose	52.1 [2.09]	9.0 [1.8]	21.1 [1.76]	82.2	21.8 [1.68]	83.0	23.5 [1.57]	84.7
Right Lung	Max. Dose	52.5 [2.1]	10.5 [2.1]	25.2 [2.1]	88.2	27.3 [2.1]	90.3	31.5 [2.1]	94.5
	Avg. Dose	11.7 [0.47]	1.5 [0.3]	3.5 [0.29]	16.7	3.6 [0.28]	16.9	3.7 [0.25]	17.0
Left Lung	Max. Dose	52.5 [2.1]	9.8 [1.95]	23.1 [1.93]	79.3	25.6 [1.97]	80.6	29.7 [1.98]	83.7
	Avg. Dose	6.7 [0.27]	0.8 [0.15]	1.8 [0.15]	9.4	1.8 [0.14]	9.3	1.8 [0.12]	9.3
Heart	Max. Dose	50.5 [2.02]	6.1 [1.22]	14.1 [1.17]	66.8	14.6 [1.13]	66.3	18.7 [1.25]	61.0
	Avg. Dose	2.9 [0.12]	0.3 [0.06]	0.7 [0.06]	4.0	0.7 [0.05]	3.9	0.6 [0.04]	3.9
Esoph.	Max. Dose	52.5 [2.1]	6.0 [1.19]	15.8 [1.32]	74.2	13.0 [1.0]	71.5	9.9 [0.66]	68.3
	Avg. Dose	11.5 [0.46]	0.9 [0.17]	2.2 [0.18]	14.6	2.1 [0.16]	14.5	1.6 [0.11]	14.0
N.O.S.	Max. Dose	52.5 [2.1]	10.5 [2.1]	25.2 [2.1]	88.2	27.3 [2.1]	90.3	31.5 [2.1]	94.5
	Avg. Dose	5.2 [0.21]	0.7 [0.14]	1.6 [0.14]	7.5	1.7 [0.13]	7.6	1.8 [0.12]	7.6
Spinal Cord	Max. Dose	7.2 [0.29]	2.3 [0.45]	5.3 [0.44]	11.2	3.6 [0.27]	9.0	1.6 [0.1]	8.0
	Avg. Dose	1.1 [0.04]	0.2 [0.03]	0.4 [0.03]	1.6	0.5 [0.04]	1.7	0.3 [0.02]	1.5
# of Fractions Given		25	5	12	42	13	43	15	45

[11] The fraction size doses are given in brackets below the cumulative doses. PTV2 represents the secondary target. "N.O.S." is abbreviation of "Not Otherwise Specified" tissue.

Appendix J[12]: Detailed Biological Data Information for Two Base Cases

Tumor Regions	Possible SUV Range	First Base Case: Input Values			Second Base Case: Input Values		
		SUV	pO_2 (mmHg)	*OMF*	*SUV*	pO_2 (mmHg)	*OMF*
Red	5.75-7.00	6.5	7.4	0.82	6.7	5.1	0.77
Yellow	5.00-5.75	5.2	12.1	0.88	5.2	12.1	0.88
Green	3.50-5.00	3.6	14.7	0.91	3.6	14.7	0.91
Light Blue	2.00-3.50	2.5	17.5	0.92	2.5	17.5	0.92
Dark Blue	0.00-2.00	0.25	46.6	0.98	0.25	46.6	0.98

[12] *SUV* denotes Standardized Uptake Value, *OMF* denotes Oxygen-Modification Factor, pO_2 denotes Oxygen Tension

Appendix K[13]: Physical and Biological Optimization Results for the Head and Neck Base Case 1 ("bDose" refers to biological dose, "pDose" refers to physical dose)

Structure	Dose Statistics (Gy)	Physically Optimized Plan with 0.9 Physical Homogeneity	Biologically Optimized Plan with 0.9 Physical Homogeneity	Biologically Optimized Plan with 0.9 Biological Homogeneity
		Total	Total	Total
Primary Target	Max. bDose	86.6 [2.22]	86.4 [2.27]	77.5 [2.04]
	Min. bDose	66.9 [1.71]	68.4 [1.8]	69.7 [1.84]
	Avg. bDose	78.9 [2.02]	78.5 [2.07]	74.5 [1.96]
Primary Target	Max. pDose	88.5 [2.27]	88.2 [2.32]	88.9 [2.34]
	Min. pDose	79.6 [2.04]	79.4 [2.09]	74.9 [1.97]
	Avg. pDose	85.0 [2.18]	84.6 [2.23]	80.4 [2.11]
Target1	Max. Dose	88.5 [2.27]	88.2 [2.32]	87.6 [2.30]
	Min. Dose	70.2 [1.8]	68.4 [1.80]	68.4 [1.8]
	Avg. Dose	78.5 [2.01]	77.9 [2.05]	76.3 [2.01]
Target2	Max. Dose	88.5 [2.27]	88.2 [2.32]	87.6 [2.3]
	Min. Dose	70.2 [1.8]	68.4 [1.80]	68.4 [1.8]
	Avg. Dose	76.5 [1.96]	75.3 [1.98]	75.5 [1.99]
Target3	Max. Dose	88.5 [2.27]	88.2 [2.32]	87.6 [2.30]
	Min. Dose	64.3 [1.65]	62.7 [1.65]	62.7 [1.65]
	Avg. Dose	73.8 [1.89]	72.7 [1.91]	72.7 [1.91]
Mandible	Max. Dose	72.0 [1.85]	72.0 [1.89]	72.0 [1.89]
	Avg. Dose	40.0 [1.03]	40.0 [1.05]	40.0 [1.05]
Brainstem	Max. Dose	58.0 [1.49]	58.0 [1.53]	58.0 [1.53]
	Avg. Dose	34.1 [0.87]	33.4 [0.88]	29.6 [0.78]
Spinal Cord	Max. Dose	50.0 [1.28]	50.0 [1.32]	50.0 [1.32]
	Avg. Dose	18.5 [0.47]	17.0 [0.45]	18.5 [0.49]
Not Otherwise Specified	Max. Dose	80.0 [2.05]	79.8 [2.10]	79.8 [2.10]
	Avg. Dose	25.7 [0.66]	25.5 [0.67]	25.2 [0.66]
# of Fractions Given		39	38	38

[13] The fraction size doses are given in brackets besides the cumulative doses.

Appendix L[14]: Physical and Biological Optimization Results for the Head and Neck Base Case 2 ("bDose" refers to biological dose, "pDose" refers to physical dose)

Structure	Dose Statistics (Gy)	Physically Optimized Plan with 0.8 Physical Homogeneity	Biologically Optimized Plan with 0.8 Physical Homogeneity	Biologically Optimized Plan with 0.8 Biological Homogeneity
		Total	Total	Total
Primary Target	Max. bDose	95.9 [2.52]	96.5 [2.54]	84.7 [2.23]
	Min. bDose	63.5 [1.67]	64.8 [1.7]	67.8 [1.78]
	Avg. bDose	81.6 [2.15]	78.8 [2.07]	75.2 [1.98]
Primary Target	Max. pDose	97.9 [2.58]	98.6 [2.59]	98.0 [2.58]
	Min. pDose	78.4 [2.06]	78.9 [2.08]	69.8 [1.84]
	Avg. pDose	88.1 [2.32]	85.2 [2.24]	81.3 [2.14]
Target1	Max. Dose	97.9 [2.58]	98.6 [2.59]	95.7 [2.52]
	Min. Dose	68.4 [1.80]	68.4 [1.80]	68.4 [1.80]
	Avg. Dose	79.4 [2.09]	78.7 [2.07]	77.2 [2.03]
Target2	Max. Dose	97.9 [2.58]	94.3 [2.48]	95.7 [2.52]
	Min. Dose	68.4 [1.80]	68.4 [1.80]	68.4 [1.80]
	Avg. Dose	76.5 [2.01]	76.6 [2.01]	76.1 [2.00]
Target3	Max. Dose	97.9 [2.58]	98.6 [2.59]	95.7 [2.52]
	Min. Dose	62.7 [1.65]	62.7 [1.65]	62.7 [1.65]
	Avg. Dose	73.9 [1.94]	74.2 [1.95]	72.9 [1.92]
Mandible	Max. Dose	72.0 [1.89]	72.0 [1.89]	72.0 [1.89]
	Avg. Dose	40.0 [1.05]	40.0 [1.05]	40.0 [1.05]
Brainstem	Max. Dose	58.0 [1.53]	58.0 [1.53]	58.0 [1.53]
	Avg. Dose	28.5 [0.75]	27.9 [0.73]	27.0 [0.71]
Spinal Cord	Max. Dose	50.0 [1.32]	50.0 [1.32]	50.0 [1.32]
	Avg. Dose	19.2 [0.5]	16.2 [0.43]	15.6 [0.41]
Not Otherwise Specified	Max. Dose	79.8 [2.10]	79.8 [2.10]	79.8 [2.10]
	Avg. Dose	23.9 [0.63]	25 [0.66]	24.1 [0.63]
# of Fractions Given		38	38	38

[14] The fraction size doses are given in brackets besides the cumulative doses.

Appendix M: Sensitivity of TCP to the Change in Standardized Uptake Value (SUV)

Throughout the computational experiments on biology, the sensitivity of tumor control probability (*TCP*) to the change in the standardized uptake value (*SUV*) was realized. This is illustrated in Table M.1 where the cumulative tumor biological and physical dose statistics as well as the achieved *TCP* are given for both physical and biological plans computed for second and third base cases. The third base case differs from the second base case by having higher hypoxia in red region (*SUV*=6.8 vs. 6.7). As the results in Table M.1 show, although the average biological doses in physical (biological) plans are very similar between second and third base case, the reduction in the minimum biological dose (63.5 Gy vs. 58.6 Gy for physical plans, 64.8 Gy vs. 59.8 Gy for biological plans) has reduced the *TCP*s from 0.63 to 0.05 and 0.70 to 0.20 for physical and biological plans, respectively. The significant decline in *TCP* relative to the change in *SUV* shows the sensitivity of the *TCP* function. However, the improvement in *TCP* obtained by biological plan still holds for the third base case (from *TCP*=0.05 to *TCP*=0.20).

Table M.1: Illustrating the Sensitivity of Tumor Control Probability to the Change in Standardized Uptake Value (*SUV*) by Comparing Physical and Biological Plans between Second and Third Base Cases (Numbers in bold are referred in the text.)

Cumulative Tumor Dose Statistics	Second Base Case (*SUV*=6.7 for Red Region)		Third Base Case (*SUV*=6.8 for Red Region)	
	Physically Optimized Plan with 0.8 Tumor Physical Dose Homogeneity	Biologically Optimized Plan with 0.8 Tumor Physical Dose Homogeneity	Physically Optimized Plan with 0.8 Tumor Physical Dose Homogeneity	Biologically Optimized Plan with 0.8 Tumor Physical Dose Homogeneity
Max. bDose (Gy)	95.9	96.5	95.9	96.5
Min. bDose (Gy)	**63.5**	**64.8**	**58.6**	**59.8**
Avg. bDose (Gy)	81.6	78.8	81.4	78.5
Max. pDose (Gy)	97.9	98.6	97.9	98.6
Min. pDose (Gy)	78.4	78.9	78.4	78.9
Avg. pDose (Gy)	88.1	85.2	88.1	85.2
Tumor Control Probability (*TCP*)	**0.63**	**0.70**	**0.05**	**0.20**

For the physical plan enforcing 0.8 physical homogeneity, Figure M.1 shows how its *TCP* changes relative to the different values of red region *OMF*. The graph shows that the *TCP* becomes sensitive when red region's *OMF* value falls below 0.8. The reason behind higher sensitivity at lower *OMF* values is due to the mathematical function of the surviving fraction. After leaving the re-population effect term off the surviving fraction equation (5.15) in Section 5.2.4 due to being independent of *OMF*, the surviving fraction formula only includes the cell killing effect which has the form of $1/e^x$. This function decreases slower as x increases. Since the higher values of *OMF* ($\geq$0.8) would correspond to higher values of x, the change in the higher x values wouldn't change the surviving fraction as much the change in the lower x values (corresponding to lower *OMF* values) would create. As a result, the change in the lower *OMF*

values would change the surviving fraction with a higher rate resulting in a more significant change in *TCP*.

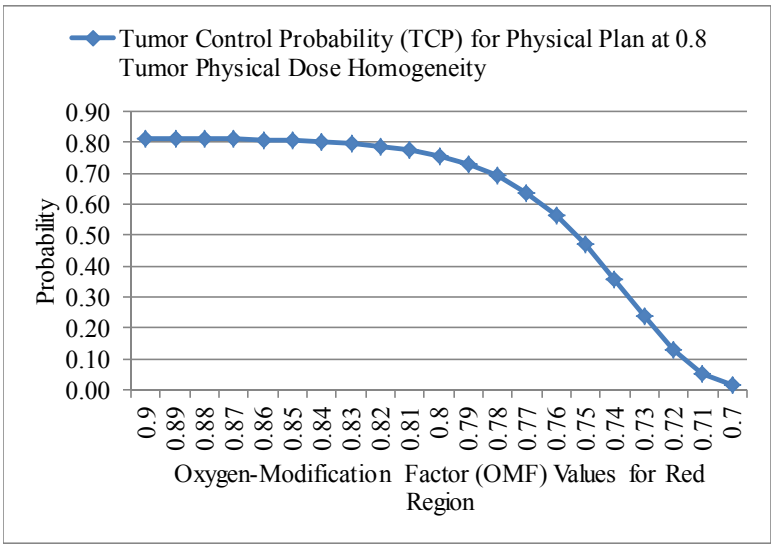

Figure M.1: Tumor Control Probability Relative to the Change in Oxygen-Modification Factor of Red Region